DISCLAIMER NOTICE

THIS DOCUMENT IS BEST QUALITY PRACTICABLE. THE COPY FURNISHED TO DDC CONTAINED A SIGNIFICANT NUMBER OF PAGES WHICH DO NOT REPRODUCE LEGIBLY.

THIS DOCUMENT IS BEST QUALITY PRACTICABLE. THE COPY FURNISHED TO DDC CONTAINED A SIGNIFICANT NUMBER OF PAGES WHICH DO NOT REPRODUCE LEGIBLY.

The Early Years of Vacuum UV

Radiation Physics at USC,

a 30th Anniversary

Final Report, 1 May 1978

by

Gerhard L. Weissler
Professor

DDC
RECEIVED
JUL 21 1978
E

78 07 13 025

(6)

"The Early Years of Vacuum UV Radiation Physics

at USC, a 30th Anniversary,"

(9) Final rept. 1947 - Dec 76

(14) **FINAL REPORT**
(USC-Vac-UV-200)

(10)

by Gerhard L. Weissler, Professor
and Principal Investigator of various
ONR Contracts from 1947 to 1977

(11) 1 May 1978

(12) 156p.

Department of the Navy
U. S. Office of Naval Research
Arlington, VA 22217
Attn: Physics Program (Code 421)

(15)

ONR Contract No.: N00014-76-C-0103
(for the period from 1 July 72 to 31 Dec. 1976)

Department of Physics
University of Southern California
Los Angeles, CA 90007

361 580

The findings of this Final Report are
not to be construed as an Official
Department of the Navy Position, un-
less so designated by other authorized
documents.

SECURITY CLASSIFICATION OF THIS PAGE (When Data Entered)

REPORT DOCUMENTATION PAGE		READ INSTRUCTIONS BEFORE COMPLETING FORM
1. REPORT NUMBER Internal Report No: USC VacUV-200 ✓	2. GOVT ACCESSION NO.	3. RECIPIENT'S CATALOG NUMBER
4. TITLE (and Subtitle) The Early Years of Vacuum UV Radiation Physics at USC, a 30th Anniversary.		5. TYPE OF REPORT & PERIOD COVERED Final Report 1947 to 31 Dec. 1976
		6. PERFORMING ORG. REPORT NUMBER
7. AUTHOR(s) Gerhard L. Weissler Professor of Physics		8. CONTRACT OR GRANT NUMBER(s) N0014-76-C-0103
9. PERFORMING ORGANIZATION NAME AND ADDRESS Department of Physics University of Southern California Los Angeles, CA 90007		10. PROGRAM ELEMENT, PROJECT, TASK AREA & WORK UNIT NUMBERS
11. CONTROLLING OFFICE NAME AND ADDRESS Office of Naval Research Branch Office 1030 East Greet Street Pasadena, California		12. REPORT DATE 1 May 1978
		13. NUMBER OF PAGES 150
14. MONITORING AGENCY NAME & ADDRESS(if different from Controlling Office)		15. SECURITY CLASS. (of this report) Unclassified
		15a. DECLASSIFICATION/DOWNGRADING SCHEDULE NA

16. DISTRIBUTION STATEMENT (of this Report)

Approved for public release; distribution unlimited except for availability of copies.

17. DISTRIBUTION STATEMENT (of the abstract entered in Block 20, if different from Report)

18. SUPPLEMENTARY NOTES

The findings of this report are not to be construed as an official Department of the Navy position, unless so designated by other authorized documents.

19. KEY WORDS (Continue on reverse side if necessary and identify by block number)

Photoionization, Vacuum Ultraviolet Spectroscopy, Plasma Spectroscopy, Photoelectric Yields, Optical Properties of Solids.

20. ABSTRACT (Continue on reverse side if necessary and identify by block number)

This final report summarizes the general area of research done during the 30-year period from 1947 to 1977, and it gratefully acknowledges the continuing sympathetic and financial support of the Office of Naval Research during this long period. Without this support, the research reviewed here would have been severely limited. ⌐ The main body of the report is divided into essentially two parts: "Photoionization in Gases" and "Optical and

DD FORM 1473 EDITION OF 1 NOV 65 IS OBSOLETE
1 JAN 73
S/N 0102-014-6601 |

20.   Abstract (continued)

Photoelectric Effects in Solids. While this material is generally in the nature of a survey, ordered in historical sequence, the last few years from 1972 to 1977 on "Plasma Research" are dealt with in some detail in Section II h) in order to satisfy the formal requirements of this Final Report. Two lists of references are appended, and a total of about 200 individual references are listed.

FOREWORD

For a report such as this, spanning a period of 30 years, a little
needs to be said about the guidelines used in its preparation. Since this
investigator came to the general area of the "Interactions of Vacuum Ultra-
Violet Radiation with Matter" via the broader area of "Gas Discharge Physics,"
it was obvious from this particular vantage point that there were two principal
areas of research: namely as presented in Chapter II: "Photon Interactions
with Gases," and in Chapter III: "Photon Interactions with Solids." In both
of these chapters, our researches are presented in overview only.

References quoted there will appear as numbers enclosed in square
brackets, [ ], if they may be found in Weissler's list of references at the end
of this report, or they may be numbers enclosed in curly brackets, { }, if found in
Professor Masaru Ogawa's list of references, also placed at the end of this report.
(M. Ogawa was a close collaborator of the undersigned at USC. He died on Dec.23, 1974.)

Certain areas of research are presented in somewhat greater detail than
the general overview nature:

In Chapter II, paragraph f) on "Bimolecular Ion-Molecule Reactions," a
large number of data are presented in form of both figures and tables, since
this material has only appeared in dissertation form or in various conference
reports.

For the same reason, namely publication only in form of another disser-
tation, the material in Chapter III, paragraph d) on "Optical and Photoelectric
Properties of Au and Aℓ in the XUV, down to 173 Å," is also presented more
extensively.

More specifically, the research done in the last few years on "Vacuum UV

<u>Interactions with stable Arc Plasmas</u>" has been presented in complete detail in Chapter II, paragraph h).

For reasons given, some researches have been written up in expanded form. In contrast, advances made during this 30 year period by us and others in <u>Instrumentation</u> has been totally omitted here, except for some quotation by title in the appended lists of references. With the rapid development of various technologies, it was felt that this otherwise very necessary phase of investigation could be outdated at the time of this writing and would contribute little to the thought processes leading the experimentalist from one problem to the next.

Finally, it is hoped that while this is a survey of one laboratory's experimental work only, the uninitiated reader will be able to glean an idea as to how a field of research grew and how it branched out into new and different directions.

ACKNOWLEDGEMENTS

In reviewing 30 years of research, certain important facts come to mind immediately:

First, the undersigned as a student and also in later years was profoundly influenced in his attitude towards physics research by his professor,

> Dr. Leonard B. Loeb
> Professor Emeritus of Physics
> Univ. of California, Berkeley

Whatever the contributions here reported may be, it was Professor Loeb who taught me how to recognize important problems and how to tackle them. He alone was more influencial than any other individual in helping me develop my "hunter's nose" or, as he put it, my "Spürnase" towards research, and I owe to Prof. Loeb whatever successes my scientific career has brought me.

Second, the researches reviewed here would have been severely limited in scope, if it had not been for the sympathetic and, most important, continuing financial support over a period of 30 years by the
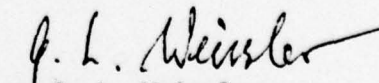
> Department of the Navy
> U.S. Office of Naval Research
> Arlington, Virginia   22217

Third, and by no means least, it is with pleasure that I wish to acknowledge here the active encouragement and assistance over these many years of my home institution, the

> University of Southern California,

and many thanks to my graduate students and associates for their help and inspiration.

To Professor L. B. Loeb, to ONR, and to USC and my co-workers I wish to express my sincerest gratitude.

G. L. Weissler
Professor of Physics
1 May 1978

"THE EARLY YEARS OF VACUUM UV RADIATION PHYSICS AT USC, A 30th AMMIVERSARY"

TABLE OF CONTENTS

LIST OF FIGURES

I. INTRODUCTION

This report covers the research activities of the undersigned and his associates, as supported by the Office of Naval Research, for approximately 30 years from 1947 to 1977. The general title for these activities, namely the "Interaction of Vacuum Ultraviolet Radiation with Gases and Solids," while not specific is never-the-less indicative of the general scope. While we will try to present our progress in historical sequence, we will start with the "Interactions with Gases" first under the sub-heading of "PHOTOIONIZATION IN GASES" and then "OPTICAL AND PHOTOELECTRIC EFFECTS IN SOLIDS" under a second sub-heading.

Since the List of References at the end of this report lists in chronological order the publications, dissertations, conference contributions, etc., many of which have been aided over these years by ONR contracts, the reader will find reference numbers cited out of numerical sequence in the text. In addition, it should be noted here that for purposes of avoiding distracting details, the discussion of innovative instrumentation has been held to a minimum, even though instrumentation references have been included in the final list. In order to make this list more meaningful to the reader, the full titles of these research reports are given as a further guide to their respective contents, with Weissler's references in [ ] and Ogawa's in { } brackets.

Finally, it may not be inappropriate to point out that the initial impetus of these researches was provided by a desire to increase our understanding of various types of electrical discharges through gases, such as glow discharges, arcs, and sparks, and not least of all, of atmospheric electrical phenomena, the orgin of ionospheric layers, and other astrophysical problems. All of these involve to a greater or lesser degree the "Interaction of Vacuum UV Radiation with Gases and Solids."[33,63]

II. PHOTOIONIZATION IN GASES.[33,63,87]

a)   Overview

In order to orient the reader, it is best to start off
with a summary of the various methods of measurement of photoionization
as presented in Fig. 1:

I.   In the upper left-hand corner, we are measuring
Attenuation. This attenuation, measured by the total absorption co-
efficient k or cross section σ, does not inquire into the details of
the atomic or molecular mechanism involved. It only measures a decrease
in intensity versus λ.[8,9,13,17,20-22,24,25,36-38,55,61,74,75]
{11-13,15-21,23-26,28,32,35-38,42-49,52,55-57}

II.   In Photoionization, we determine the number of ion
pairs produced by photoionization per photon absorbed, and we begin to
inquire into the mechanism.[18,23,27-30,33,61,63]

III. Fluorescence occurs when in the process of photoion-
ization a resonance transition leaves the ion in an excited state, which
may then decay to a lower one. Such fluorescence can then be measured
with a second monochromator, or with a filter and a photomultiplier, or
with some similar device. In this fashion, we obtain further information
about specific absorption mechanisms.[56,63,65,69,80,86,91,105]
{30,41,51-54}

I Attenuation

Detector

Specimen I_λ

$I_{o\lambda}$

D $I = I_0 e^{-n\sigma\ell}$

I_λ

$I_{o\lambda}$

D

$\gamma = \text{eff.} = \dfrac{\text{ions formed}}{\text{photon abs.}}$

$I_0\gamma = \dfrac{(i_1)^2/e}{i_1 - i_2}$

i_1 i_2

II Photoionization

$I_{o\lambda}$ D

$h\nu_{Flu}$

D
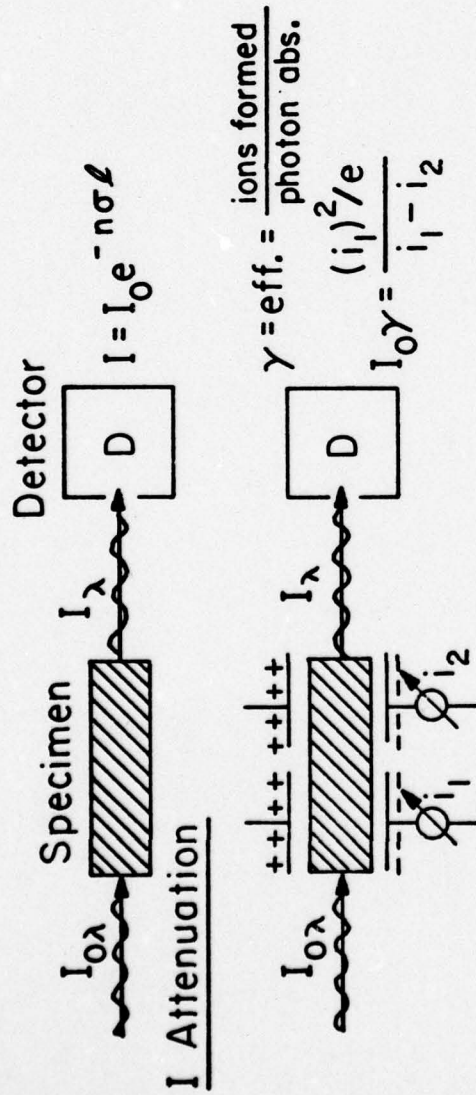
III Fluorescence

$I_{o\lambda}$ D

B D
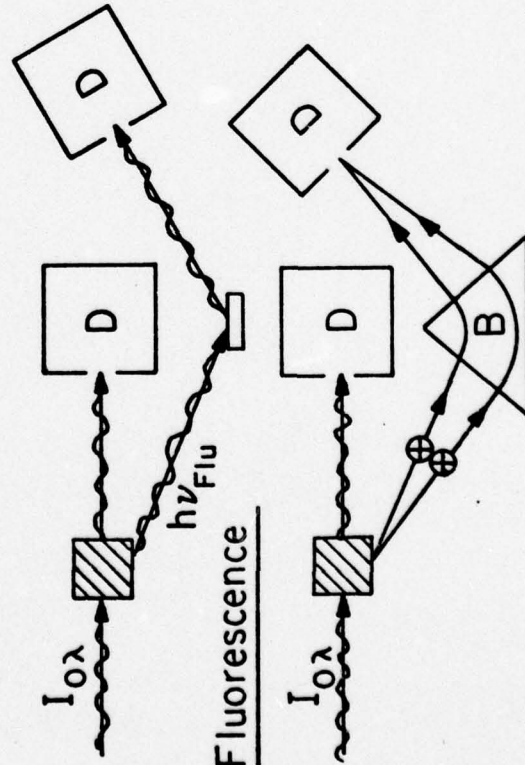
V Ion Mass Spectrometer
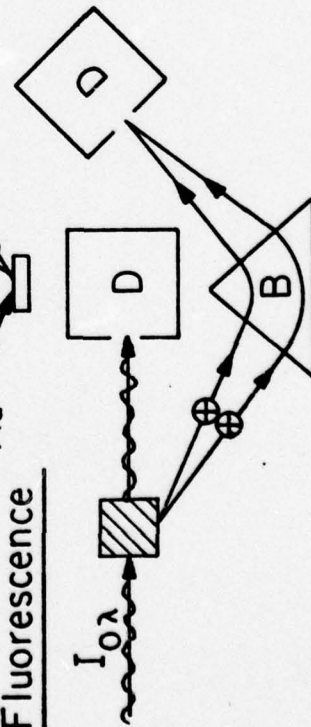
V Photo Electron Energy Analysis

$I_{o\lambda}$ D D

I_λ

$I_{o\lambda}$ D
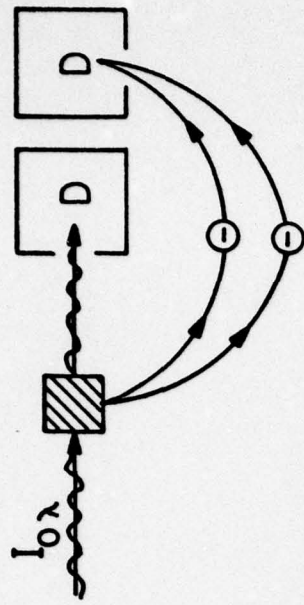
VI Ion Neutral Beam Absorption

Hot Plasma

Black Body $T°K$

Source   Spectrograph
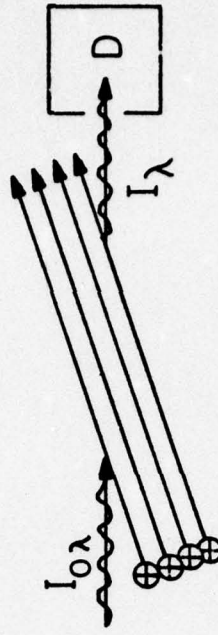
VII Plasma Spectroscopy
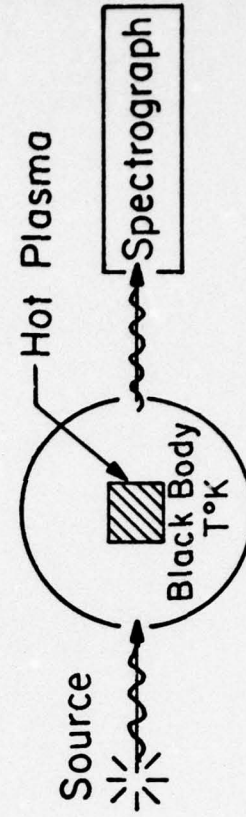
Fig. 1. Methods of Measurement of Photoionization Processes.

IV. A combination of a monochromator with a <u>mass spectrometer</u> provides information on cases where a photon of a given frequency, $h\nu$, may either produce a molecular ion by direct photoionization, or it may form by dissociative photoionization an atomic ion and a neutral, either of which may be in an excited or in the ground state.[39,40,44,50,52-54,63,64,66,81,87,105,106] {14}

V. A new method has been perfected during the last decade, which concerns itself with energy analysis of ejected photoelectrons, the so-called ESCA <u>method</u> (Electron Spectroscopy for Chemical Analysis).[63,87]

VI. An <u>ion beam</u> or a beam of neutrals may be used as the absorbing medium when light is traversing it. This allows the study of those particular species, which can be most easily produced in beam form, for instance, atomic hydrogen. But this would probably be the last to be so studied, because our theoretical knowledge of hydrogen is more complete than that of any other atom. However, this method seems most suitable for some metallic vapors of particular significance to astrophysical problems. The difficulty with this approach is accuracy, because one needs to know the precise geometry of and atom density in the beam which is traversed by the radiation.[87]

VII. Finally, the last method shown in the bottom right corner of Fig. 1 is <u>plasma spectroscopy</u>.[*] The hot plasma, either in a low pressure shock tube or in a high pressure arc, is utilized either as an emitting or absorbing medium. High pressure means about one atmosphere, and the plasma is assumed to be in thermodynamic equilibrium, or at least in L.T.E. (Local Thermodynamic Equilibrium). If this is true, then we can utilize various laws, for instance Kirchhoff's law, which states that the emissivity is proportional to the absorptivity, and that the proportionality constant is the Planck functiona B_λ. By measuring emission intensities, we thereby can obtain the absorption coefficient or the photoionization cross section, provided that we measure first the Planck

[*][68,84,85,96,101-104,108-125]

function. Some very careful and beautiful work has been done on vacuum ultra-violet plasma emission spectroscopy by the late Günther Boldt in Munich, who was unfortunately taken from us at a very early age.

In Table I, I wish to make use of nitrogen and oxygen as examples of the interactions of photons with different molecular electrons, as they accur in the processos of light absorption. The first and 7th lines give the electron configurations of the atoms and the second and 8th lines describe the corresponding ground states of the molecules. The absorption giving rise to the excitation of a neutral state as the upper state of the Schumann-Runge bands, line, 9, occurs when a photon interacts with a $(\pi_u 2p)$-electron of O_2. In the case of molecular ions, one of the $(\sigma_g 2p)$-electrons of N_2 (line 3) or a $(\pi_g 2p)$-electron in O_2 (line 10) is removed to infinity. For still higher lying excited states of the two ions, N_2^+ and O_2^+ (lines 4,5,6, and 11,12), more tightly bound electrons are ejected.

This example may suffice to show the various possible interactions between different molecular electrons and photons and to show the significance of studying specific photon absorption transitions as a function of wavelength, to shorter and shorter wavelengths down into the soft x-ray region.

Figure 2 represents some potential energy curves of a hypothetical molecule. We consider first a phtoon of energy $h\nu_1$ slightly above the ionization threshold, XM_2^+. In this particular case, we obtain primarily photoions of the molecule in the ground state. I would like to remind the reader of one easily overlooked fact, namely that the various excited states of the molecular ion have neutral Rydberg states converging towards each. The neutral Rydberg states are schematically indicated by short, thick horizontal bars, sometimes marked "Ry". One of these Rydberg states is shown in terms of its potential energy curve, marked M_2^* on the right and "Ry" on the left. It is located between the X- and the A-states of the molecular ion. The significance of the neutral states will

Table I. The electron configurations of some states of atomic and molecular nitrogen and oxygen

1.	N	ground state:	$1s^2$	$2s^2$	$2p^3$	: $^4S_{3/2}$
2.	N_2	graund state:	kk	$(\sigma_g2s)^2(\sigma_u2s)^2$	$(\pi_u2p)^4(\sigma_g2p)^2$	: $X\ ^1\Sigma_g^+$
3.	N_2^+	ground state:	kk	$(\sigma_g2s)^2(\sigma_u2s)^2$	$(\pi_u2p)^4(\sigma_g2p)$	: $X\ ^2\Sigma_g^+$
4.	N_2^{+*}	excited ion :	kk	$(\sigma_g2s)^2(\sigma_u2s)^2$	$(\pi_u2p)^3(\sigma_g2p)^2$	: $A\ ^2\Pi_u$
5.	N_2^{+**}	excited ion :	kk	$(\sigma_g2s)^2(\sigma_u2s)$	$(\pi_u2p)^4(\sigma_g2p)^2$	: $B\ ^2\Sigma_u^+$
6.	N_2^{+***}	excited ion :	kk	$(\sigma_g2s)(\sigma_u2s)^2$	$(\pi_u2p)^4(\sigma_g2p)^2(\pi_g2p)$	: $C\ ^2\Sigma_u^+$
7.	O	ground state:	$1s^2$	$2s^2$	$2p^4$	: $^3P_2$
8.	O_2	ground state:	kk	$(\sigma_g2s)^2(\sigma_u2s)^2$	$(\sigma_g2p)^2(\pi_u2p)^4(\pi_g2p)^2$	: $X\ ^3\Sigma_g^-$
9.	O_2	Upper state of Schumann- Runge bands :	kk	$(\sigma_g2s)^2(\sigma_u2s)^2$	$(\sigma_g2p)^2(\pi_u2p)^4(\pi_g2p)^3$	: $B\ ^3\Sigma_u^-$
10.	O_2^-	ground state:	kk	$(\sigma_g2s)^2(\sigma_u2s)^2$	$(\sigma_g2p)^2(\pi_u2p)^4(\pi_g2p)$	: $X\ ^2\Pi_g$
11.	O_2^{-*}	excited ion :	kk	$(\sigma_g2s)^2(\sigma_u2s)^2$	$(\sigma_g2p)^2(\pi_u2p)^3(\pi_g2p)^2$	: $a\ ^4\Pi_u$ $A\ ^2\Pi_u$
12.	O_2^{-**}	excited ion :	kk	$(\sigma_g2s)^2(\sigma_u2s)^2$	$(\sigma_g2p)^1(\pi_u2p)^4(\pi_g2p)^2$	: $b\ ^4\Sigma_u^-$

Fig. 2. Photon absorption transitions in a hypothetical molecule, M_2.

become apparent a little later. The three photons, $h\nu_1$, $h\nu_2$, and $h\nu_3$, show the general complexity of the various interactions with a simple diatomic molecule.

For instance, $h\nu_1$ may be absorbed by interacting with a $(\sigma_g 2P)$-electron of the molecule, raising it to a continuum state above its ionization limit. This electron will then be ejected with a kinetic energy, KE_1, leaving the molecular ion in its ground electronic state and in a vibrational state, say v'=0, as shown by the downward arrow.

If $h\nu_1$ happens to have jsut the right amount of energy, then this photon may also interact with a more tightly bound electron, say $(\pi_u 2p)$, and excite it to the Rydberg state shown as a full curve M_2^* in its v'=2 state. (This is one of the Rydberg states converging toward the excited state of the molecular ion, $A\ M_2^*$). Since the Ry-state lies above the ionization limit, $X\ M_2^+$, in other words, since it is immersed in the ionization continuum above $X\ M_2^+$, therefore configuration interaction between the Rydberg and the adjacent continuum states may occur, giving rise to a more broadened or diffuse absorption band than in the absence of neighboring continuum states. The electron may then make a horizontal transition into the continuum, a pre-ionization process, which results in its ejection, leaving behind as before a molecular ion, $X\ M_2^+$ (v'=0,1...).

As the photon energy is increased, say to a value $h\nu_2$, the choice of absorption mechanisms increases. Not only are those processes mentioned for $h\nu_1$, also possible for $h\nu_2$, namely direct photoionization and perhaps pre-ionization, leaving the molecular ion in various vibrational states of its ground state with the emission of an electron of considerable energy (as shown by the three long downward arrows on the extreme left, labelled KE_2). In additon, a second direct photoionization process may occur, when $h\nu_2$ is absorbed by a $(\pi_u 2p)$-electron, thereby raising it into one of its corresponding continuum states above the $A\ M_2^{+*}$ limit. When this electron is ejected, it may leave the ion in its A state, v'=0,1,...,

In this case, the three shorter downward arrows on the near left of curve A indicate the magnitude of the energy of the photo-electrons, and the three groups of downward arrows of three each illustrate the emission of the associated fluorescence radiation marked $h\nu_{F1}$, provided that the transition from A→X is allowed.

There is yet another photon interaction mechanism possible, which has been illustrated for a photon of still greater energy, $h\nu_3$. If this photon is absorbed by a $(\sigma_u 2s)$-electron, raising it to a continuum state above the B M_2^+* limit, then this electron may be ejected with an energy KE_3. This may leave the molecule in the excited state of the ion, B M_2^+* in the vibrational state v'=1. As a result, dissociative photoionization may occur, because a repulsive potential curve, C, crosses B at v'-1. Therefore, we would observe a photo-electron of energy KE_3 (downward arrow to the near left) and two atomic dissociation products, M^+ and M, of total kinetic energy E_D (downward double arrow to the right).

Of course, dissociation may not occur when a photo-electron of slightly greater energy KE_3 is observed (downward arrow on far left) leaving M_2^+ in the vibration state v'=0 of the B state, which in turn may decay by way of fluorescence (three downward arrows, labelled $h\nu'_{F1}$), if some transition to a lower state is possible.

b) Photoelectron Energy Analysis[*][87]

With a variety of different specific absorption transitions as illustrated in Fig. 2 in mind, it becomes immediately obvious that a specific cross section for each absorption transition is needed, and this then requires a brief review of the capabilities of some of the measuring techniques. Therefore, some examples will be quickly discussed as, for instance, the absorption of the He resonance line at 584 Å (hν=21.21 eV) by molecular hydrogen, as shown schematically in Fig. 3 by the upward arrow.

*"Electron Spectroscopy", D.A. Shirley, ed.; North-Holland Publishing Co., Amsterdam 1972.
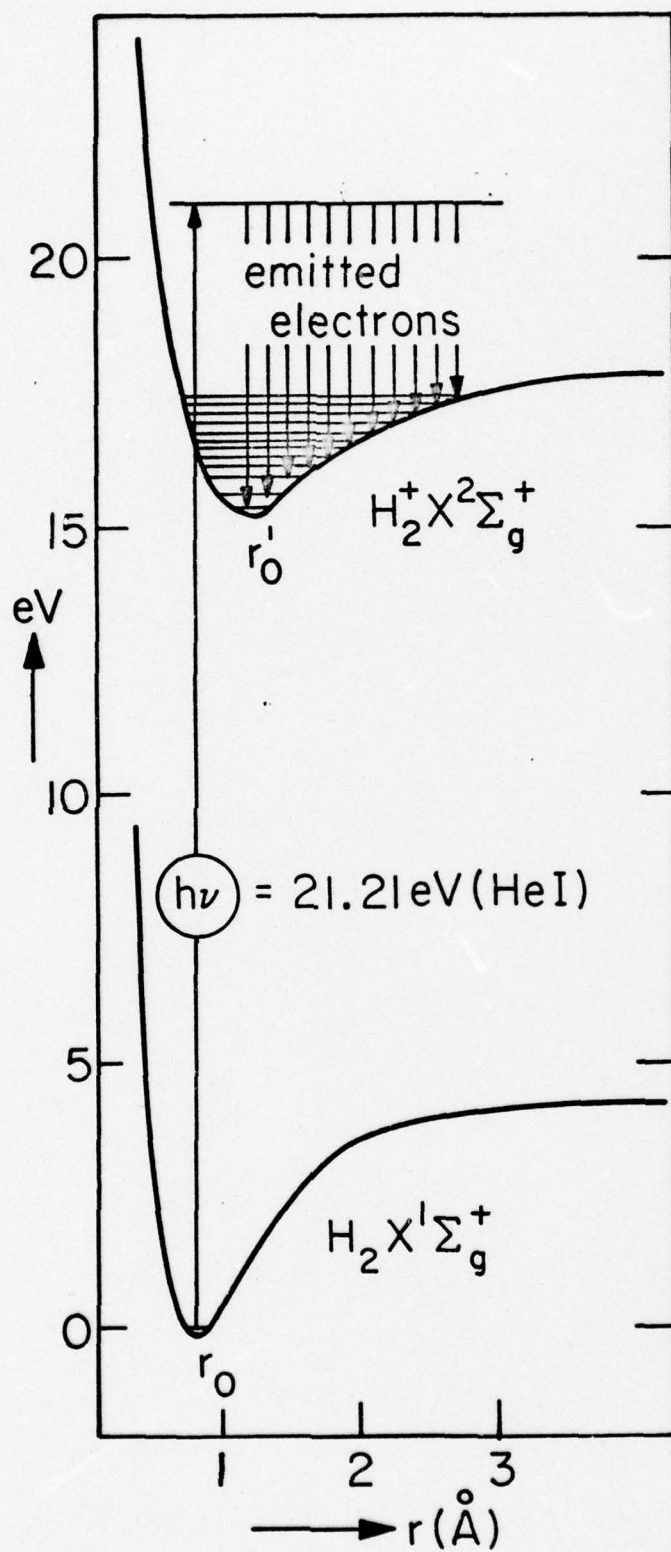
Fig. 3. Photoionization in H_2.

Here, the incident photon raises an electron to a continuum state above the ionization limit of 15.47 eV of the ground state of the molecular ion, H_2^+ X $^2\Sigma_g^+$. From there, the electron is released with discrete amounts of energy, downward arrows, leaving the ion in v'=0,1,...12,13. In Fig. 4 we present the ESCA results of the Uppsala group [*] which shows these sharply defined groups of electron energies. The assuracy of the electron energy determination is seen to be about ±0.010 eV, which is comparable to the resolution of a 1 meter normal incidence spectrograph with a grating of 600 grooves per millimeter and with entrance and exit slits of 20 to 100 micron width each. The relative peak heights in Fig. 4 not only allows the assignment of the relative cross section for a photon absorption transition, which leaves the ion in one specific vibrational state, provided the total photoionization cross section to the X H_2^+ state is known. In addition, the distribution of the peak heights allows conclusions as to the nature of the removed electron, bonding or anti-bonding, since this distribution will indicate the position of the upper potential curve, X H_2^+, with respect to the lower one, X H_2, in Fig. 3: $r'_o > r_o$, therefore a bonding electron has been removed; if in another molecule $r'_o < r_o$, as for instance, for the states A or B M_2^+ in Fig. 2, then an antibonding electron will have been removed by an absorption transition involving either of these two states, and a very different distribution of peak heights will be observed in electron energy measurements. This is clearly related to the asymmetry of all potential energy curves, which are very steep to the left of the minimum, for small internuclear distances, and much shallower to the right, as shown more clearly in Fig. 3.

The remarkable accuracy of the ESCA method illustrated in Fig. 4 was achieved by the Uppsala group [*] by use of electrostatic deflectors in the shape of concentric spherical surfaces. Alternate methods of photoelectron energy analysis are concentric cylinder electrostatic deflectors (which have an

[*] "ESCA, ATOMIC, MOLECULAR AND SOLID STATE STRUCTURE etc.", K. Siegbahn et al., Nova Acta Regiae Soc. Sci. Upsaliensis, Series IV, Vol. 20, Uppsala 1967.
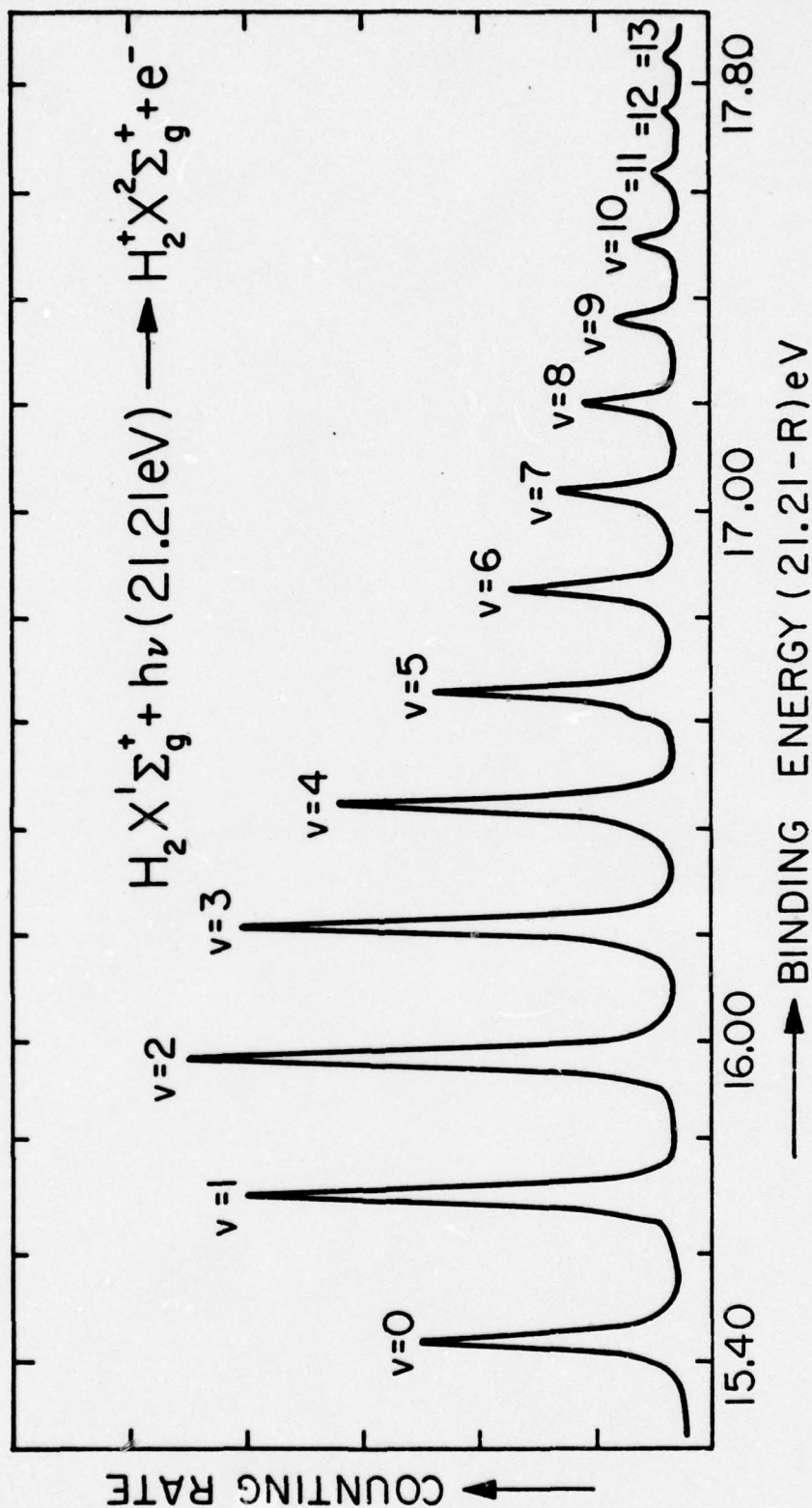
Fig. 4. Energies of Photoelectrons[1] in H_2 by He I 584 Å

advantage of very roughly 2π in electron collection efficiency over the spherical analyzers), and the spherical grid retarding potential methods. The last one is only capable of much lower accuracy than the first two (as will become obvious when inspecting later Figs. 6 and 7), but it has the advantage of collecting substantially all photoelectrons released by a given photon. This, in turn, allows for a better assignment of specific photoionization cross sections in terms of relative currents than is possible by the first two methods, which rely on counting rates.

On the other hand, the spherical electrostatic analyzer is particularly useful for the determination of the angular distribution of photoelectrons which has a bearing on the bonding character of the concerned electron. Since this instrument accepts only electrons from a relatively small solid angle, this angle of electron emission with respect to the E-vector of a polarized photon beam and with respect to the photon beam direction itself can be varied. This is not true for the other two methods.

Figure 5 shows a select number of Gilmore's Franck-Condon curves for N_2 and N_2^+ and will be used to illustrate further what has been said before. Here, the incident photon, $h\nu_i$=21.21 eV, He I 584 Å, is shown to be absorbed by nitrogen in one of its continuum states, well above the first (X N_2^+), second (A N_2^+), and third (B N_2^+) ionization limits. As a consequence, three energy groups of photoelectrons have been measured (the downward arrows to the different vibrational states of the three electronic states marked X, A, and B), depending on whether $h\nu_i$ interacted with one or the other of the molecular electrons of N_2: $(\sigma_g 2p)$, $(\pi_u 2p)$, or $(\sigma_u 2s)$ as shown in Table I.

Figure 6 shows these three groups of photoelectrons measured with the spherical grid retarding potential method. If the total photoionization cross section is known, say from measurements with ion chambers (Fig. 1, II),

---

* "ESCA Applied to Free Molecules", K. Siegbahn et al., North-Holland Publ. Co. Amsterdam 1969.

Fig. 5. Some Franck-Condon Curves of Gilmore's for N_2 and N_2^+.

then the specific cross section which leaved the ion in v'=0 of the B-state is simply obtained from the measured current ratio, I_1/I_{MAX}, shown in Fig. 6.

The ESCA method represented in Fig. 7 measures those photoelectron transitions which leave the ion in its A-state, and the high accuracy is self-evident, when this figure is compared to the central part of the retarding potential versus current curve of Fig. 6.

While the accuracy of the ESCA method is remarkable in terms of the determination of energies of atomic and molecular states, conventional emission and absorption spectroscopy using modern gratings and photographic emulsions must still be regarded as one of the most accurate probes of atomic and molecular physics.

As an example, Fig. 8 represents M. Ogawa's absorption spectrum of N_2 between 800 Å and 1000 Å, in the top-half with a reciprocal linear dispersion of 2.85 Å/mm in the first order. In the bottom-half of the figure, the region A marked above, from 822 Å to 834 Å, is shown in the third order with 0.95 Å/mm. The significance of this becomes obvious, when one recognizes that the sharpness of the fine rotational lines within the vibrational bands allows for analysis of these rotational states, which are not seen by any of the photoelectron energy analyzers. Another way of saying this, is to compare the ESCA resolution of about 0.01 eV, or about 80 cm^{-1}, with that in Fig. 8, bottom, of about o.0002 eV to 0.001 eV at 800 Å and 1000 Å, respectively, or 1 to 10 cm^{-1}.

c) <u>Fluorescence Produced in Photoionization Processes</u> [58,63,65,69,80,81,91,105]

Of those photoionizing transitions in Fig. 5, which leave the molecule in its B-state, some will spontaneously decay to the X-state of the molecular ion (indicated in Fig. 5 by two groups of downward arrows and labelled as $h\nu_{F1}$: fluoresc. radiation). Such wavelength resolved fluorescence as a function of the incident radiation can be observed, when a vacuum monochromator is coupled

* {30,41,51-54}
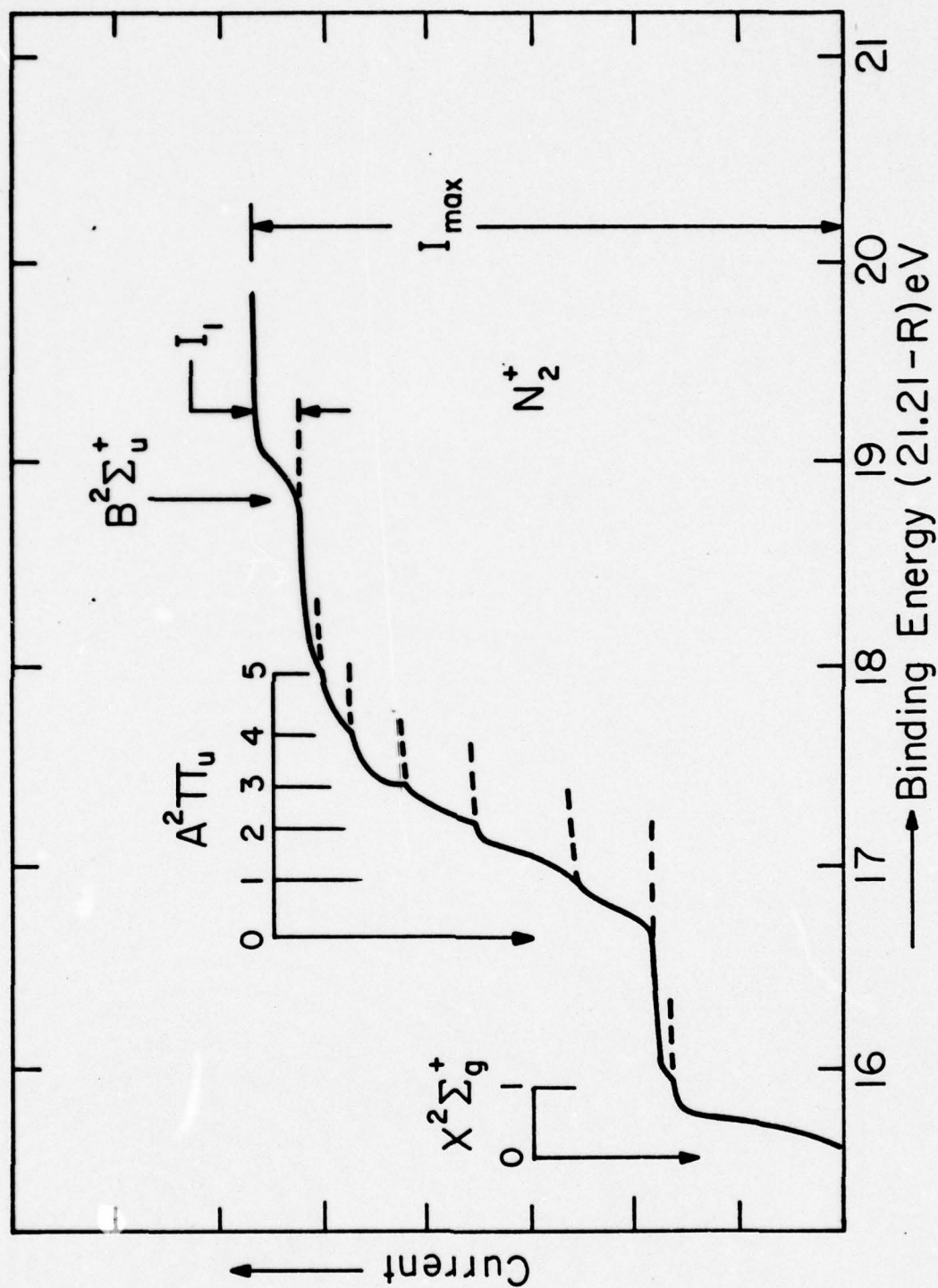
Fig. 6. Energies of Photoelectrons in N_2 by He I 584 Å, measured with the Spherical Grid Retarding Potential Method (as per Samson).
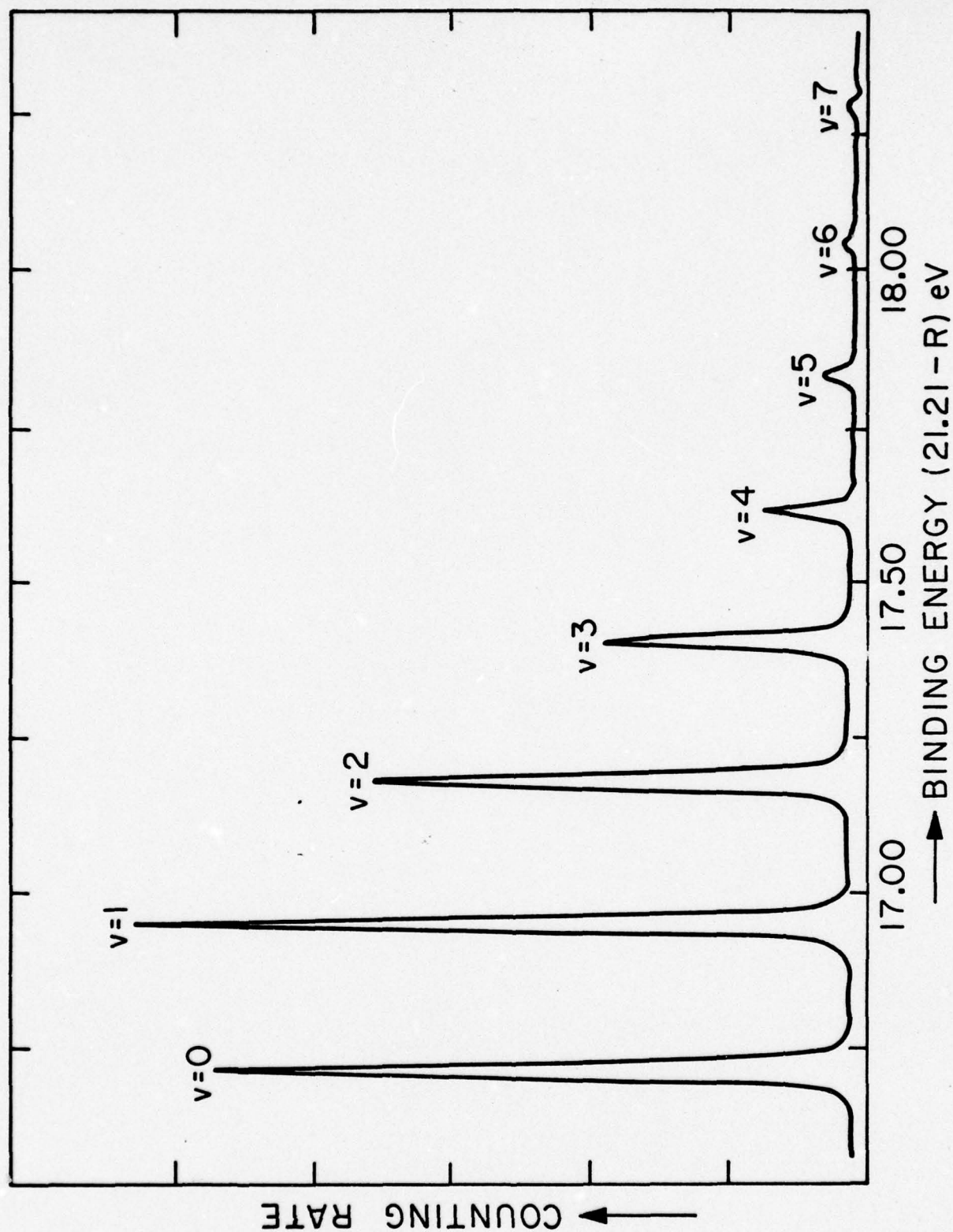
Fig. 7. Energies of Photoelectrons in N_2 by He I 594 Å, measured with a Spherical Electrostatic Analyzer (as per Uppsala ESCA work).
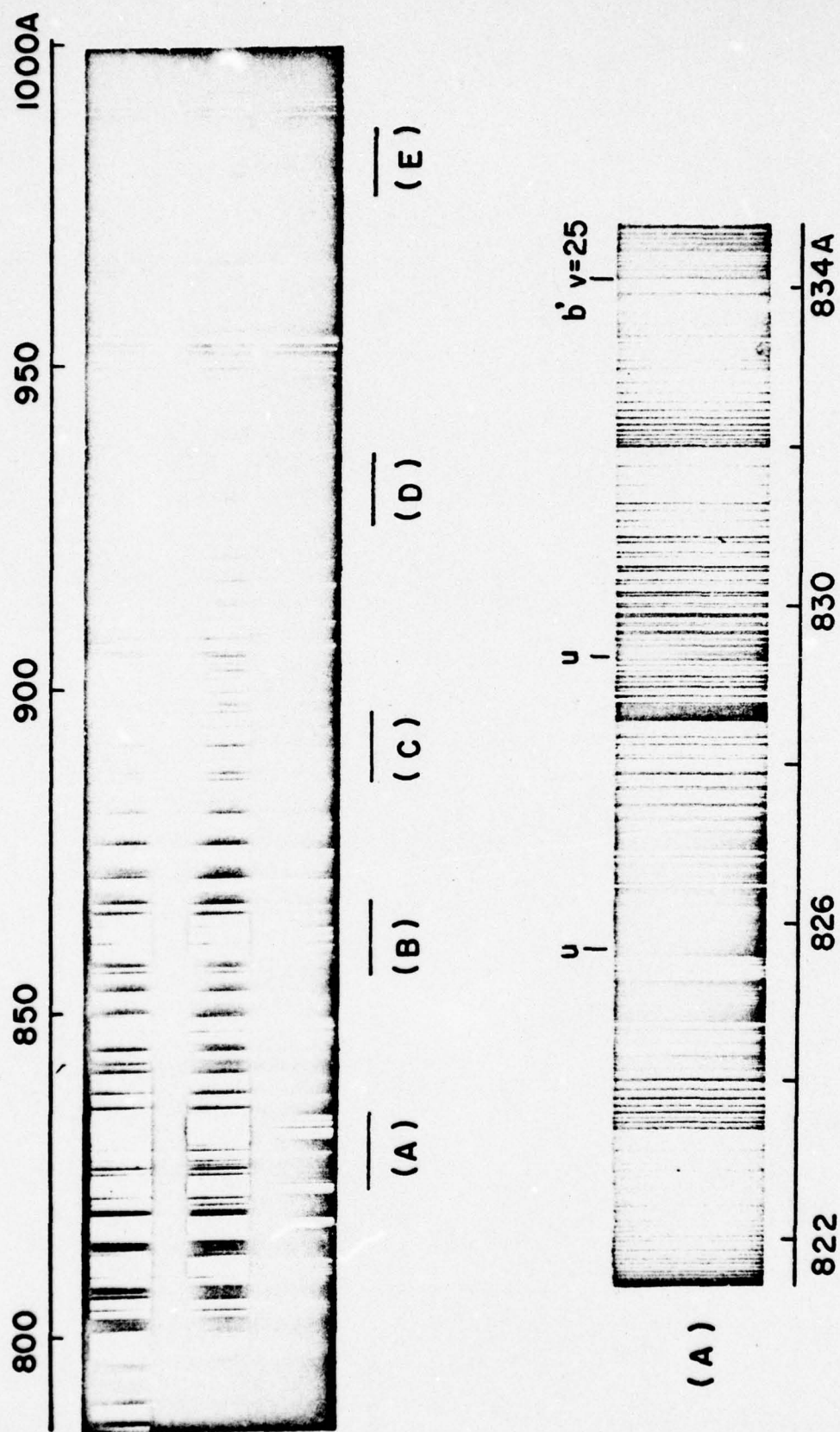
Fig. 8. Ogawa's N_2 Absorption Plate between 800 Å and 1000 Å.

to a second spectrometer   which looks at the photoionization region, as shown in Fig. 9.

When experimental results, obtained in this fashion, are corrected for detector and instrument response, then the fluorescent intensities in Fig. 10 appear as four pronounced peaks for the transitions from B, $v'=0$ to X, $v''=0,1,$ $2,3$ (left group of four downward arrows in Fig. 5) and as four subsidiary peaks or shoulders for the much weaker fluorescence from B, $v'=1$ to X, $v''=0,1,2,3$. The ratios of these band intensities are then proportional to the Franck-Condon factors for these transitions.

It is obvious, that these fluorescence techniques ought to be extended toward the observation of both shorter and longer wavelengths.

Furthermore, by studying the fluorescence radiation also as a function of the time-delay, i.e., following the light-source spark which produces the primary photons, $h\nu_i$, it is possible to observe radiation characteristic of species which are the result of collisions between photoions in known states and neutrals.

Thus, from the analysis of photoelectron energies and currents and from such fluorescence work just described, much more information can be obtained not only about molecular states, but also about details of specific photo-ionization transitions. In particular, the work so far reported is of such promise that its extension into the shorter wavelength region is imperative

d) Mass Spectrometer Analysis of Photoionization Products [*]

While referring to shorter wavelengths, it is obvious from Fig. 5 that if the incident photon is of energy $h\nu_i \geq 24.5$ eV, the minimum value to form $N^+ + N$, then it should be possible to observe atomic ions (also shown in Fig. 2 for the absorption of $h\nu_3$). This requires that a mass spectrometer be coupled to a vacuum monochromator   as in Fig. 11. There, the photon beam from a Seya-Namioka type instrument is allowed to pass through the ionization chamber

[*][39,40,44,50,52-54,63,64,66,81,87,105,106] {14}
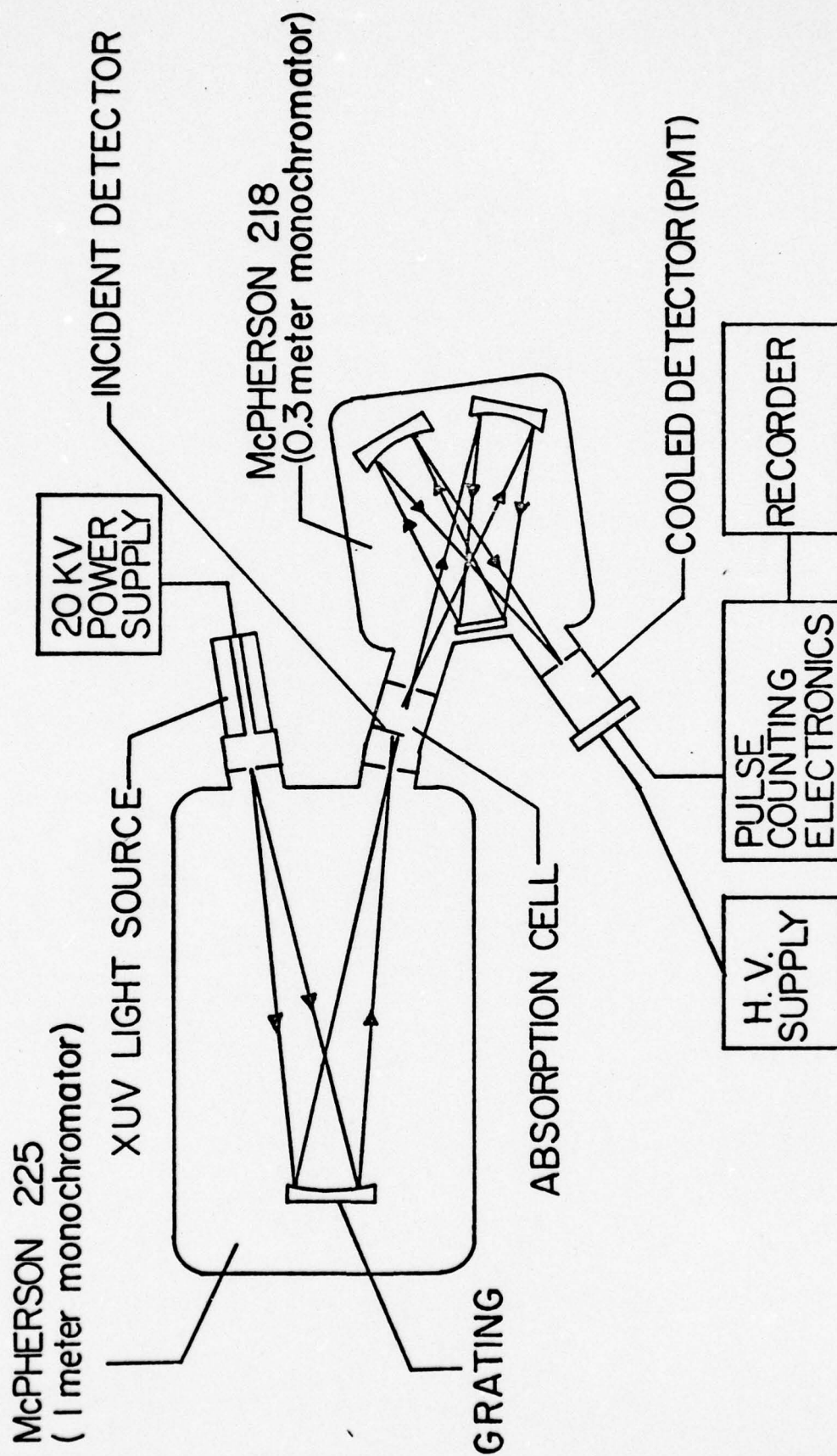
Fig. 9. U.S.C. Vacuum Monochromator Coupled to a Czerny-Turner Spectrometer for Fluorescence Analysis.
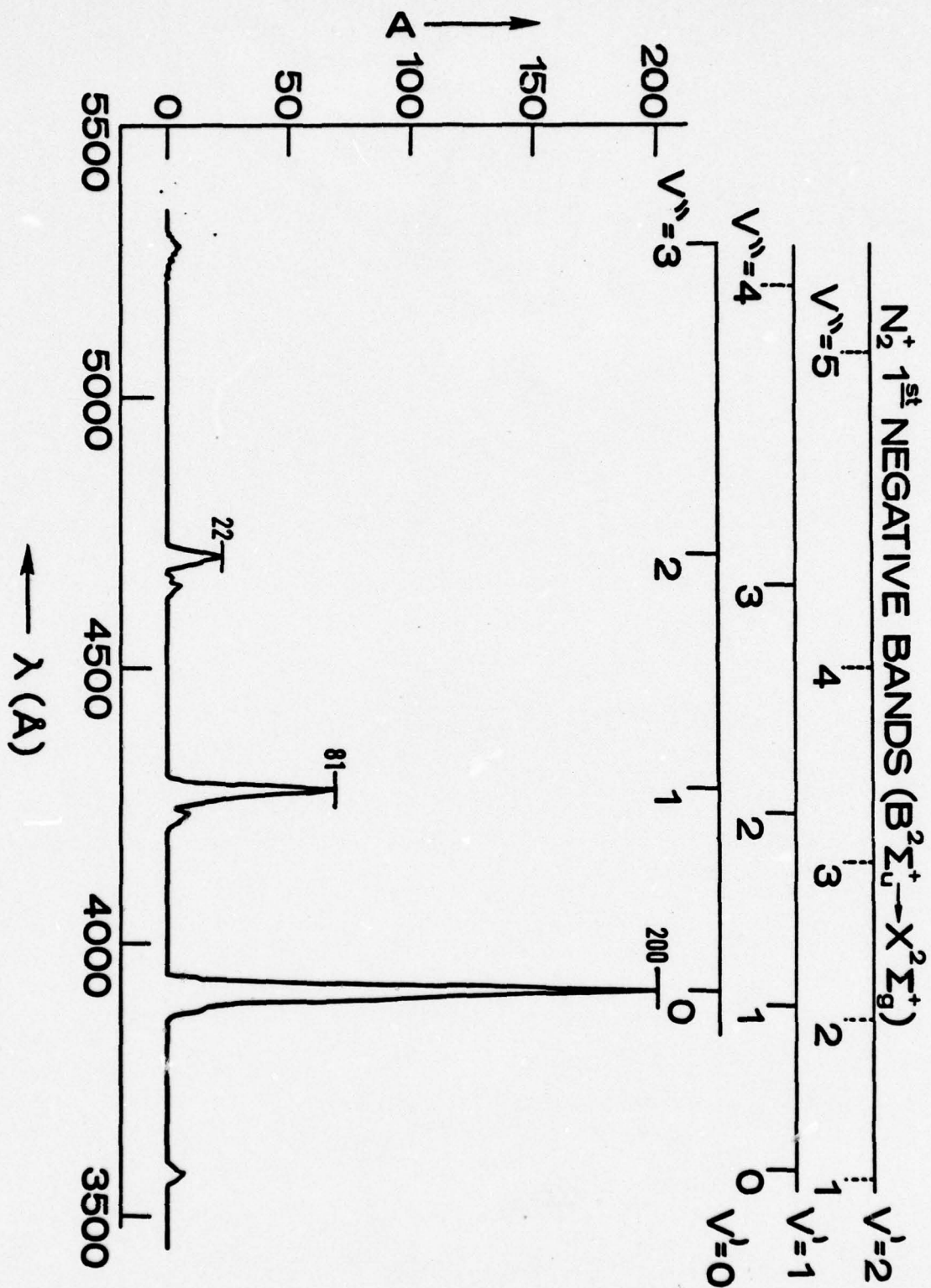
Fig. 10. Fluorescence from N_2^+ ($B^2\Sigma_u^+ \rightarrow X^2\Sigma_g^+$).
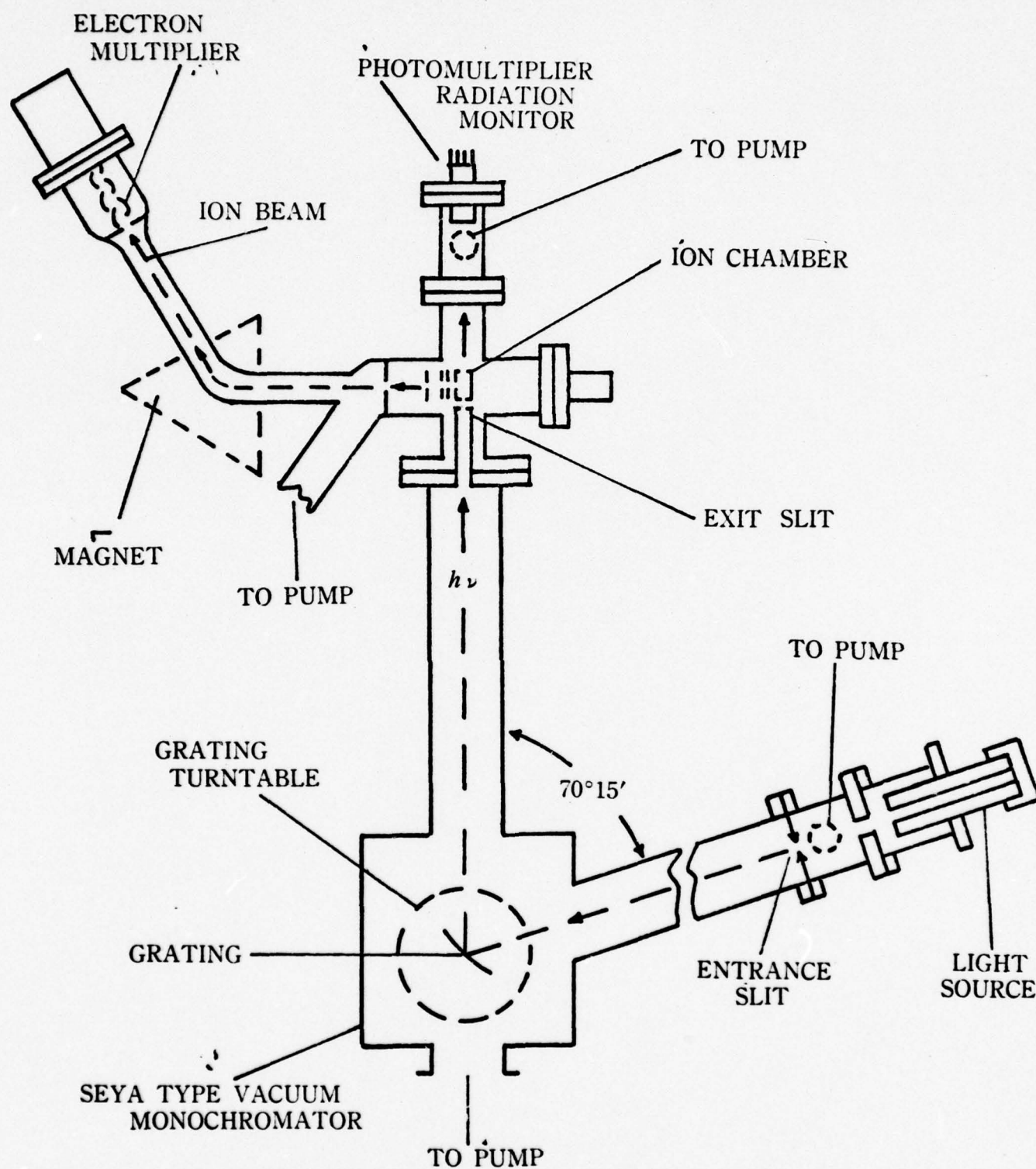
Fig. 11. U.S.C. Seya-Namioka Monochromator Coupled to a Nier-type Mass Spectrometer.

of a Nier-type mass spectrometer.

The results for N_2 are shown in Fig. 12, where the intensity of ions produced per unit photon flux is plotted against photon energy. The different ionization limits for the formation of N_2^+, the X-, A-, B-, and C-states, are marked there with downward arrows. Of particular importance is the upper right inset, which shows the appearance of the atomic ion, N^+, at a value slightly above the C-state limit, in agreement with the fact that the Franck-Condon regime (indicated by 2 vertical lines in Fig. 5) intersects the C-state at $v' \sim 1$ or 2, i.e., above $v'=0$. It is worth noting that the intensity ordinate of the inset is by a factor of 1/100 smaller than the ordinate on the main Fig. 12.
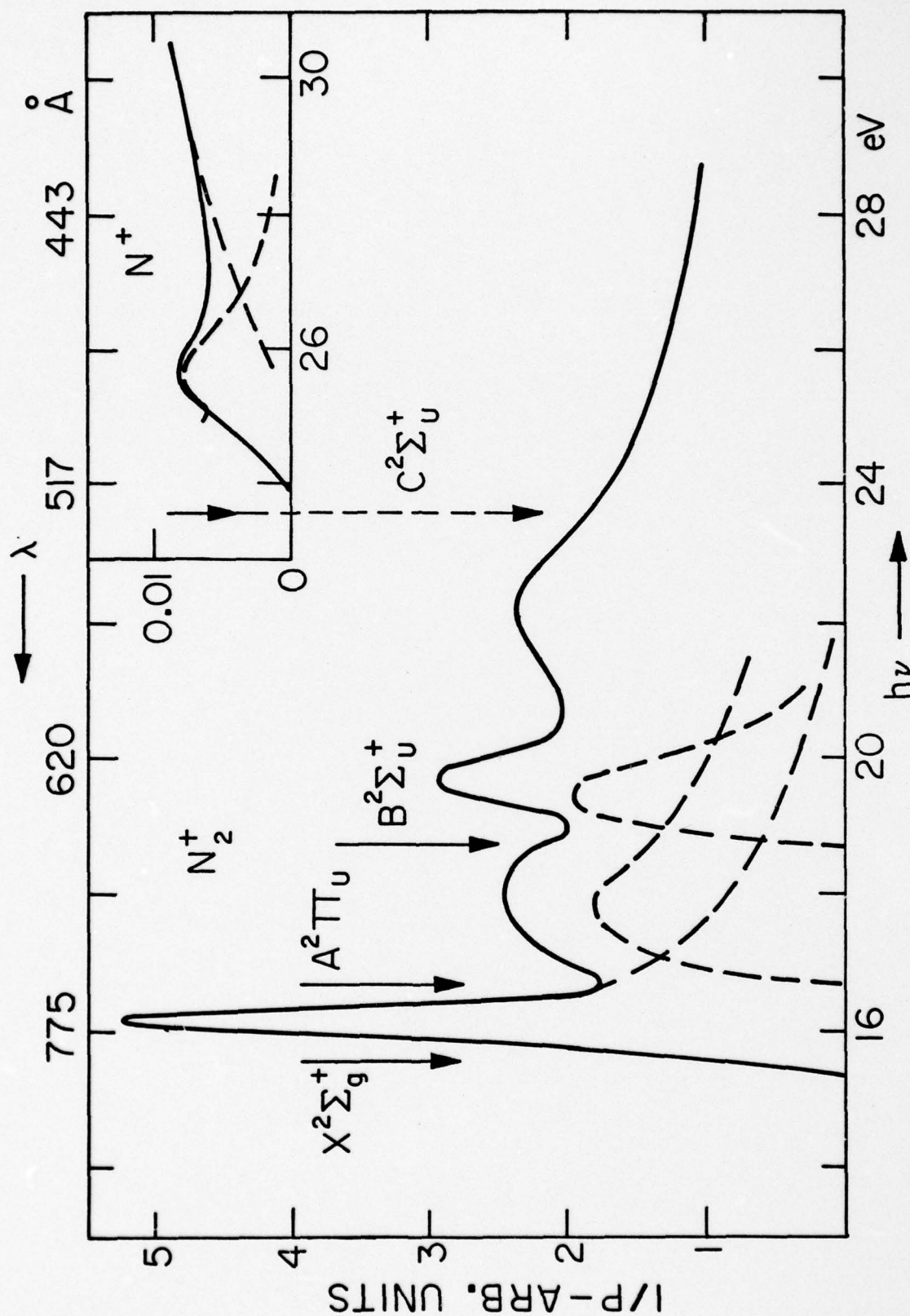
Fig. 12. Ion Intensities, N_2^+ and N^+, per unit Photon Flux versus Wavelength.

e) Ion-Molecule Reactions[46,50,63]

Ionization of a gas in a mass spectrometer is sometimes followed by an ion-molecule reaction. When this process occurs the reaction is often described by the equation

$$W + X^+ \rightarrow Y^+ + Z,$$

in which an electrically neutral gas molecule W and an ionized molecule X^+ collide to form a product ion Y^+ plus a neutral Z. For such bimolecular reactions the intensities of the reactant and product ions are found to vary directly and as the square of the gas pressure, respectively, and are usually observed at pressures higher than those ordinarily used in a mass spectrometer. Two quantities of interest in an ion-molecule reaction are the reaction rate and cross section for the process. The cross section is defined in the usual way as that area about the neutral molecule W through which the ionized molecule X^+ must pass for the reaction to occur, while the reaction rate constant is that number which, when multiplied by the concentration of X^+ and W, will equal the time rate of increase of the concentration of the product ion Y^+.

The usual method of ionizing the neutral molecule X is by electron impact, but in this research, X^+ has been produced by photoionization using monoenergetic photons from a grating monochromator. Photoionization has been found to possess several advantages over electron impact methods. First, the temperature in the ionization chamber of the mass spectrometer was essentially room temperature, while with an electron beam the heat of the filament causes temperature gradients to exist, thereby making a precise determination of both temperature and density of the gas in the ion chamber difficult. Furthermore, heat from the filament causes the release of impurity molecules from surfaces, making extreme cleanliness mandatory for this type of source. With a photo-

ionization source, no particular precautions were necessary to reduce background peaks due to impurities. It was also possible to work at higher pressures without taking special precautions to prevent the filament from evaporating and, of course, no magnetic field was necessary to align the ionizing beam.

The primary aim of this research was to look for the occurance of ion-molecule raactions and to determine their reaction rate and cross section. The gases studied were hydrogen, methane, and a one-to-one mixture of hydrogen and nitrogen, and the observed product ions detected were H_3^+, CH_5^+, and N_2H^+, respectively. (For results, see fig's. 13 to 25 and Table II.)

Of secondary interest were the appearance potentials of ions and the dependence of ion intensities on photon energy. In many instances ion intensity variations could be correlated with the onset of higher ionization potentials, corresponding to an ion in an excited state, or with a dissociative ionization process.

It is hoped that the results obtained will advance our knowledge of chemical kinetics and contribute to our understanding of molecular structure and the properties of matter when interacting with radiation of the vacuum ultraviolet region.
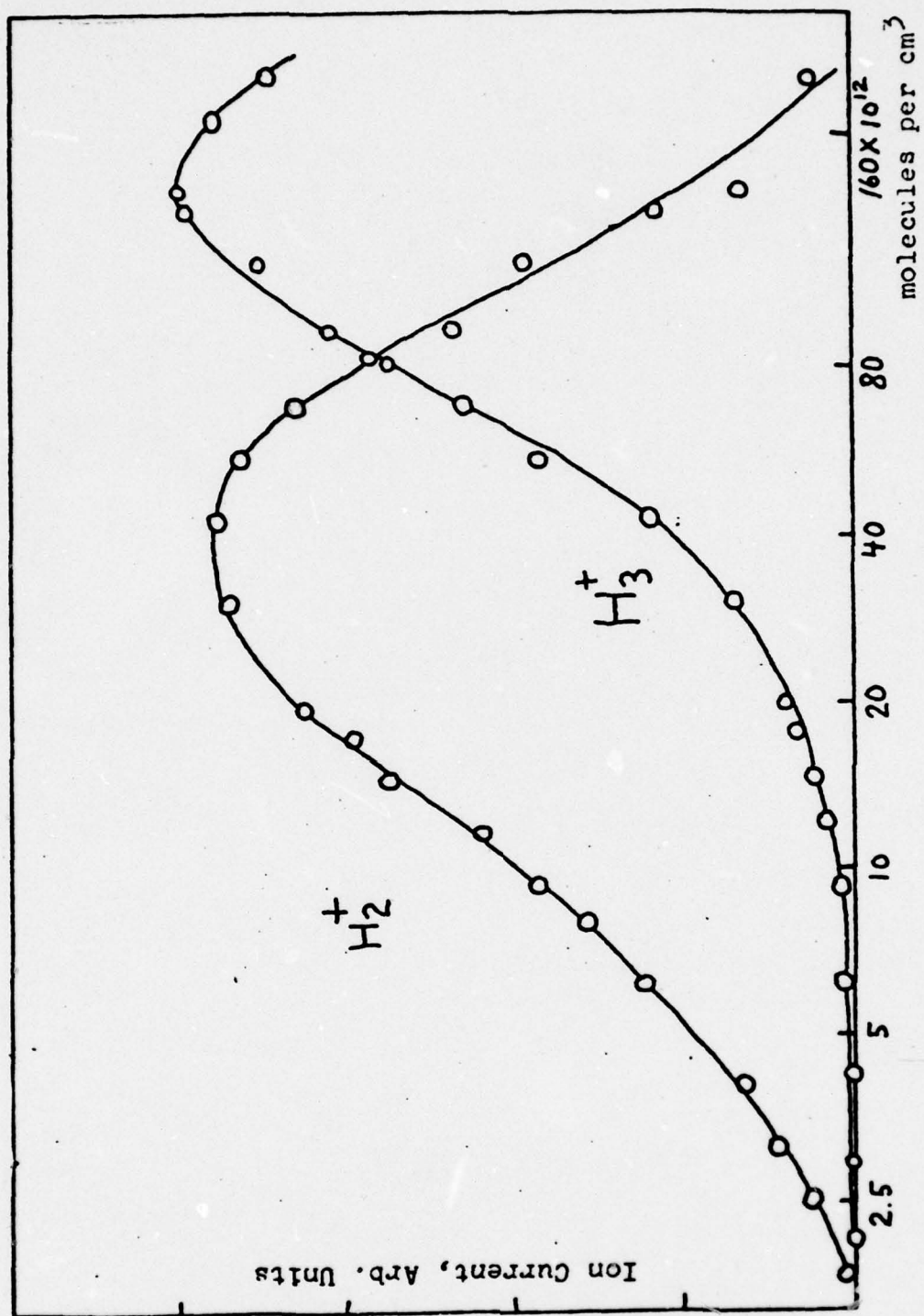
Figure 13. H_2^+ and H_3^+ currents versus H_2 concentration at λ = 765 Å.
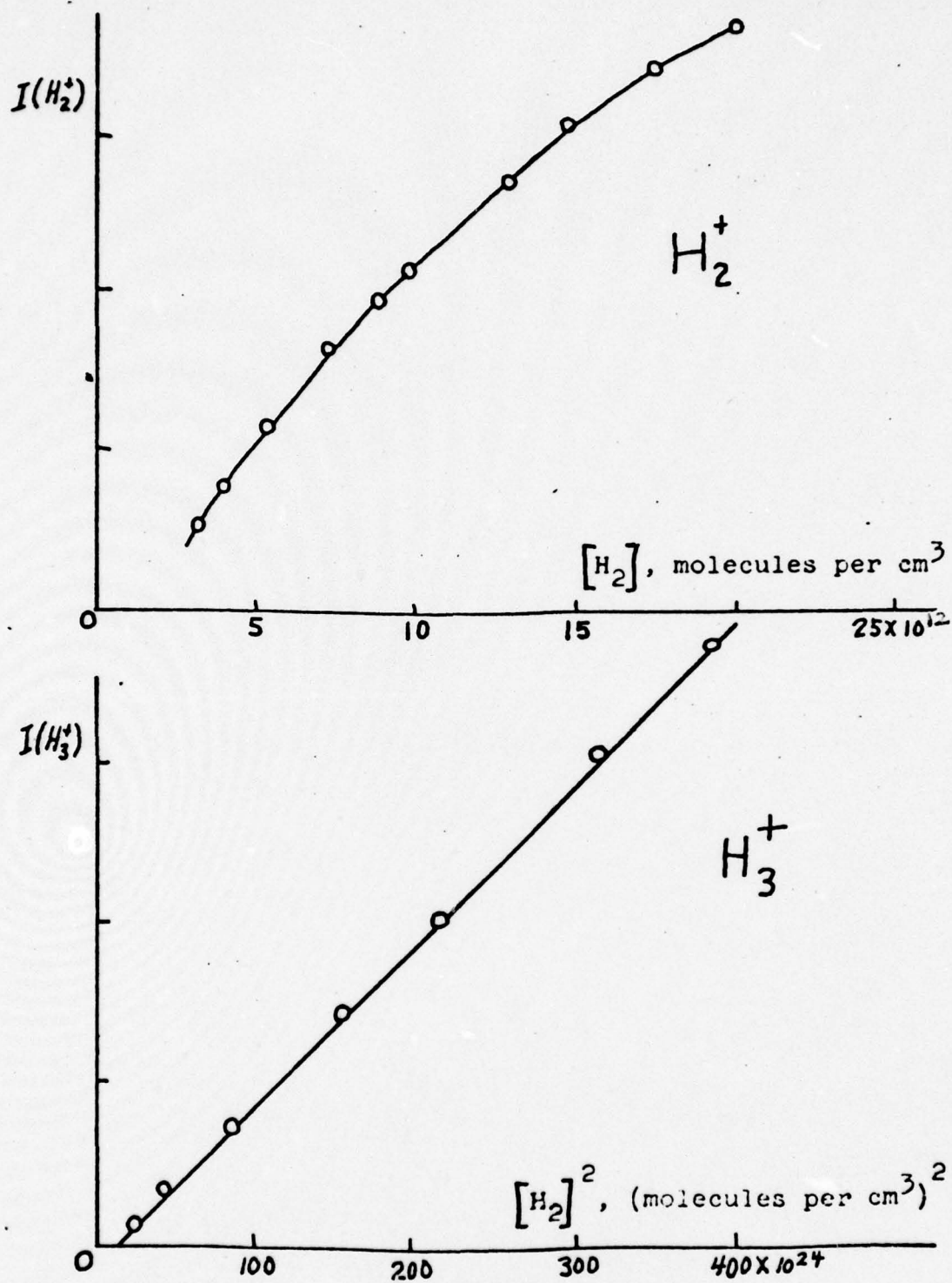
Figure 14. Linear and Quadratic Dependence of H_2 Concentration versus H_2^+ and H_3^+ Currents.
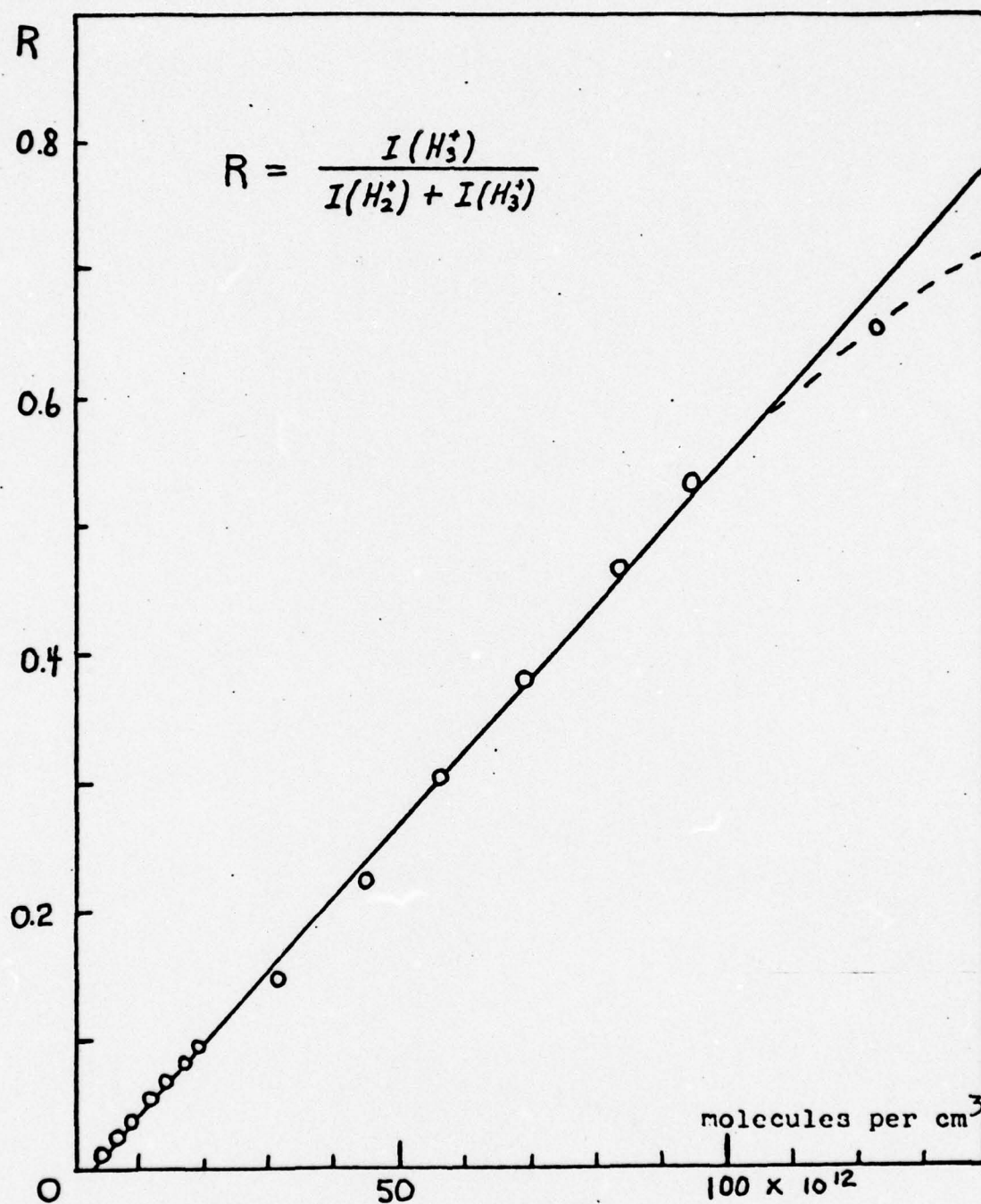
Figure 15.   Ion ratio R versus Hydrogen Concentration for

$H_2^+ + H_2 \rightarrow H_3^+ + H$ at $\lambda = 765$ Å.
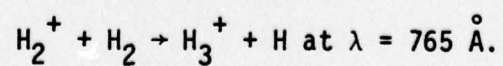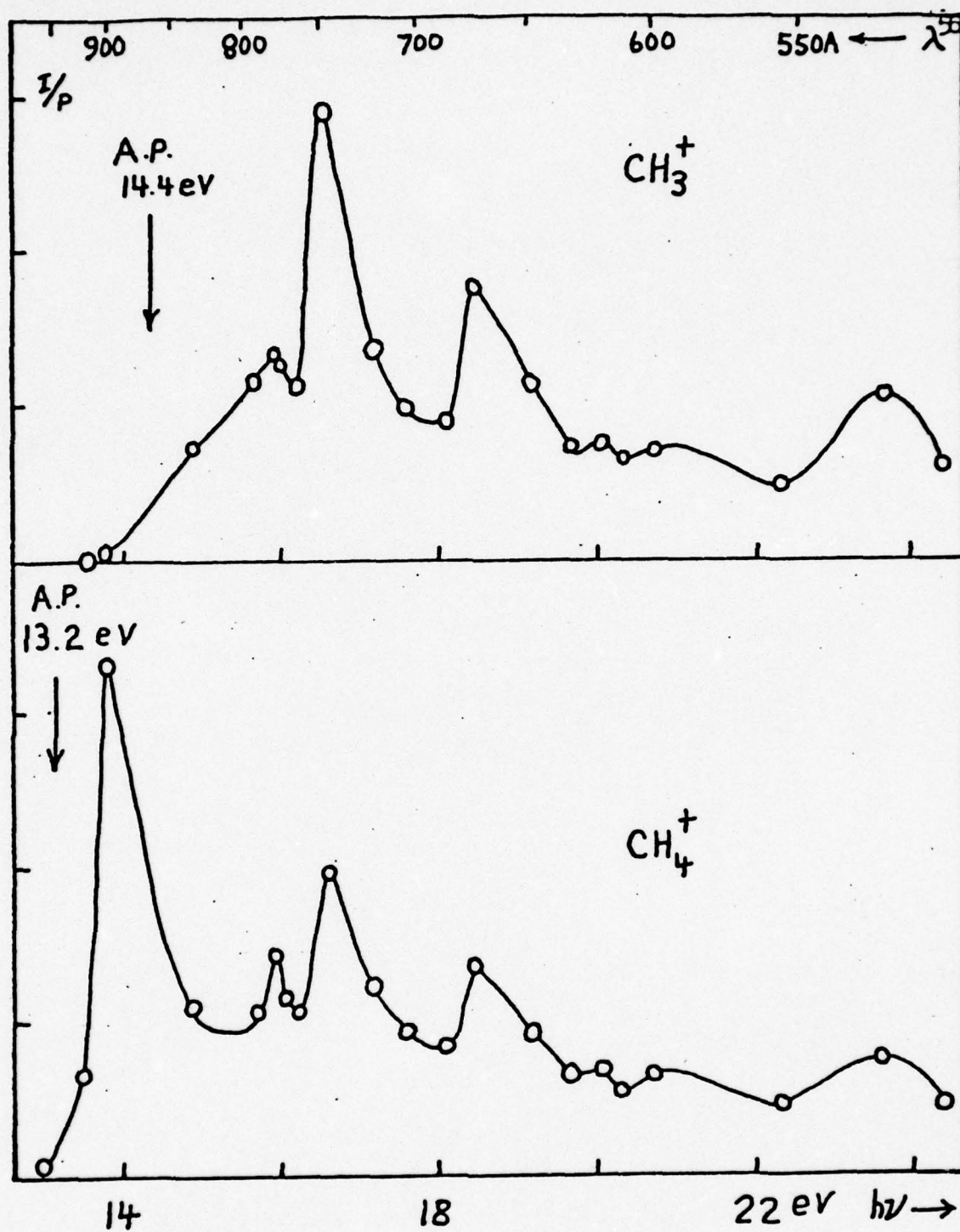
Figure 16. CH_4^+ and CH_3^+ Currents per unit Photon Flux versus Wavelength.
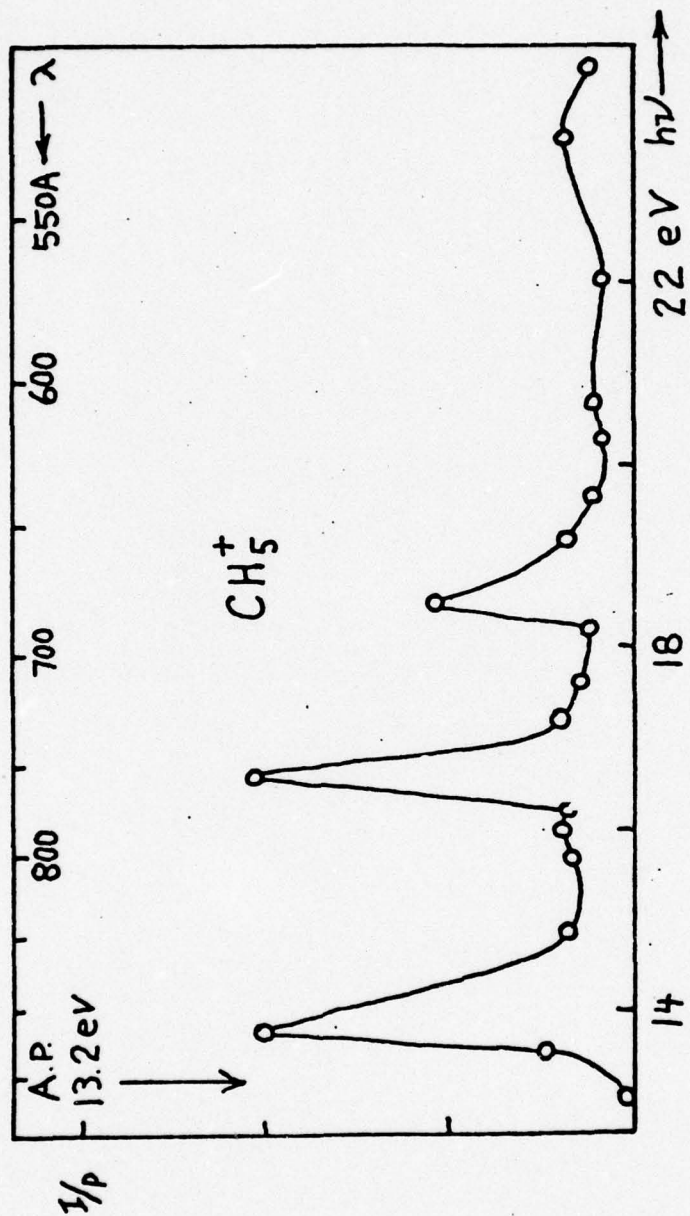
Figure 17, CH_5^+ current per unit photon flux versus wavelength.
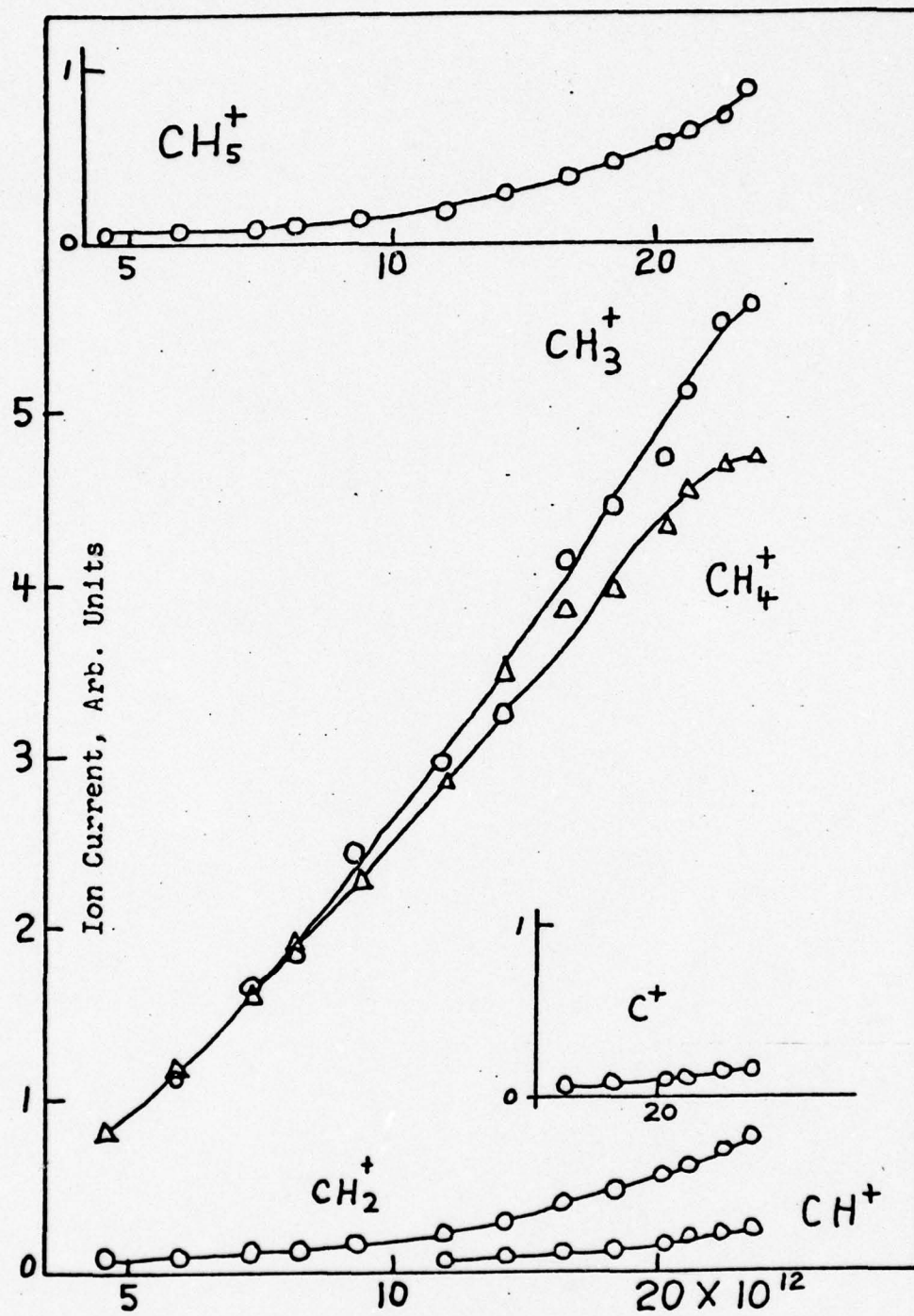
Figure 18. CH_5^+, CH_4^+, CH_3^+, CH_2^+, CH^+, and C^+, Currents versus Concentration of CH_4 at $\lambda = 765$ Å.
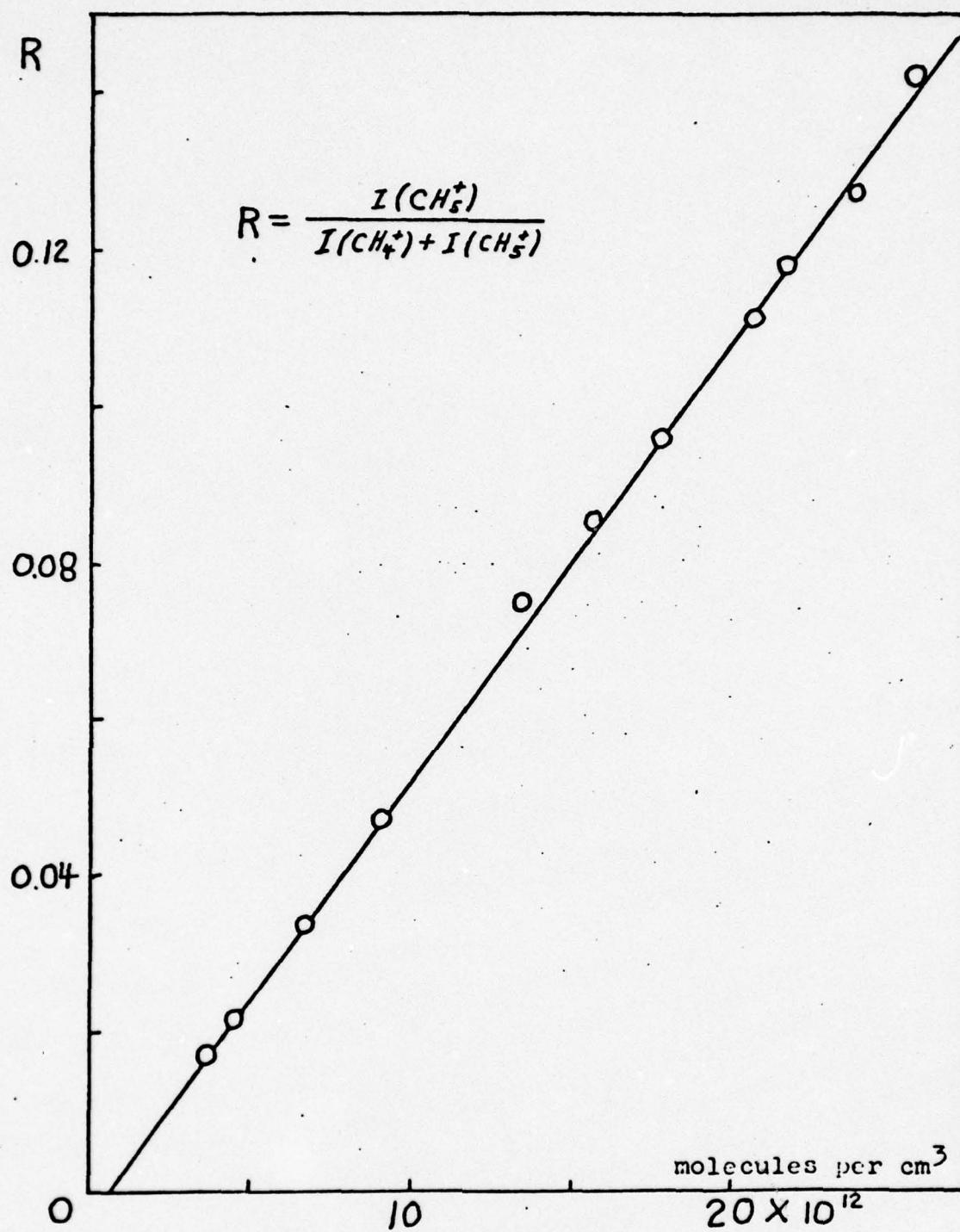
Figure 19. Ion Ratio R versus CH_4 Concentration for
$CH_4^+ + CH_4 \rightarrow CH_5^+ + CH_3$ at λ = 765 Å.
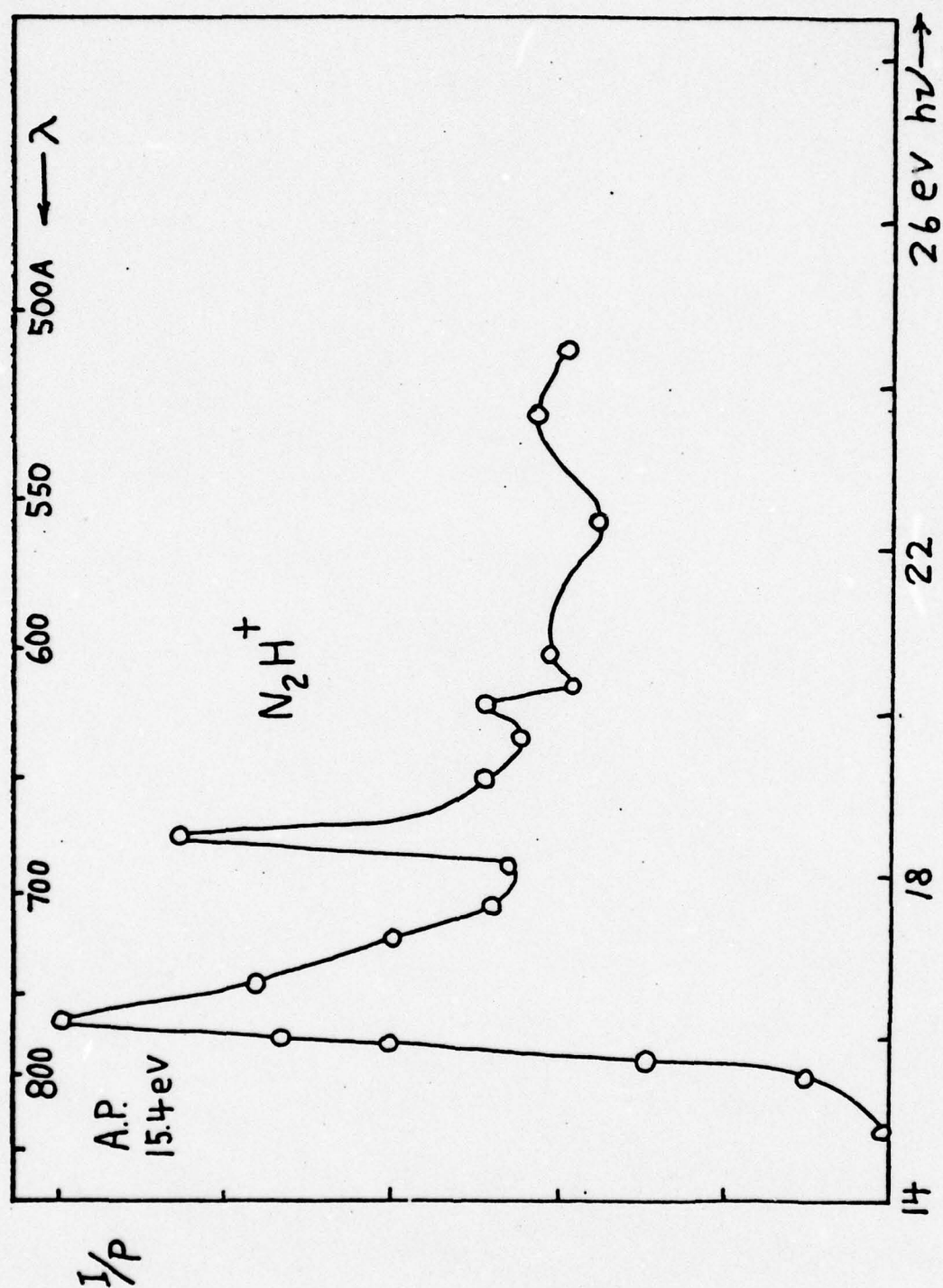
Figure 20. N_2H^+ current per unit photon flux versus wavelength.
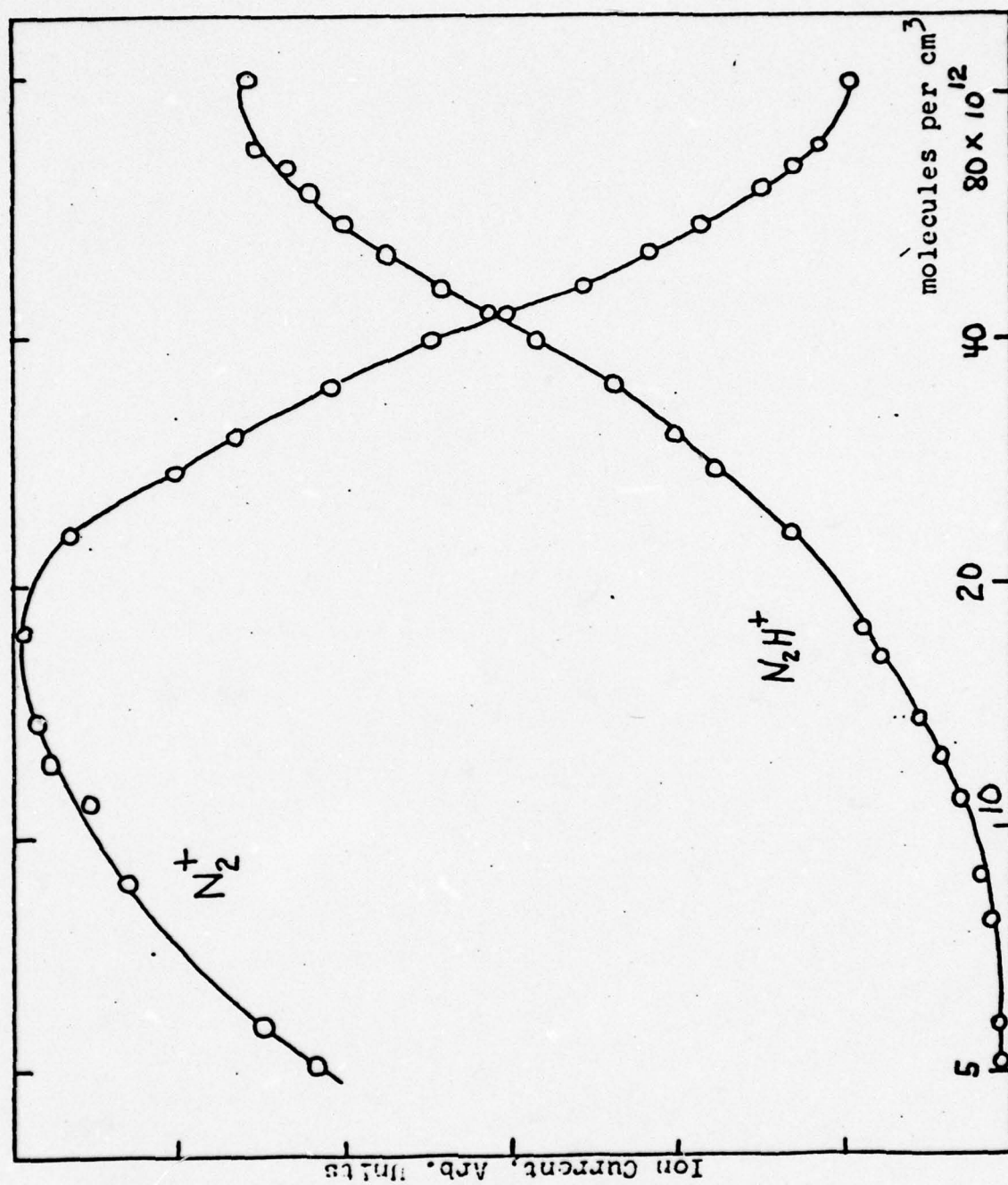
Figure 21. N_2^+ and N_2H^+ Currents versus Concentration at $\lambda = 765$ Å.
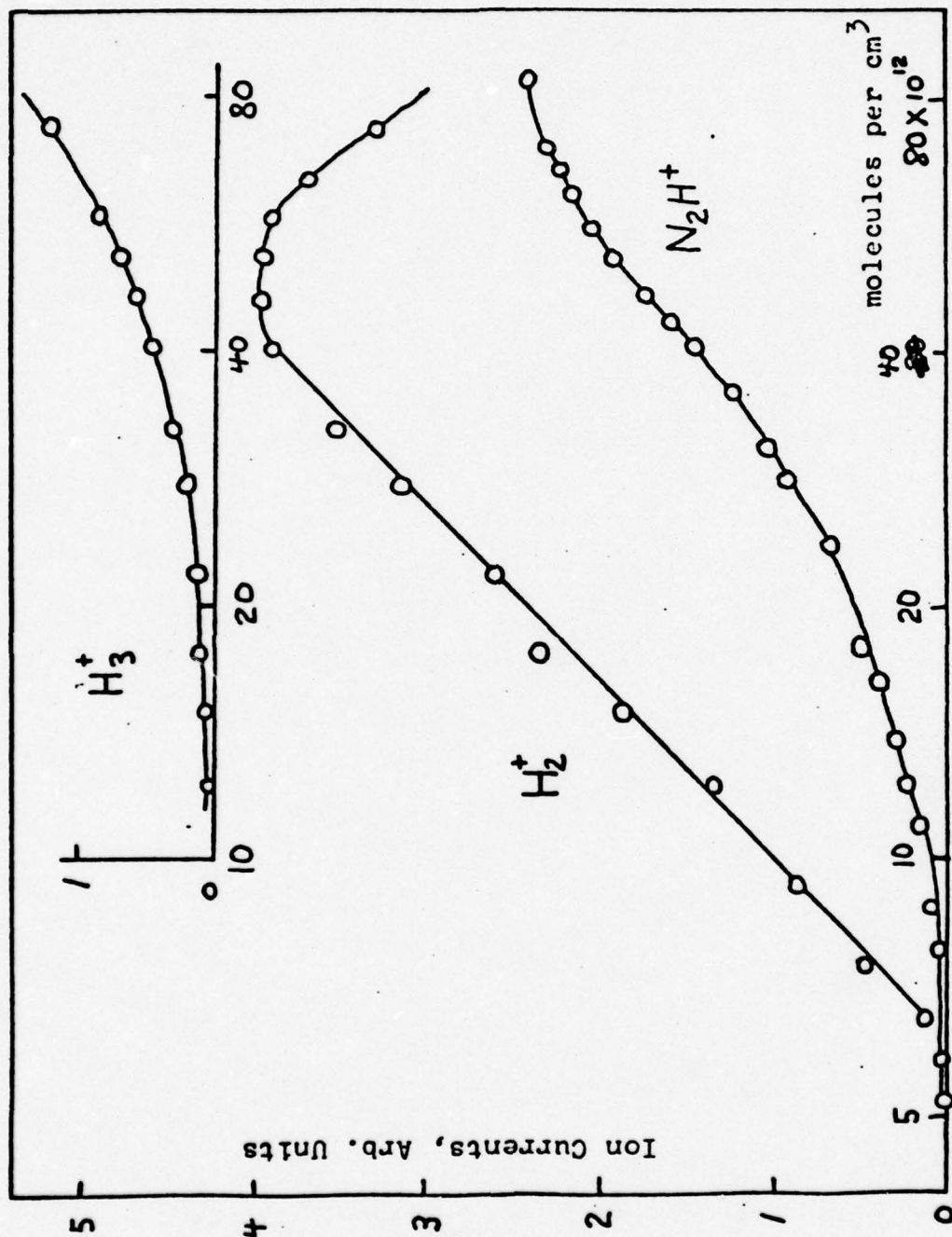
Figure 22. H_2^+, H_3^+, and N_2H^+ currents versus total concentration of N_2 and H_2 at λ = 765Å.
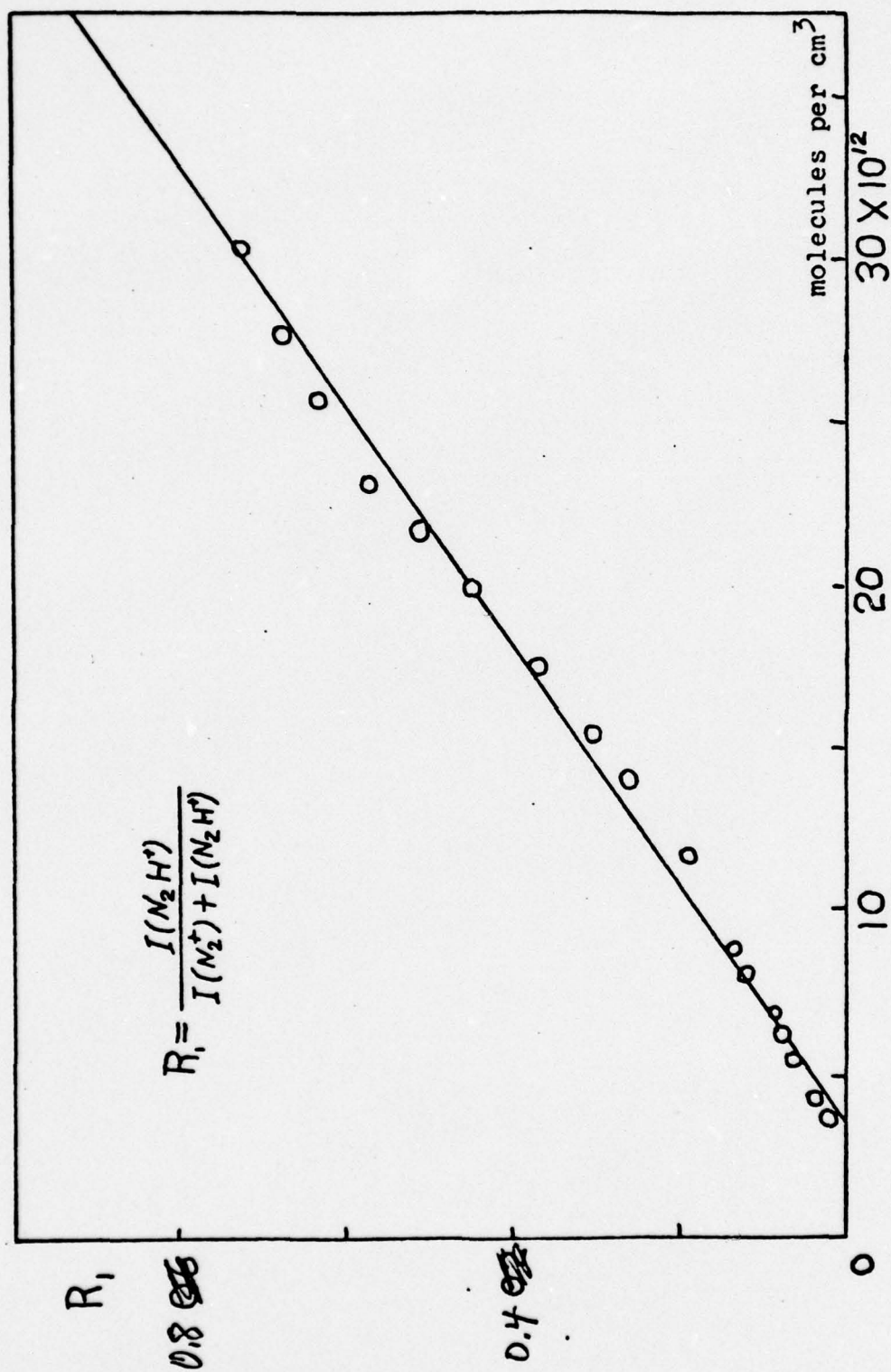
Figure 23. Ion ratio R versus H_2 concentration for

$N_2^+ + H_2 \longrightarrow N_2H^+ + H$ at $\lambda = 765A$.

$$R_2 = \frac{I(N_2H^+)}{I(H_2^+) + I(N_2H^+)}$$

molecules per cm^3

20 X 10^{12}
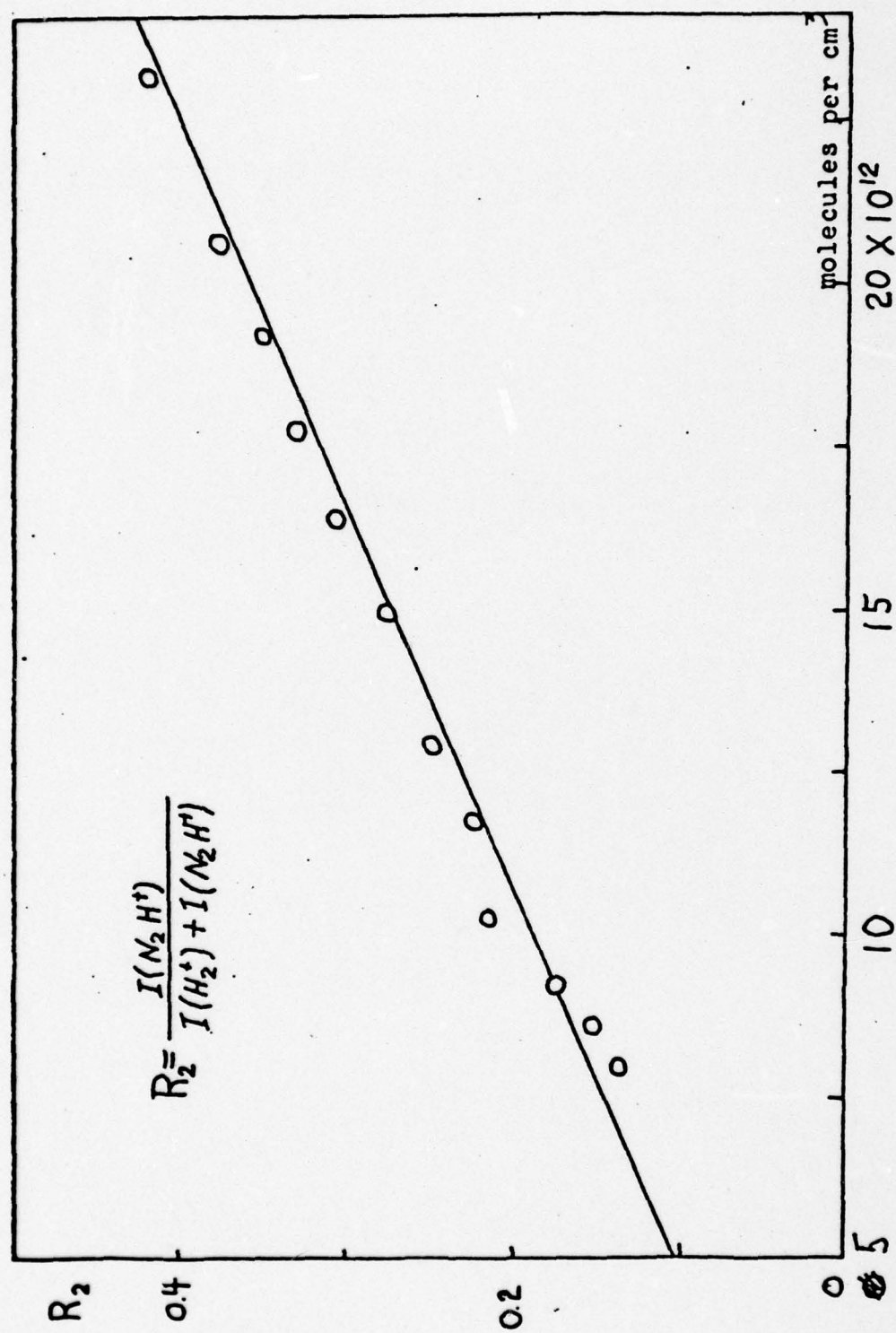
Figure 24. Ion ratio R versus N_2 Concentration for
$N_2 + H_2^+ \rightarrow N_2H^+ + H$ at $\lambda = 765$ Å.
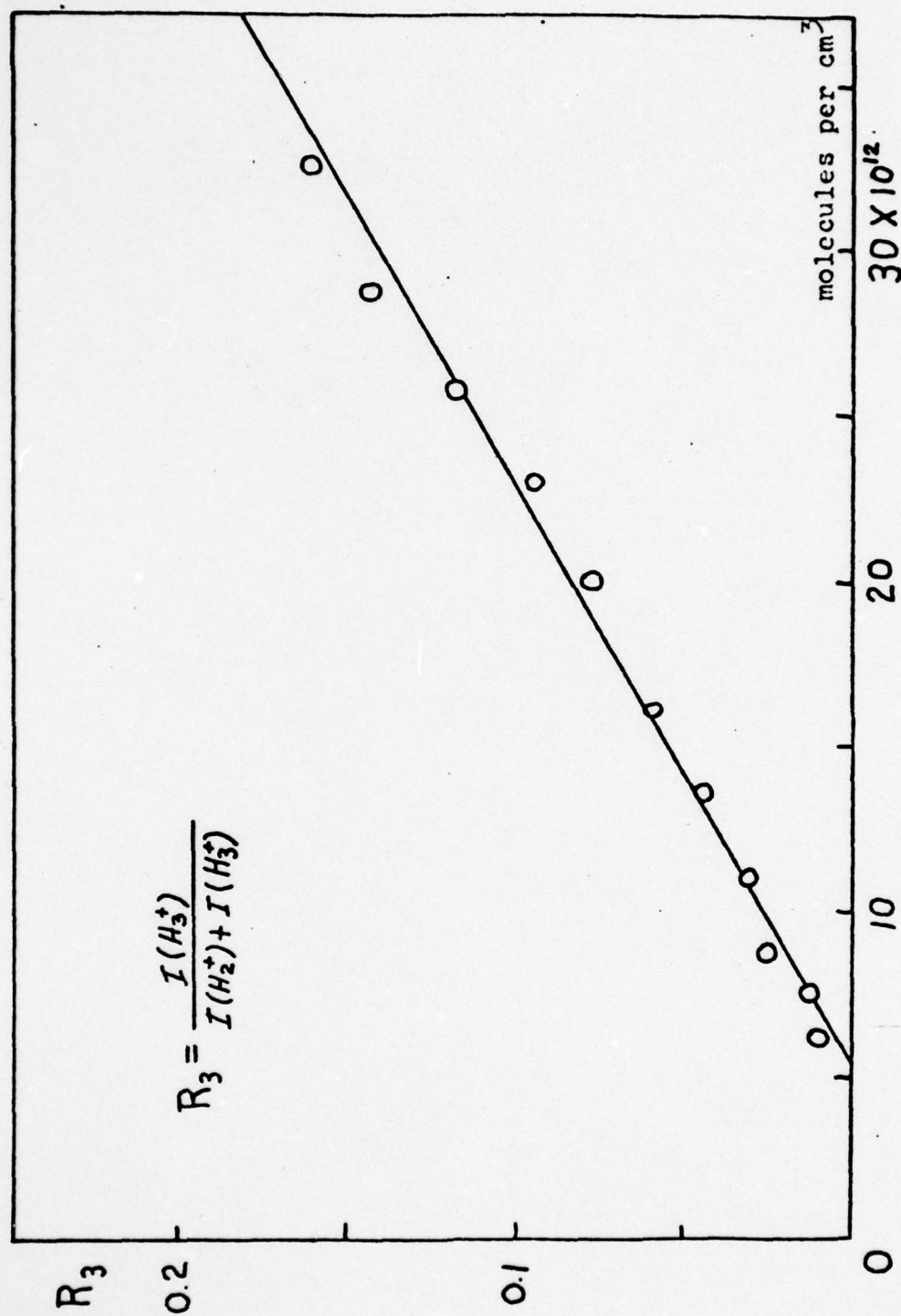
Figure 25. Ion ratio R versus H_2 concentration for
$H_2^+ + H_2 \longrightarrow H_3^+ + H$ in a mixture of N_2 and H_2 at $\lambda = 765A$.

TABLE II

SUMMARY OF EXPERIMENTAL RESULTS

I. Photoionization Potentials

Molecule	Energy ev	Type
H_2	15.4 ± 0.3	—
CH_4	13.3 ± 0.3	IP_1
CH_4	18	IP_2

II. Dissociative Ionization Processes

Ion	Energy ev	Reaction
H^+	18.0 ± 0.5	$H_2 + h\nu \longrightarrow H_2^+ \longrightarrow H^+ + H$
CH_3^+	14.4 ± 0.4	$CH_4 + h\nu \longrightarrow CH_4^+ \longrightarrow CH_3^+ + H$

III. Secondary Ion Appearance Potentials

a) Associations

Ion	Energy ev	Reaction
H_3^+	15.4 ± 0.3	$H_2 + H_2^+ \longrightarrow H_3^+ + H$
CH_5^+	13.3 ± 0.3	$CH_4 + CH_4^+ \longrightarrow CH_5^+ + CH_3$
N_2H^+	15.3 ± 0.3	$N_2^+ + H_2 \longrightarrow N_2H^+ + H$

TABLE II   (Continued)

b) Dissociation from Collisions

Ion	Energy ev	Reaction
CH_2^+	13.3 ± 0.3	——
CH^+	14.4 ± 0.4	——
C^+	14.4 ± 0.4	——

IV.   Reaction Rate and Cross Sections

Ion	$Q \times 10^{16}$ cm^2	$k \times 10^9$ cm^3 per molecule sec	$k_t = 2\pi e \sqrt{\dfrac{\alpha}{\mu}} \times 10^9$ cm^3 per molecule sec
H_3^+	170	3.9	2.1
CH_5^+	130	1.6	1.3
N_2H^+	620	6.2	1.5

f) <u>Dissociation into Neutrals and Other Absorption Processes Below 1000 Å</u> [*]

Now, we come to some speculation, as indicated at the beginning, Figure 26 shows in part (a) at the very top the total absorption coefficient in O_2, measured by two very well known and highly competent groups, namely by the late Professor Ken'ichi Watanabe and his student Matsunaga at the University of Hawaii (labelled M), and by Drs. Gilbert R. Cook and Masaru Ogawa (identified by open circles). The curves in the middle, (b), by the same two groups, represent measurements of the total photoionization by all possible mechanisms. The differences in the coefficients in both (a) and (b) are obvious. However, it is really astounding, when these differences, $k_d = k - k_i$, in the observed values of these two groups are plotted, as in the bottom part, (c), of Fig. 26. Not only is the difference coefficient, k_d, very substantial for each group, but the trends of k_d versus λ are the same for both, and both groups differ drastically in the absolute value of this difference coefficient, in some instances by as much as a factor of two or more.

These difference curves in (c), which extend over the wavelength region of the ionization continuum in oxygen, are thought to represent a photodissociation process. The plausibility of this if further supported by the different dissociation limits of O_2, D_7 to D_{18}, indicated by vertical bars in Fig. 26(c). While these absorption transitions have not been specifically indicated earlier, say in Fig. 2, they clearly correspond to the lifting of an electron to a neutral state, either Rydberg or non-Rydberg or repulsive, which in this example of O_2 lies in energy above the first ionization limit of 1040 Å (other ionization limits of O_2 are shown as vertical bars IP_2 to IP_5 in Fig. 26 (b)).

As already mentioned, the differences in k_d by two otherwise highly regarded experimental groups obviously are unacceptable and necessitate the

[*][105,108] {50,55,56}
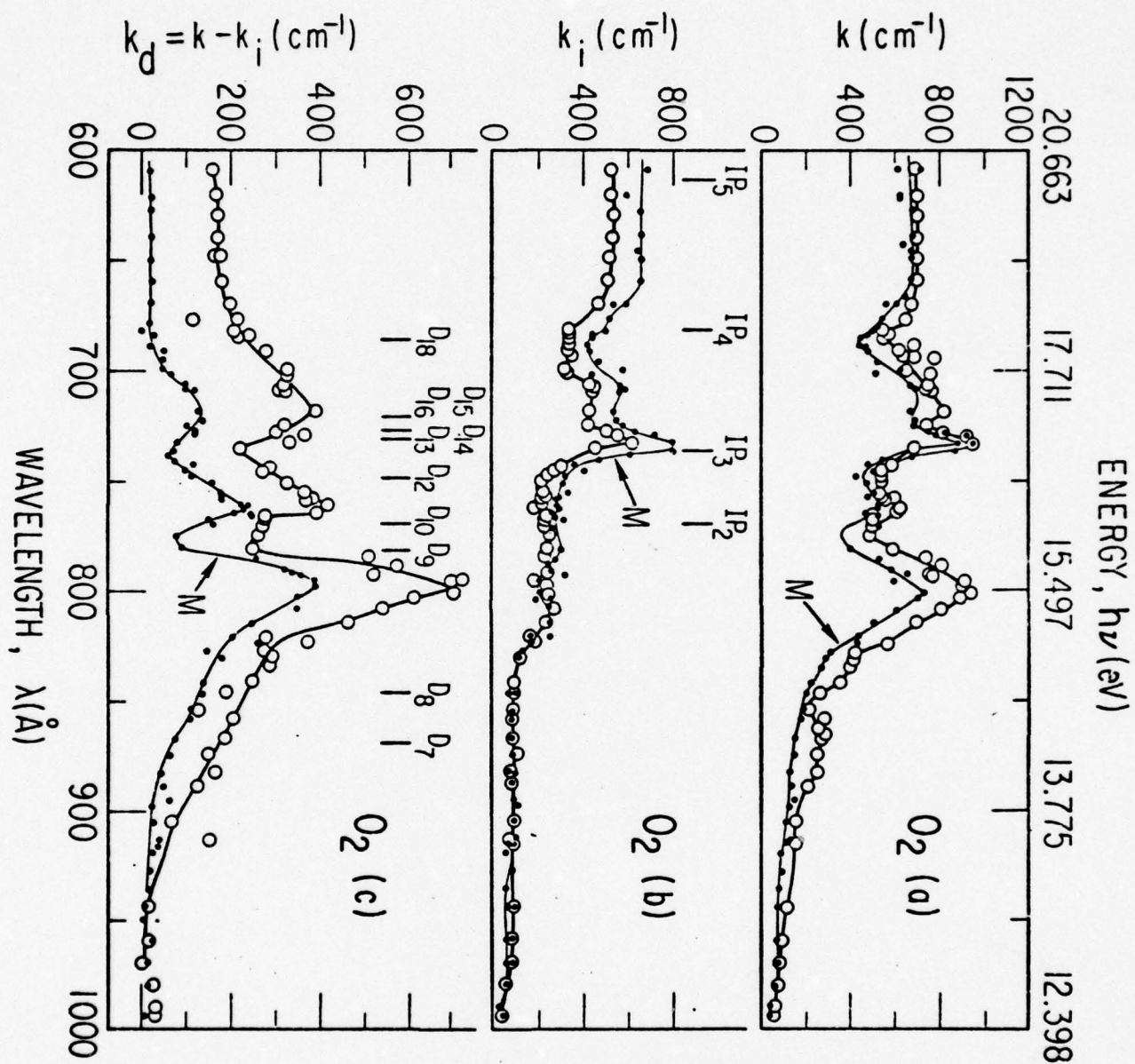
Fig. 26. O_2, Total Absorption Coefficients, k, in (a), Photoionization k_i in (b), and the Difference Coefficient, $k_d = k - k_i$, in (c).

development of new and better measurement techniques.

Again, in Fig. 27, Cook and Ogawa have plotted the difference coefficient, $k_d=k-k_i$, for H_2 in the upper half and for N_2 in the lower half of the figure. As before, ionization limits are labelled IP and dissociation by D. The reality of k_d is perhaps best born out by the fact that it goes to zero in H_2 towards shorter wavelengths.

In Table III, Professor M. Ogawa has compiled a list of electronic states in N_2 and their corresponding dissociation limits. It is interesting to note there that the neutral products from D_2 onward have either one or both atoms in a metastable state. Thus, to continue our speculation, it seems quite feasible to measure dissociation coefficients resulting in metastables by yet another method than the one indicated above ($k_d=k-k_i$), namely by making use of metastable detectors developed by Dr. Homer Hagstrum. In this case, a metastable impinging on a surface may release an electron, if the work function is lower than the energy of the metastable level.

By utilizing a repetitive low-pressure capillary spark source, which provides vacuum ultraviolet radiation during a time interval of say 1 to 5 microseconds, it should be possible to collect all ions and electrons formed by photoionization processes during and immediately following the light pulse. Then one allows all neutrals, including metastables, to drift towards Hagstrum-type detectors, where the resulting electron pulse is a direct measure of the metastables produced. In addition, these electrons could be energy-analyzed, and/or the Hagstrum detecting surfaces could be chosen to have different work functions, say by cesiating. Either or both procedures would allow us to differentiate between metastable levels of different energies. In this way, it should again be possible to obtain photodissociation cross sections for the formation of specific metastable species.
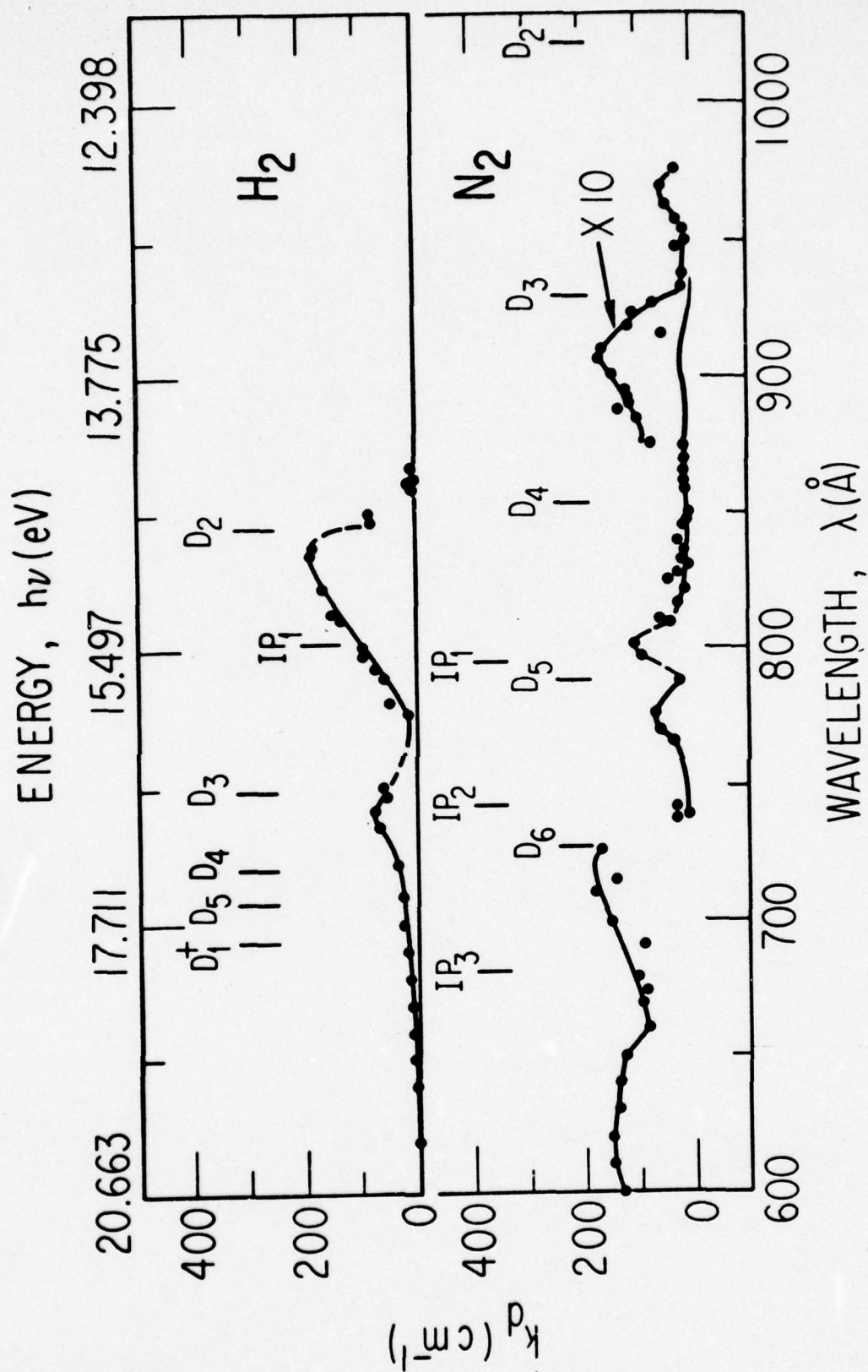
Fig. 27. The Difference Coefficient, $kd=k-k_i$, in H_2 (top) and N_2 (bottom).

Table III. Electronic states and their dissociation limits, N_2

Limits	Products $N+N$	Energy (eV) (λ in Å)	Electronic States
D_1	$2p^3\,{}^4S_u + 2p^3\,{}^4S_u$	9.756 (1270.7Å)	$X\,{}^1\Sigma_g^+,\ A\,{}^3\Sigma_u^+,\ {}^5\Sigma_g^+,\ {}^1\Sigma_u^-$
D_2	$2p^3\,{}^4S_u + 2p^3\,{}^2D_u$	12.140 (1021.2)	${}^3\Sigma_g^+,\ {}^3\Sigma_u^+,\ B\,{}^3\Pi_g,\ {}^3\Pi_u,\ {}^3\Delta_g,\ {}^3\Delta_u,\ {}^5\Sigma_g^+,\ {}^5\Sigma_u^+,\ {}^5\Pi_g,\ {}^5\Pi_u,\ {}^5\Delta_g,\ {}^5\Delta_u$
D_3	$2p^3\,{}^4S_u + 2p^3\,{}^2P_u$	13.332 (929.9)	${}^3\Sigma_g^-,\ B'^3\Sigma_u^-,\ {}^3\Pi_g,\ {}^3\Pi_u,\ {}^5\Sigma_g^-,\ {}^5\Sigma_u^-,\ {}^5\Pi_g,\ {}^5\Pi_u$
D_4	$2p^3\,{}^2D_u + 2p^3\,{}^2D_u$	14.524 (853.6)	${}^1\Sigma_g^+(3),\ a'^1\Sigma_u^-,\ {}^1\Sigma_u^-,\ a^1\Pi_g,\ {}^1\Pi_g,\ {}^1\Pi_u(2),\ {}^1\Delta_g(2),\ w^1\Delta_u,\ {}^1\Phi_g,\ {}^1\Phi_u,\ {}^1\Gamma_g,\ {}^3\Sigma_g^+(3),\ {}^3\Sigma_u^+(2),\ {}^3\Pi_u(2),\ {}^3\Pi_g(2),\ {}^3\Delta_u(2),\ {}^3\Delta_g,\ {}^3\Phi_u,\ {}^3\Phi_g,\ {}^3\Gamma_u$
D_5	$2p^3\,{}^2D_u + 2p^3\,{}^2P_u$	15.718 (788.8)	${}^1\Sigma_g^+,\ {}^1\Sigma_u^+,\ {}^1\Sigma_g^-(2),\ {}^1\Sigma_u^-(2),\ {}^1\Pi_g(3),\ {}^1\Pi_u(3),\ {}^1\Delta_g(2),\ {}^1\Delta_u(2),\ {}^1\Phi_g,\ {}^1\Phi_u,\ {}^3\Sigma_g^+,\ {}^3\Sigma_u^+,\ {}^3\Sigma_g^-(2),\ {}^3\Sigma_u^-(2),\ {}^3\Pi_g(3),\ {}^3\Pi_u(3),\ {}^3\Delta_g(2),\ {}^3\Delta_u(2),\ {}^3\Phi_g,\ {}^3\Phi_u$
D_6	$2p^3\,{}^2P_u + 2p^3\,{}^2P_u$	16.906 (733.8)	${}^1\Sigma_g^+(2),\ {}^1\Sigma_u^-,\ {}^1\Pi_g,\ {}^1\Pi_u,\ {}^1\Delta_g,\ {}^3\Sigma_u^+(2),\ {}^3\Sigma_g^-,\ {}^3\Pi_g,\ {}^3\Pi_u,\ {}^3\Delta_u$
D_7	$2p^3\,{}^4S_u + 3s\,{}^4P_g$	20.082 (617.4)	${}^1\Sigma_g^-,\ {}^1\Sigma_u^+,\ {}^1\Pi_g,\ {}^1\Pi_u,\ E\,{}^3\Sigma_g^+,\ {}^3\Sigma_u^+,\ {}^3\Pi_g,\ C^3\Pi_u,\ {}^5\Sigma_g^+,\ {}^5\Sigma_u^+,\ {}^5\Pi_g,\ {}^5\Pi_u,\ {}^7\Sigma_g^+,\ {}^7\Sigma_u^+,\ {}^7\Pi_g,\ {}^7\Pi_u$
D_8	$2p^3\,{}^4S_u + 3s\,{}^2P_g$	20.434 (606.7)	${}^3\Sigma_g^+,\ {}^3\Sigma_u^+,\ {}^3\Pi_g,\ {}^3\Pi_u,\ {}^5\Sigma_g^+,\ {}^5\Sigma_u^+,\ {}^5\Pi_g,\ {}^5\Pi_u$
	$N+N^+$		
D_1^+	$2p^3\,{}^4S_u + 2p^2\,{}^3P_g$	24.304 (510.2)	$X^2\Sigma_g^+,\ B^2\Sigma_u^+,\ D^2\Pi_g,\ A^2\Pi_u,\ {}^4\Sigma_g^+,\ {}^4\Sigma_u^+,\ {}^4\Pi_g,\ {}^4\Pi_u,\ {}^6\Sigma_g^+,\ {}^6\Sigma_u^+,\ {}^6\Pi_g,\ {}^6\Pi_u$
D_2^+	$2p^3\,{}^4S_u + 2p^2\,{}^1D_g$	26.203 (473.1)	${}^4\Sigma_g^-,\ {}^4\Sigma_u^-,\ {}^4\Pi_g,\ {}^4\Pi_u,\ {}^4\Delta_g,\ {}^4\Delta_u$
D_3^+	$2p^3\,{}^2D_u + 2p^2\,{}^3P_g$	26.688 (465.0)	${}^2\Sigma_g^+(2),\ {}^2\Sigma_u^+(2),\ {}^2\Sigma_g^-,\ {}^2\Sigma_u^-,\ {}^2\Pi_g(3),\ {}^2\Pi_u(3),\ {}^2\Delta_g(2),\ {}^2\Delta_u(2),\ {}^2\Phi_g,\ {}^2\Phi_u,\ {}^4\Sigma_g^+(2),\ {}^4\Sigma_u^+(2),\ {}^4\Sigma_g^-,\ {}^4\Sigma_u^-,\ {}^4\Pi_g(3),\ {}^4\Pi_u(3),\ {}^4\Delta_g(2),\ {}^4\Delta_u(2),\ {}^4\Phi_g,\ {}^4\Phi_u$

A third way of detecting atomic dissociation products has been suggested by our colleague, Professor Darrell L. Judge at U.S.C. He proposes to make use of the very strong absorption of resonance lines as a sensitive detector: for instance, the absorption of Ly-α (1215 Å) by atomic hydrogen.

One might conclude this particular section by referring to absorption measurements of atomic vapors by heating certain metals in King furnaces or other electric ovens, or more recently by producing reasonably high density atomic and ionic beams. When one extends this to ovens of very high temperatures, we make the transition to my last subject, namely the absorption and emission properties of hot gaseous plasmas.

g) Plasma Spectroscopy [68,84,85,96,101-104,108-125]

The applications of hot gaseous plasmas to problems of photoionization go back to Millikan's vacuum spark or Lyman's low-pressure capillary spark as light sources in this field. I wish to limit this discussion to quantitative emission and absorption properties of those specific plasmas, which can be shown to be in Local Thermodynamic Equilibrium (L.T.E.). This condition of L.T.E. is crucial, since the eventual calculation of number densities of certain species (singly-and/or doubly ionized or neutral atoms or radicals) depends on it. In particular, two types of highly ionized plasmas have been shown to be in L.T.E., those produced in low-pressure shock tubes [51-68] and in high-current wall-stabilized arcs. (In addition, partial equilibrium has been shown to exist in magnetically stabilized low pressure discharges, such as the Philips-type d.c. discharge or the thetapinch impulse discharge.)

1) Shock Tube Plasmas [51,68]

Because of the fact that Tee-type or Cone-type shock tubes can be driven by high voltage condenser discharges at relatively low neutral gas pressure (of the order of 10-50 mm Hg), we guessed that it would be easier to couple such a low pressure shock tube to our vacuum spectrographs. Such a mating, with appropriate differential pumping, would then allow us to study the absorption properties of certain constituents present in calculable number-densities in the high temperature shock tube plasma. Our experimental arrangement is shown in Fig. 28, where the Tee-tube S is placed in front of the primary slit of a normal incidence vacuum spectrograph-monochromator. Two 1 mm diameter holes were drilled into the quartz envelope of the shock tube, alligned with the optic axis (dashed line), and a light source could shine radiation through the shock plasma (if both were properly triggered by the photomultipliers PM1 and PM3). We used Xenon gas for the convenience of the experimentalist: The thresholds of the photoionization continua of the neutral and the ion can both be probed conveniently with a normal incidence vacuum spectrograph since

$$(1) \quad Xe + h\nu \xrightarrow{\sigma} Xe^+ + e^- \qquad \begin{aligned} IP_1 &= 12.127 \text{ eV} \\ \lambda_1 &= 1022 \text{ Å} \end{aligned}$$

and

$$(2) \quad Xe^+ + h\nu \xrightarrow{\sigma^+} Xe^{++} + e^- \qquad \begin{aligned} IP_2 &= 21.2 \text{ eV} \\ \lambda_2 &= 584 \text{ Å} \end{aligned}$$

The photoionization cross section σ of neutral Xenon was measured in the cold gas, using the arrangement in Fig. 28, and the results are shown in Fig. 29. (The rapid variation of σ in the autoionization region between the
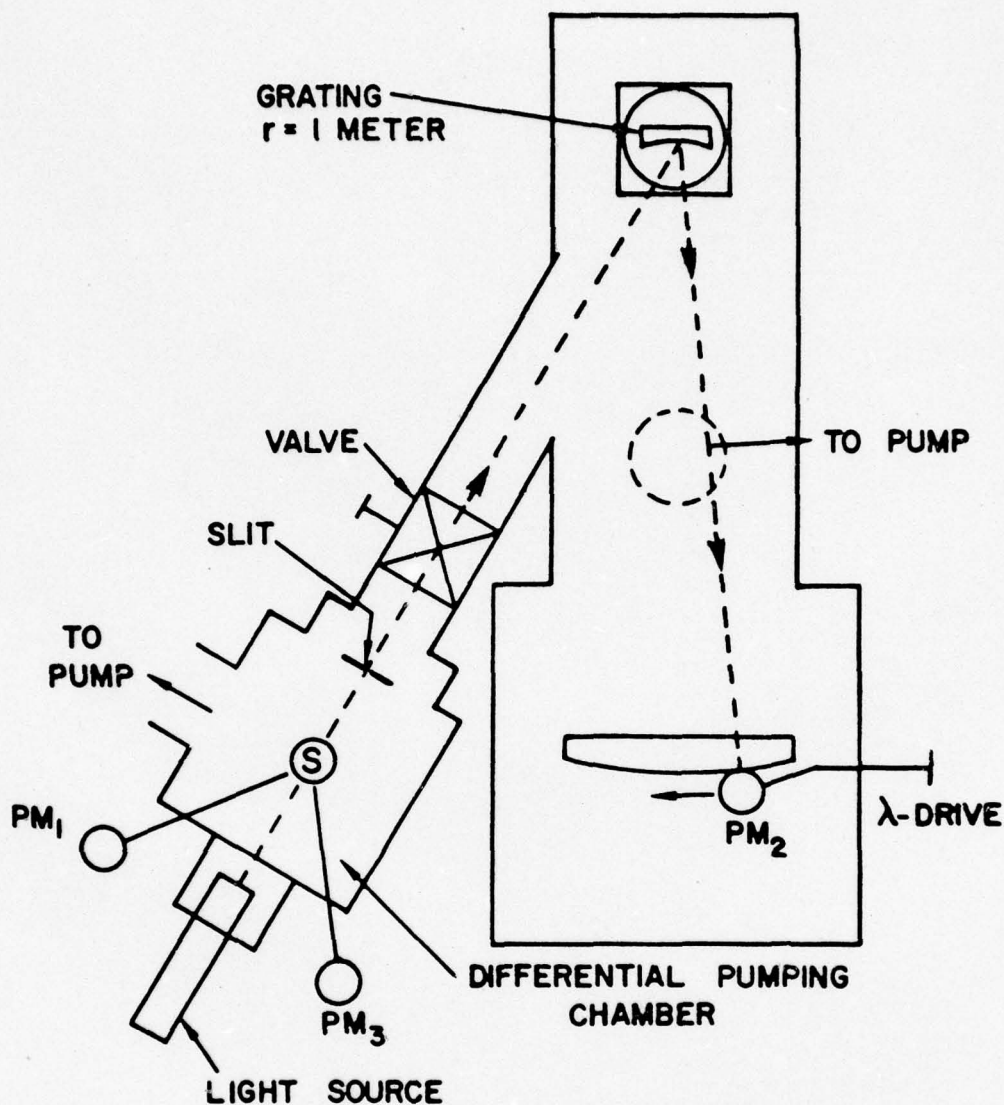
Figure 28. Arrangement of vacuum spectrograph, light source and shock tube. (S) denotes the position of the shock tube. The axis of the long arm of this tube (see Fig. 5) is perpendicular to the plane of the paper.
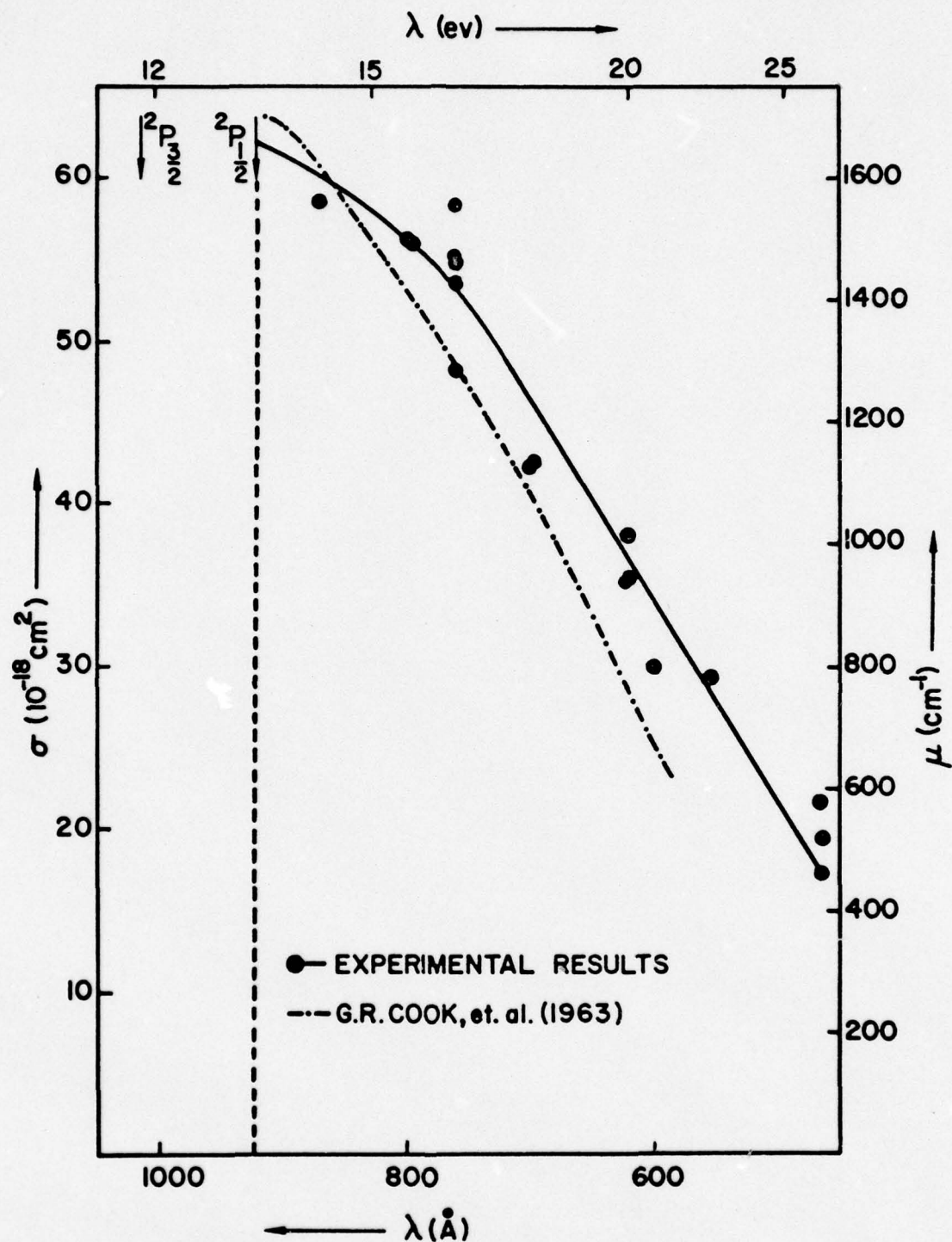
Figure 29. Photoionization cross section of neutral xenon.

$2p_{3/2}$- and the $2p_{1/2}$- limits due to broad autoionization lines has not been shown there.)

If then the shock tube is activated and a high temperature Xenon plasma is generated on the optic axis (Fig. 28), then one would expect the two wavelengths emitted by the light source, namely $\lambda_1 = 760$ Å and $\lambda_2 = 555$ Å, to be attenuated differently by the cold gas and by the hot Xenon plasma, as inspection of Fig. 30 will show.

In this manner, it was possible to obtain values for the cross section σ^+ in the above eq. (2), and its magnitude is also shown in Fig. 30. The large error limit on these data permit us to neglect any serious falsification due to transitions from metastable states into the corresponding continuum:

$$X_e^M + h\nu \xrightarrow{\sigma^M} Xe^+ + e^- ,$$

and

$$Xe^{+M} + h\nu \xrightarrow{\sigma^{+M}} Xe^{++} + e^- .$$
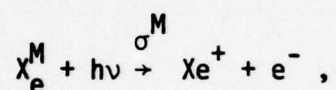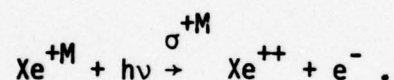
While such shock tube plasmas could be made to serve some of our purposes, their plasmas variability in time suggested to us that the time-independent, stable high-current arcs would be more suitable to our plasma absorption and emission work.
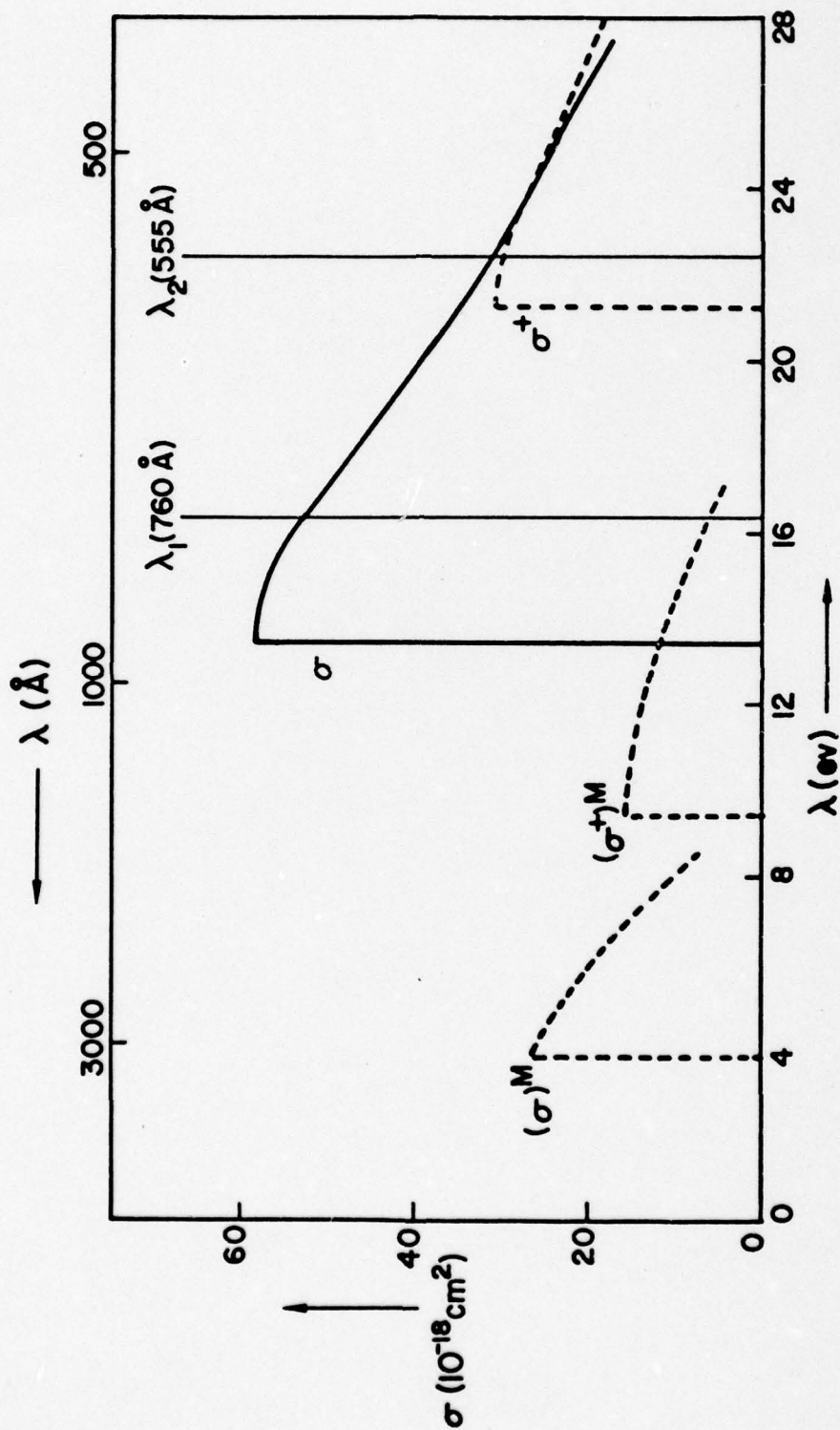
Figure 30. Photoionization cross sections for the xenon atom and ion. The curves σ and σ^+ correspond to transitions from the ground states of the atom and ion into their respective continua. $(\sigma)^M$ and $(\sigma^+)^M$ represent photoionization from the first metastable state of the excited xenon atom and ion.

2) High Current DC Arc Plasmas [84,101,102,106,108-125]

The principal equations which govern a plasma in L.T.E. are, for instance in the case of a pure argon arc, given by the conditions that the net charge in such a plasma is zero:

$$n_{Ar}^{+} = n_e^{-} , \quad \text{(charge neutrality)}$$

that the partial pressures are additive:

$$n_{Ar} + n_{Ar}^+ + n_e^- = p/kT, \quad \text{(Dalton's law)}$$

and that the condition of L.T.E. justifies the Saha-Boltzmann-type of particle distribution as a function of the temperature $S(T)$:

$$(n_{Ar}^+ + n_e^-)/n_{Ar} = S_{Ar}(T). \quad \text{(Saha equation)}$$

In addition, one can make use of the fact that most plasmas contain trace elements of hydrogen, and therefore it is possible to measure the width of the Stark-broadened Balmer line, say H-β, and determine from this the electron density, n_e^-:

$$n_e^- = \beta(\Delta\lambda)^{3/2}. \quad \text{(Stark broadening) electron density, } n_e^-:$$

Finally, measurements of intensity ratios of spectral lines provide alternate ways of determining the temperature.

Between all of these equations, the temperature and the density of each of the particles present can be obtained.

If such an arc is used with its axis coincident with the optical axis of a spectrograph, then the arc plasma emission intensity, $I_\lambda(x)$, with x along the direction of observation, is

$$dI_\lambda(x)/dx = \epsilon_\lambda - \tau_\lambda I_\lambda(x),$$

where the emissivity ϵ_λ is proportional to the absorptivity τ_λ, and the Planck function B_λ is the proportionality constant, as required by Kirchhoff's law

$$\epsilon_\lambda = B_\lambda \tau_\lambda.$$

B_λ is the intensity of blackbody radiation, given by

$$B_\lambda = [2hc^2/\lambda^5][\exp(hc/\lambda kT) - 1]^{-1}.$$

Thus

$$dI_\lambda(x)/dx = \tau_\lambda[B_\lambda - I_\lambda(x)].$$

After integration,

$$I_\lambda(1) = B_\lambda + (I_{0\lambda} - B_\lambda) \exp(-\tau_\lambda 1).$$

If there is no external light source to the plasma, then $I_{0\lambda}=0$, and for an arc of length 1:

$$I_\lambda(1) = B_\lambda[1-\exp(-\tau_\lambda 1)].$$

The optically thin case is obtained for small values of $(\tau_\lambda \ell)$:

$$I_\lambda = B_\lambda\tau_\lambda\ell.$$

For large $(\tau_\lambda \ell)$, the plasma is optically thick:

$$I_\lambda = B_\lambda.$$

From these additional equations, one can then obtain values for B_λ for various lines which are optically thick $(\tau\ell>>1)$, together with intensity values of, say a recombination spectrum (the reverse of photoionization) which is optically thin $(\tau\ell>>1)$ and which then finally allows the determination of τ_λ, the absorption coefficient, in units of cm^{-1}, or the cross section σ, in cm^2.

If one employs an external light source, say a vacuum uv low-pressure capillary spark or, for that matter, a second wall-stabilized arc, then one can shine light from this second source through the plasma of the first arc and obtain the number density of one species, say neutral argon in the ground state, from the attenuation of the source radiation at, say, 780 Å. For this wavelength, the absorption coefficient of argon is accurately known. Thus, if the first arc were operated in an atmosphere of helium, which is transparent down to about 500 Å, and if this arc were seeded with a small amount of argon,

Then the number density of argon could be checked in this way with an external light source. This value can then be compared with the one obtained by using the emission intensities of one arc only, together with the equations given above for a plasma in L.T.E.

Figure 31 shows an experimental arrangement in the author's laboratory, which has been used to measure the photoionization cross section, σ_i, of atomic carbon.

$$C + h\nu \overset{(\sigma_i)}{\rightarrow} C^+ + e^-.$$
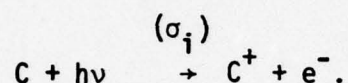
If an argon arc, Fig. 32, was seeded with CO_2 in its central region, then at a temperature of 12,500°K the arc contained only atoms and atomic ions as its sole constituents. As a consequence, C^+ could recombine with free electrons in the plasma with the emission of a photon, and the reverse of the above absorption or photoionization equation could be seen in emission:

$$C^+ + e^- \overset{(I_\lambda)}{\rightarrow} C + h\nu.$$
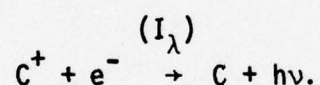
Thus, the optically thin intensity of this recombination spectrum was measured as a function of λ, and the corresponding σ_i values obtained by these methods compared well with independent theoretically calculated carbon photoionization cross sections, Fig.'s 33 and 34.
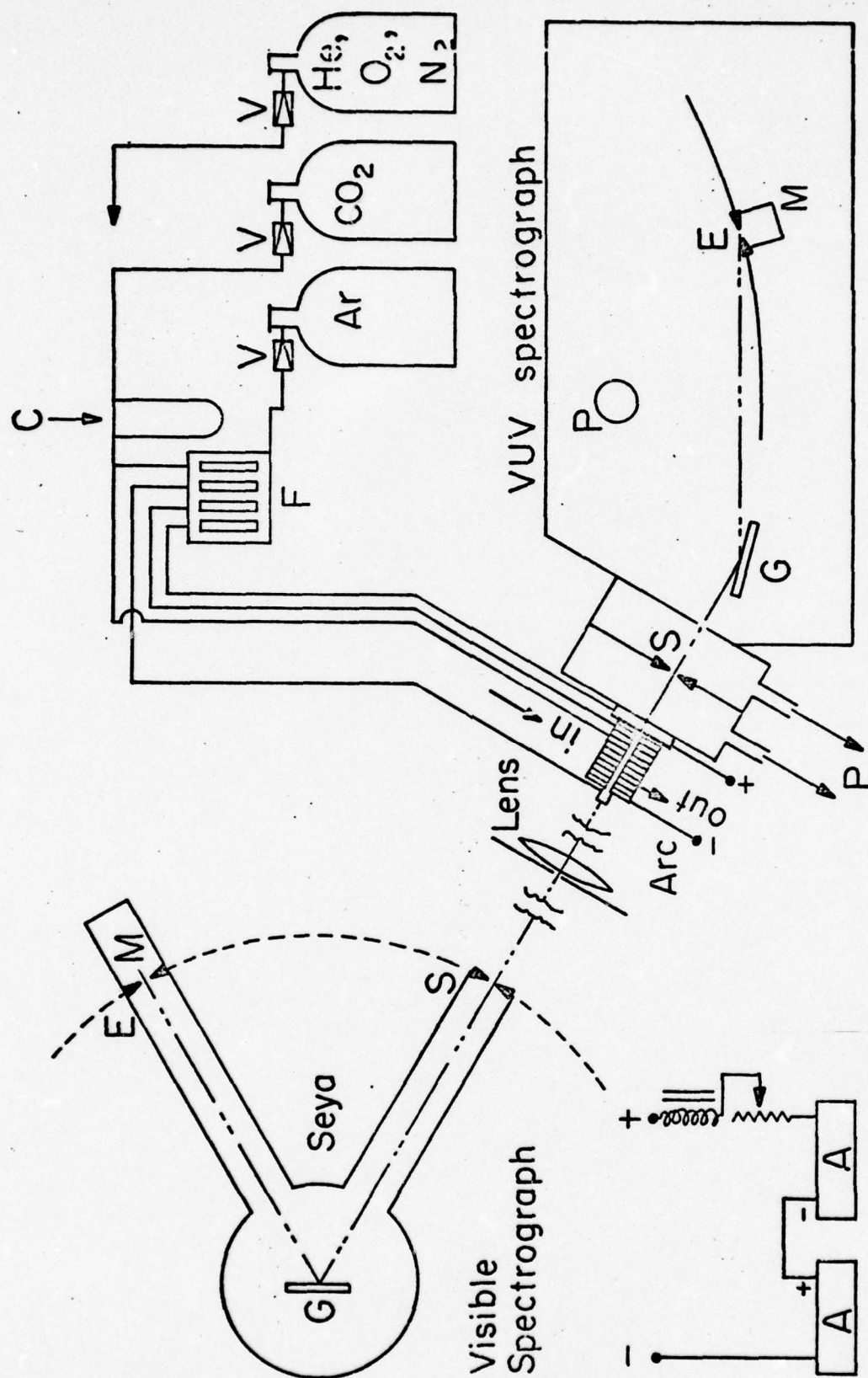
Fig. 31. Experimental arrangement. The light from the arc is viewed axially by a grazing incidence vacuum uv spectrograph and, in the visible region via a lens, by a Seya monochromator. Two power supplies, A, maintain the arc. The primary slits, gratings, exit slits, and photomultiplier detectors are marked by S, G, E, and M, respectively. Pumps are indicated by P. The various gases flow through valves V and flowmeters F into the arc. C represents the capillary flowmeter for small rates of flow.

58.
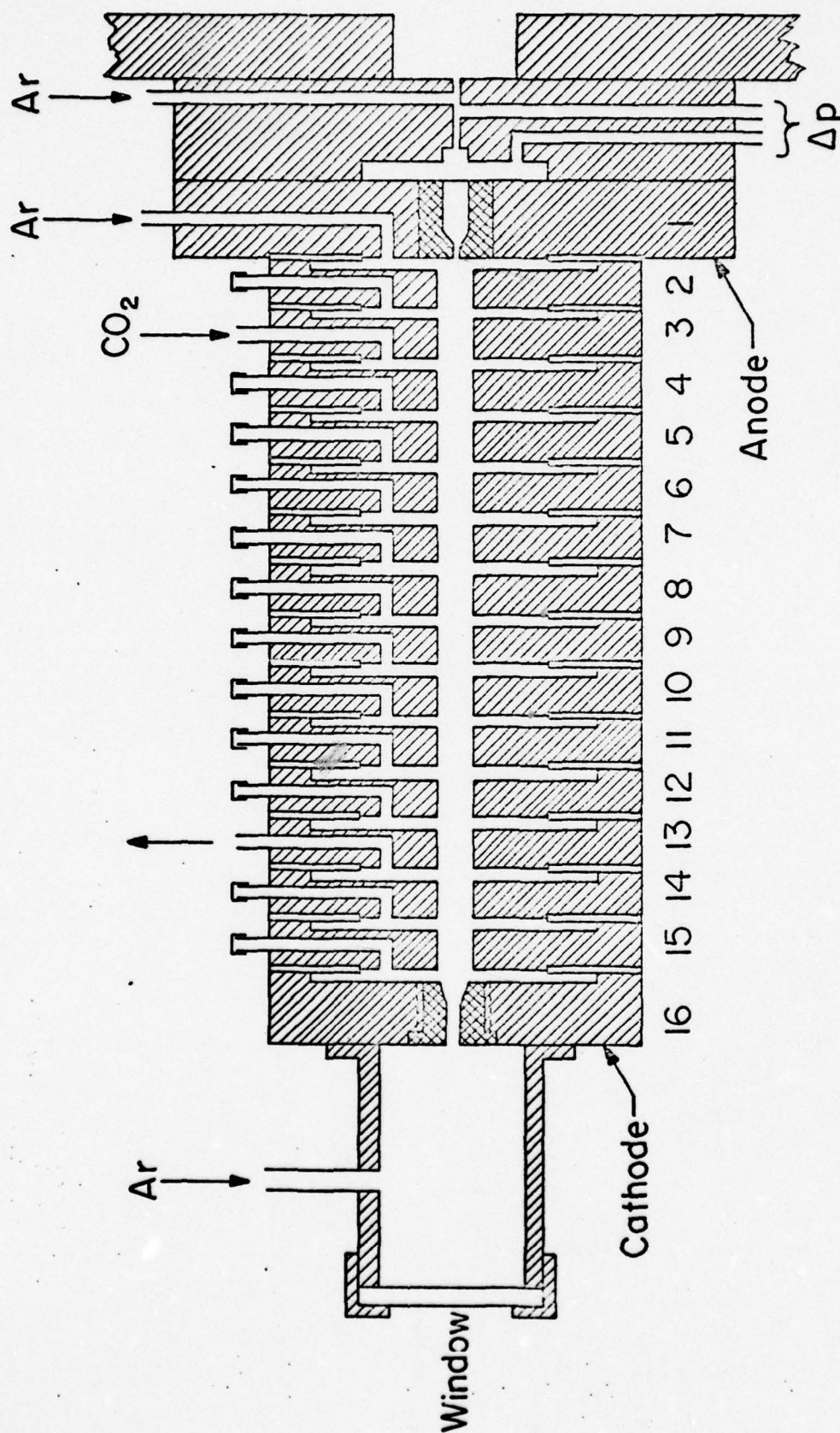
Fig. 32. The wall-stabilized arc. The anode and the cathode are tungsten inserts, cross-hatched areas, into the copper discs numbered 1 and 16, respectively. The other copper discs, 2 to 15, are electrically floating and show gas connections. Their water cooling is not shown.
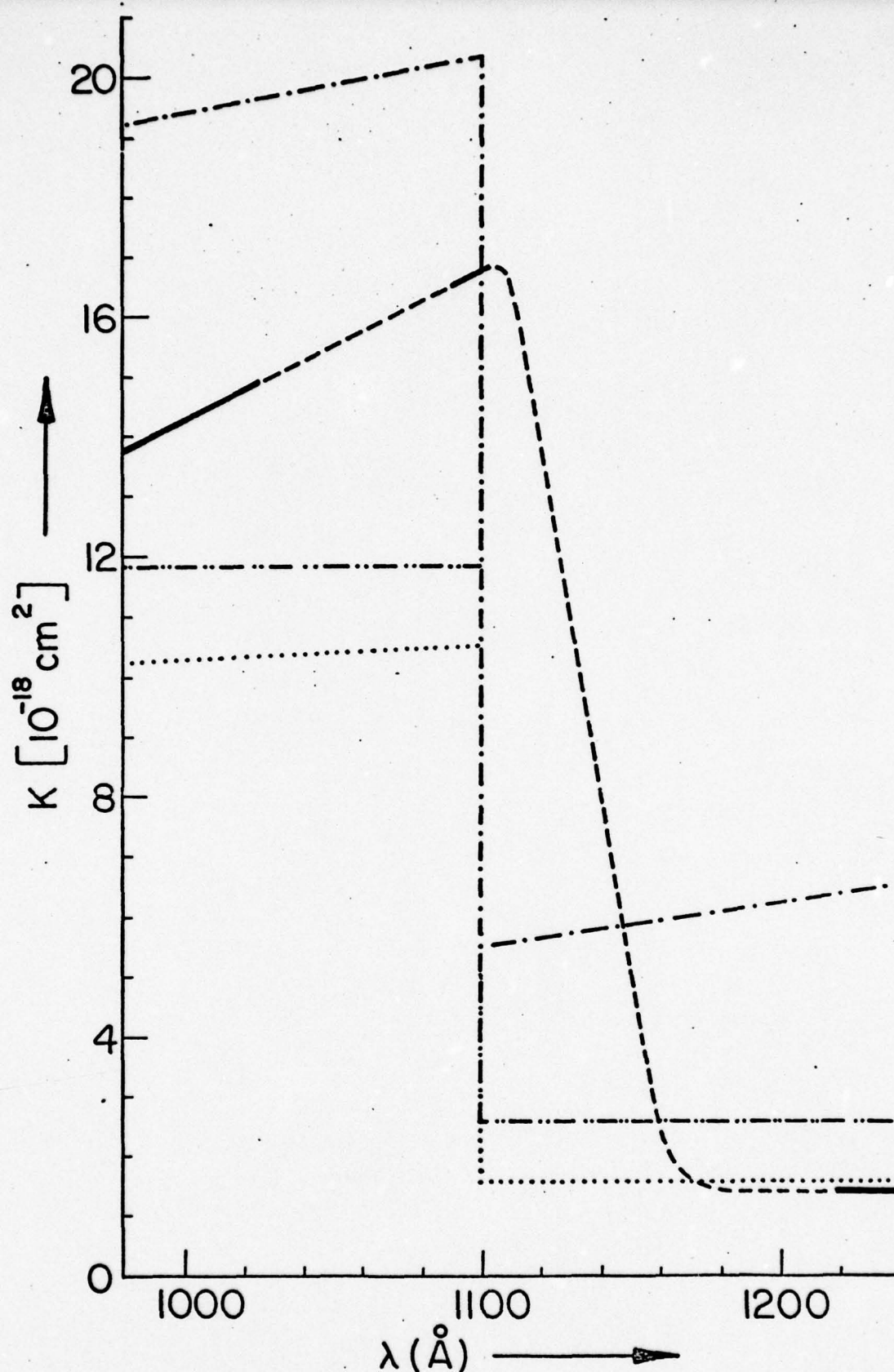
Fig. 33. Absorption cross section, K_λ, per neutral C atom for a plasma temperature of 12 500 K. The theoretical curves of Peach, ref. 12 and dotted line, Praderie, ref. 9 and dot-dash line, and Wilson and Nicolet, ref. 10 and dash-double dot-dash line, can be compared with experimental values, shown by the heavy, continuous lines.
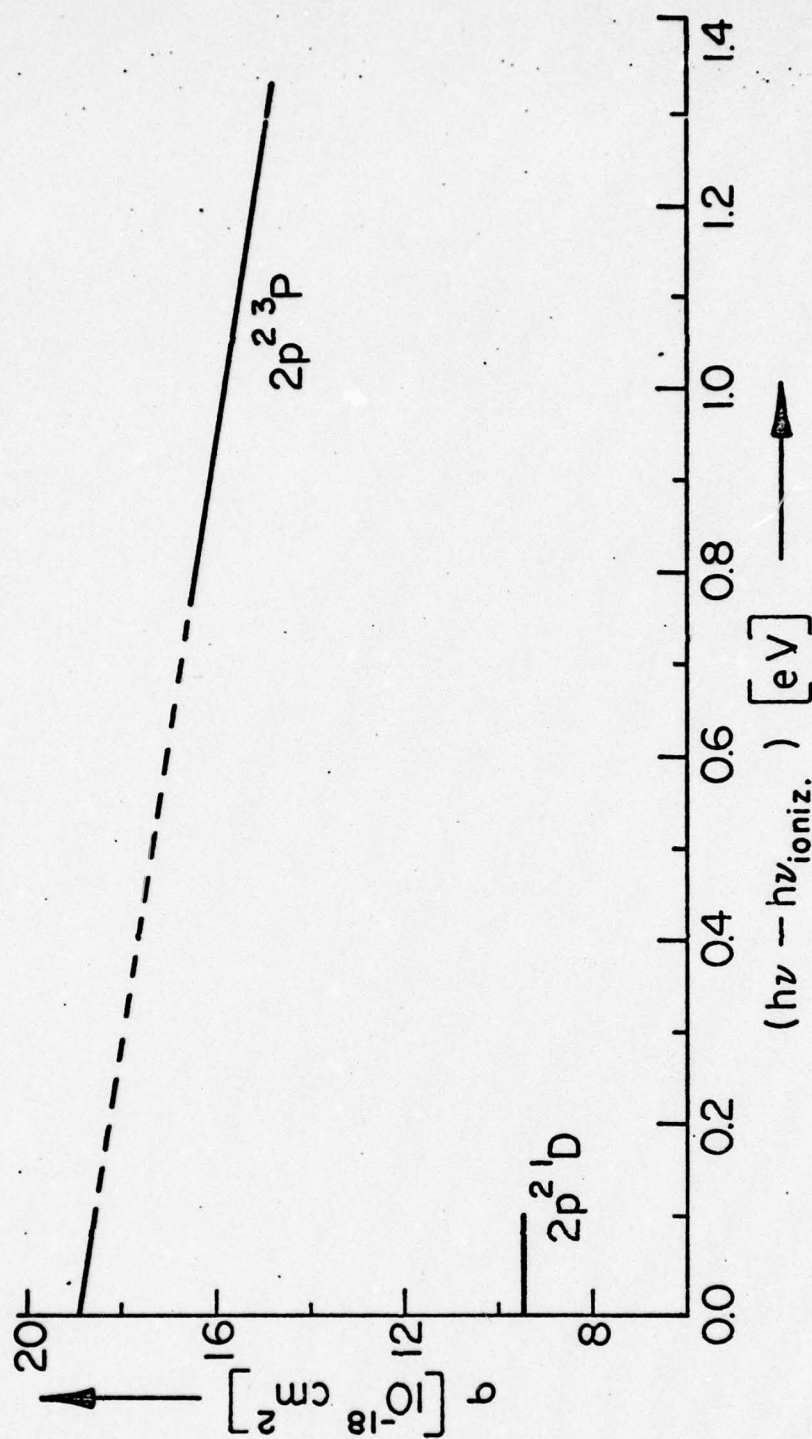
Fig. 34. Photoionization cross section from the $2p^2$ ^3P (ground state) and the $2p^2$ ^1D state of neutral carbon as a function of photon energy minus ionization energy.

h) <u>Recent Plasma Research, 1972 to 1977.</u> [108-125]

1) f-Values of Nine Argon-II Lines [114,124]

ABSTRACT

Oscillator strengths of nine ArII lines in the vuv have been measured using a wall stabilized arc operating in a helium-argon mixture. These lines, 740 Å, 730 Å, 725 Å, 723 Å, 718 Å, 679 Å, 664 Å, and 661 Å, are seen superimposed over the argon resonance continuum whose photoionization cross sections are accurately known. The f-values, so obtained, are 0.013, 0.033, 0.059, 0.024, 0.028, 0.047, 0.024, and 0.044 respectively. From various data, the experimental spread was found to be within ± 10%. However, the estimated plus experimental error is within ± 20%. These f-values have been used to calculate the emission transition probabilities and life times of the excited states which are compared with the theoretical values of Statz <u>et al</u>.

INTRODUCTION

Ar II lines in the vacuum ultraviolet (vuv) region arising from the states of $3p^4 4s$ and $3p^4 3d$ to those of $3p^5$ configuration are used as wavelength standards and were recommended by the commission 14 of the International Astronomical Union in 1962. A determination of their transition probabilities or oscillator strengths not only extends their application to the field of quantitative spectroscopy but also provides a check for the theoretical models used for calculating them. The experimental f-values of these lines are not known.

ANALYSIS AND METHOD

A Maecker[1] type wall stabilized arc was operated in helium and argon mixture. These gases were flown into the arc in such a way that helium provided a window up to about 510 Å where its ionization began and the radiation emitted by the argon atoms entered unabsorbed into a two meter grazing incidence spectrometer via a differential pumping system required for the vuv spectroscopy. The details of the wall stabilized arc and the experimental arrangement have been reported earlier.[2]

Between 800 Å and 510 Å the emitted radiation consisted of Ar II multiplets which were superimposed over argon resonance continuum. A typical spectrum, recorded photoelectrically, is shown in Fig. 35. Only nine Ar II lines (740 Å, 730 Å, 725 Å, 723 Å, 679 Å, 666 Å, 664 Å, and 661 Å) could be fully resolved.

The method of measuring the oscillator strengths of the above lines employed a comparison of intensity of an Ar II line with the intensity of the underlying neutral argon resonance continuum. It has been shown previously[3] that in a mixture of argon and helium plasma argon atoms can be described in LTE (Local Thermal Equilibrium) and the intensity, I_λ, of radiation emitted by the argon atoms is given by a modification of Kirchoff's law of emissivity being proportional to absorptivity, namely

$$I_\lambda = B_\lambda(T) \left[1-e^{-\tau_\lambda \ell}\right] , \tag{1}$$

[1] H. Maecker, Z. Naturforsch. 11a, 457 (1956).

[2] W. Hofmann and G. L. Weissler, J. Opt. Soc. Am. 61, 223 (1971).

[3] G. L. Weissler and S. K. Srivastava, Contributed paper to the "IX International Commission on Optics Conference," October 10-13, 1972; Santa Monica, California; see also "Space Optics" Proceed. IX. Int'l. Congress of the Int'l. Commission for Optics, B.J. Thompson and R.R. Shannon, Editors; National Academy of Sciences, Washington, D.C. 1974, page 772.
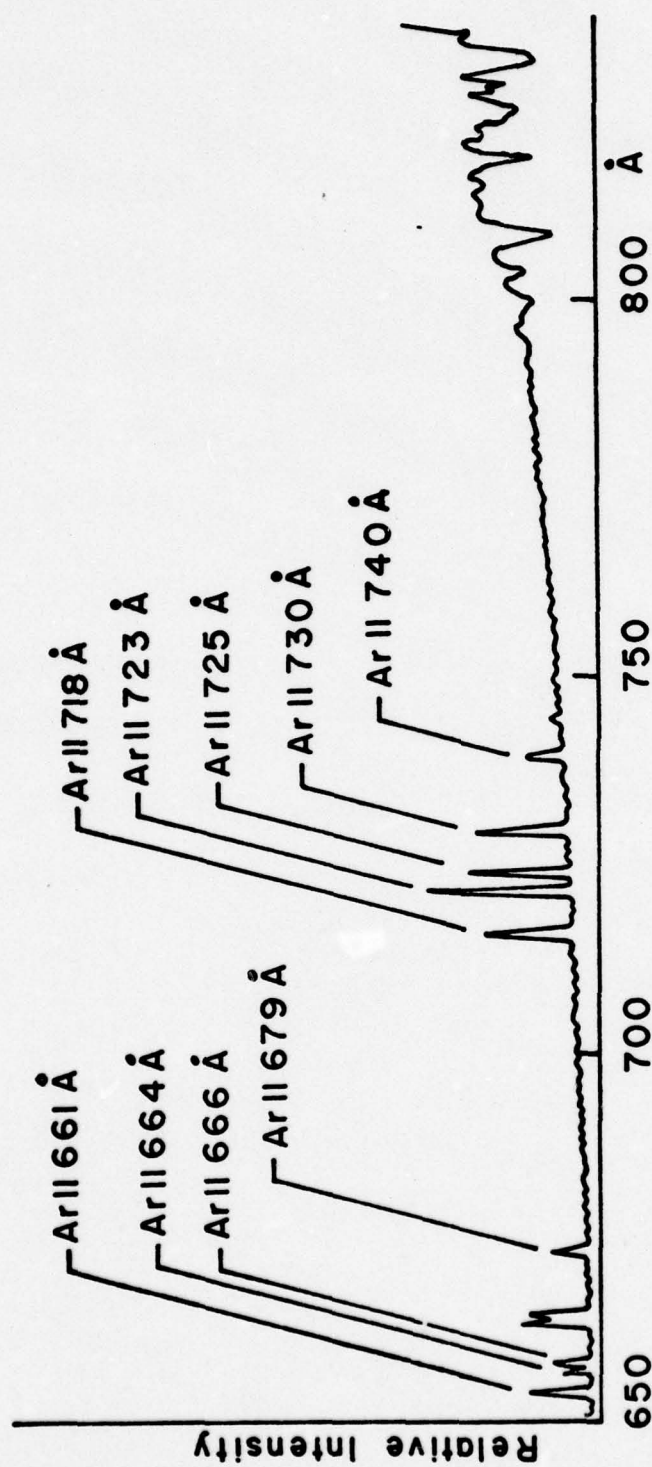
Fig. 35. A typical spectrum of Ar II lines and Ar I resonance continuum between 650A and 932Å emitted along the axis of He-Ar arc.

where $B_\lambda(T)$ is the Planck function and τ_λ is the absorption coefficient of the plasma of length ℓ at the wavelength λ. If $\tau_\lambda << 1$ the above relation reduces to

$$I_\lambda/B_\lambda = \tau_\lambda \ell ,\tag{2}$$

and the radiation at the wavelength λ is called optically thin. The intensity, I_λ, of an optically thin resonance continuum is obtained from Eq. (2)

$$I_\lambda/B_\lambda = N_g \sigma_\lambda \ell ,\tag{3}$$

where N_g is the number density of neutral argon atoms in the ground state, σ_λ the photoionization cross section at the wavelength λ, and ℓ is the length of the emitting plasma. For an optically thin spectral line the intensity is given by its profile and from Eq. (2) it is written as

$$\left[\int I_\lambda d\lambda/B_\lambda\right]^+ = (\pi e^2/m_e c^2) \; (\lambda_o^+)^2 \; f_{mn}^+ \; N_m^+ \ell ,\tag{4}$$

where $\left[\int I_\lambda d\lambda/B_\lambda\right]^+$ is the total intensity emitted by the spectral line at the wavelength λ_o^+, f_{mn}^+ its absorption oscillator strength for a transition from a lower energy level m to the upper level n, N_m^+ the density of atoms in the energy level m, and ℓ is again the length of the emitting plasma. '+' sign indicates a spectral line from the singly ionized atom.

For an Ar II line at the wavelength λ_o^+ which is superimposed over argon resonance continuum at the same wavelength, both being emitted from a plasma of length ℓ, division of Eq. (4) by Eq. (3) gives

$$\left[(I_\lambda d\lambda)^+/I_\lambda\right] = (\pi e^2/m_e c^2) \; (\lambda_o^+)^2 \; (f_{mn}^+/\sigma_\lambda) \; (N_m^+/N_g) ,\tag{5}$$

Equation (5) was used in calculating the oscillator strengths, f_{mn}^+, of Ar II

lines. The intensity, $(\int I_\lambda d\lambda)^+$, of the lines was measured in terms of the areas enclosed by them by the usual methods of planimetry and the intensity of the argon resonance continuum was obtained from its height. It was assumed that the intensity, I_λ, of the continuum remained the same over the entire width of an Ar II line. Under these conditions the ratio $[(I_\lambda d\lambda)^+/I_\lambda]$ gave the equivalent width of the line which was converted into wavelength units and substituted in Eq. (5). Temperature of the plasma was measured by the ratio of the Ar I line at 4300 Å to the Ar II line at 4806 Å in the visible. The electron density of the plasma was determined from the half width of the Stark broadened H-β line. These lines were recorded by a Seya-Namioka spectrometer and the radiation emitted by the plasma along its axis was focussed onto its entrance slit. The theoretical details of this measurement are given by Stuck and Wende.[4] The photoionization cross sections σ_λ of argon resonance continuum have been measured previously by Samson[5] and were used in the Eq. (5).

In Eq. (5) the ratio, (N_m^+/N_g), of the population densities of Ar II atoms in the energy level m and of neutral argon atoms in the ground state is needed. This can be obtained by the use of Saha equation.[6] But due to an error of about ± 2% in the measurement of the temperature of the plasma the error in the cal- culated ratio (N_m^+/N_g) becomes high. Therefore, this quantity was obtained from the measured ratio of the intensities of the Ar II line at 4806 Å and the Ar I line at 4300 Å. These intensities are directly proportional to the population densities in the upper levels of transitions which can be used to find the ratio (N_m^+/N_g) by applying the Boltzman relation. As will be discussed later, this method gives a better accuracy for the ratio (N_m^+/N_g). This ratio is given by

$$(N_m^+/N_g)=(I^+/I)(A/A^+)(\lambda^+/\lambda)(g_e/g_e^+)(g_m^+/g_g)\exp[(E_e^+-E_e)/kT], \qquad (6)$$

[4] D. Stück and B. Wende, J. Opt. Soc. Am. 62, 96 (1972).

[5] J.A.R. Samson, J. Opt. Soc. Am. 54, 420 (1964).

[6] M. N. Saha, Phil. Mag. J. Sci. 41, 267 (1921).

where I^+, A^+, λ^+, g_e^+ and E_e^+ are the intensity, transition probability, wavelength, statistical weight and the energy of the upper level of transition respectively for the Ar II line at 4806 $\overset{\circ}{A}$ and I, A, λ, g_e and E_e are the corresponding quantities respectively for the Ar I line at 4300 $\overset{\circ}{A}$. g_m^+ and g_g are the statistical weights of the level m of the Ar II atom and ground state of the Ar I atom respectively.

RESULTS AND ERROR ANALYSIS

The absorption oscillator strengths, transition probabilities and the life times for these lines are presented in the Table I. Along with our experimental values we have presented the theoretical lifetime data based on the intermediate coupling calculations of Statz et al.[7] while writing this the lifetime for $3p^4 4s^2 P$ (725 $\overset{\circ}{A}$) was reported by Livingston et al.[9] It has also been included in the Table I.

From Eq. (5) it is seen that the errors in the measured values of f_{mn}^+ are contributed by the uncertainties in the determination of the ratio (N_m^+/N_g) and the reported[5] values of σ_λ. The ratio (N_m^+/N_g) depends on the accuracy of the measured temperature T and the ratio (A/A^+) of the transition probabilities. Our temperature measurements are accurate only to within ± 2%, contributing an error of about ± 12% to the ratio (N_m^+/N_g). This explains the experimental spread of ± 10% in our results. The values of the individual transition probabilities A and A^+ have been determined by several authors. It is found[8] that these values differ by about ± 30%. However, there is a close

---

[7] H. Statz, F. A. Horrigan, S. H. Koozekenani, C. L. Tang, and G. F. Koster, J. Appl. Phys. 36, 2278 (1965); and G. F. Koster, H. Statz, and C. L. Tang, J. Appl. Phys. 39, 4045 (1968).

[8] W. L. Wiese, M. W. Smith, and B. M. Miles, "Atomic Transition Probabilities," Vol. II, Natl. Bur. Std. (U.S.) NSRDS-NBS 22 (U.S. Govt. Printing Office, Washington, D.C.).

TABLE I

Absorption f-values, emission transition probabilities and lifetimes for some $3p^5$-$4s$ and $3p^5$-$3d$ transitions of Ar II in the vuv.

| Transitions (i→K) | λ (Å) | This Experiment | | | t_K Theoretical[a] $(10^{-9}$ sec$)$ | t_K Lifetime[b] Measurements $(10^{-9}$ sec$)$ |
		$f_{iK}\pm20\%$	$A_{Ki}\pm20\%$ (10^8sec^{-1})	t_K $(10^{-9}$ sec$)$		
$3p^5\ ^2P^0_{3/2}$	723	0.024	3.06	1.95±0.78	0.3623	-
$3p^5\ ^2P^0_{1/2}{\rightarrow}4s\ ^2P_{3/2}$	730	0.033	2.06			
$3p^5\ ^2P^0_{3/2}{\rightarrow}4s\ ^2P_{1/2}$	718	0.028	7.20	0.69±0.28	0.3564	0.909±0.059
$3p^5\ ^2P^0_{1/2}{\rightarrow}4s\ ^2P_{1/2}$	725	0.059	7.40			
$3p^5\ ^2P^0_{3/2}{\rightarrow}3d\ ^2D_{5/2}$	661	0.044	4.48	2.23±0.45	-	-
$3p^5\ ^2P^0_{3/2}{\rightarrow}3d\ ^2F_{5/2}$	666	0.016	1.604	6.23±1.25	-	-
$3p^5\ ^2P^0_{3/2}{\rightarrow}4s\ ^4P_{3/2}$	740	0.013	1.583	-	-	-
$3p^5\ ^2P^0_{1/2}{\rightarrow}4s\ ^2D_{3/2}$	679	0.047	3.399	-	-	-
$3p^5\ ^2P^0_{3/2}{\rightarrow}3d\ ^2D_{3/2}$	664	0.024	3.63	-	-	-

[a] H. Statz, F. A. Horrigan, S. H. Koozekenani, C. L. Tang, and G. F. Koster, J. Appl. Phys. 36, 2278 (1965); and G. F. Koster, H. Statz, and C. L. Tang, J. Appl. Phys. 39, 4045 (1968).

[b] A. E. Livingston, D.J.G. Irwin, and E. H. Pinnington, J. Opt. Soc. Am. 62, 1303 (1972).

agreement of the ratio (A/A^+) between many authors. This agreement is within ± 5%. Thus, the error in the measured value of the ratio (N_m^+/N_g) is within ± 15%.

The values of the photoionization cross section σ_λ are known[5] with an accuracy of ± 5%. The total error in the values of f_{mn}^+ reported here is thus ± 20%.

From Table I we find that there is a large difference between our life-time values and the theoretical values of Statz et al.[7] The lifetime values of this experiment have been calculated from the transition probabilities and are thus accurate to within ±40%. Within this limit of accuracy our results agree with the lifetime value for $3p^4 4s^2 p$ reported by Livingston et al.[9]

[9] A. E. Livingston, D. J. G. Irwin, and E. H. Pinnington, J. Opt. Soc. Am. 62, 1303 (1972).

2) Measurements of Lyman-alpha and -beta Line

Profiles in an Argon Arc. [122,125]

Introduction

At sufficiently high pressures, the shape of a spectral line, emitted from a hot gas, is mainly due to interactions between the light emitting particle and other electrons, ions and atoms of the plasma. Therefore, the profile of the line carries information about the physical condition at the place of emission and can serve as a diagnostic tool in determining for instance particle densities. Because of this application, there has been strong interest in the theoretical and experimental treatment of line profiles by astro and plasma physicists in the last decades.

The effects of electric fields due to ions and electrons in a plasma are important over a rather wide range of plasma parameters as a result of the long range of Coulomb forces. For a survey of theoretical and experimental work in the field of spectral line broadening we refer to Griem's book.[1] The Stark profiles of Hydrogen require the least theoretical effort since exact wave functions are known. Consequently the different calculations[2,3] show rather similar results. In general, there is good agreement between the experimental and theoretical profiles (except for the inner line core). This is particularly true for the Balmer lines, especially H-beta.

In the case of Lyman-alpha and -beta the situation is not so convincing. Ly-α is of special importance in comparison to the other Hydrogen lines. The

[1]Griem, Hans R., Spectral Line Broadening by Plasmas, Academic Press, N.Y. (1974).
[2]Kepple, P. and Griem, H. R., Report #831, University of Maryland (1968).
[3]Vidal, C. R., Cooper, J., and Smith, E. W., The Astrophys. J. Supplement, series 25, 37 (1973).

upper level of Ly-α is composed of only three Stark levels, and except for the very line center, there is no overlapping of different Stark levels. This, and the absence of any Stark splitting of the ground state, leads to great simplifications in the theoretical treatment and makes a comparison between calculated and measured profiles a highly sensitive test for the quality of line broadening theories.

Relative wing measurements by Elton and Griem[4] in a pulsed shock tube experiment agreed quite well with theory. In contrast, the measurements by Boldt and Cooper[5] with a wall stabilized arc deviated considerably from theory, even though their experiment was obviously carried out with great care. Fussman[6] has repeated the measurements of Boldt and Cooper with much improved accuracy and found very good agreement between his experimental data and the theoretical values of Vidal et al.[3] He attempted to explain discrepancies with the older measurements in terms of diffusion processed in the arc, which was operated in a mixture of Argon and Hydrogen. To avoid these difficulties, Behringer and Ott[7] measured the profile of Ly-α using a wall stabilized arc in pure Hydrogen, and they find excellent agreement with theory.

However, all these experimentally determined line profiles of Ly-α show more or less pronounced asymmetries, and in a recently published paper, Voslamber[8] predicts an assymmetry and, for lower temperatures, even a sattelite on the red wing of Ly-α due to proton interaction.

---

[4]Elton, R. C. and Griem, H. R., Phys. Rev. 135, A1550 (1964).

[5]Boldt, G. and Cooper, W. S., Z. Naturforsch. 19a, 968.

[6]Fussmann, G., Phys. Lett. 41A, 155-6 (1972).
———Europhysics Study Conference on Spectral Line Broadening and Related Topics, Meudon, France (1973).

[7]Behringer, K. and Ott, W. R., Europhysics Study Conference on Spectral Line Broadening and Related Topics, Meudon, France (1973). Ott, W. R., and Gieres, G., Critical Analysis of the Lyman Alpha Stark Profile Measured with a Pure Hydrogen Arc, National Bureau of Standards, Washington, D.C.

Voslamber[8] predicts an assymmetry and, for lower temperatures, even a sattelite on the red wing of Ly-α due to proton interaction.

We therefore decided to repeat the Ly-α measurements and to look for this sattelite. Similar to the Boldt experiment, a wall stabilized arc of the Maecker type[9] was used as a light source, and the arc was operated in argon with different low percentage admixtures of Hydrogen. Temperature and electron density were kept constant by checking the Argon continuum in the visible region. No attempt has been made to measure the profile absolutely, but we fitted the experimental data to the theoretical values in the far wing of the line. The relative agreement with the calculations of Vidal et al.[3] was found to be very good in the case of Ly-α and only fairly good for Ly-β.

Apparatus and Experimental Procedure

A high current cascade arc of the Maecker type[9] was used to generate a steady state plasma and Fig.s 31 and 32 show the arc configuration used here. A detailed description of the experimental arrangement can be found elsewhere.[10] The arc consisted of 18 water-cooled copper plates, each of which had a hole of 6 mm diameter in the center, forming the arc channel. The total lengths between cathode and anode was 13 cm, and the copper plates were separated by teflon

---

[8] Voslamber, D. Phys. Lett. 40A, 266-8 (1972).
LeQuang Rang and Voslamber, D., Europhysics Study Conference on Spectral Line Broadening and Related Topics, Meudon, France (1973).
———On the Interference Term in the Unified Theory IInd Int. Conf. on Spectral Lines, Eugene, Oregon (1974).

[9] Maecher, H., Z. Naturforsch. 11a, 457 (1956).

[10] Hofman, W., Measurement of the Photoionization Cross Section in the Resonance Continuum of Carbon-I Using a Wall-Stabilized Arc (1970).
Tech. Report No.: USC-Vac UV-121.

gaskets which provided a gas tight seal and electrical insulation between the plates. The electrodes were round plates of Tungsten, screwed into water cooled copper plates, and both had holes in the center for end-on observation. Each copper plate has a gas inlet and two openings for cooling water. Power was provided by two Harnishfeger Corp. Welding Power Supplies, and the arc was usually operated between 80 and 100 Amps. With a 1 Ohm water cooled resistor limiting the current.

In order to start the arc, it was evacuated and then filled with 5-6 Torr of Argon. The power supply was turned on and a glow discharge was initiated by discharging a 0.1 uF, 3000 volt capacitor between anode and cathode. As soon as the low pressure discharge was burning, the pressure in the arc was increased to 1 atm. Finally, a 2o Ohm resistor originally connected in series to the water-cooled 1 Ohm resistor was bridged and the high-current arc was operative.

A schematic diagram of the optical arrangement is shown in Fig. 31. The anode side of the arc is directly connected to the differential pumping system of a 2 m grazing incidence vacuum uv spectrograph and monochromator combination. The instrument had been designed by Weissler[11] and built in the USC Physics Department machine shop. It is equipped with an uncoated lightly ruled glass grating with 690 lines per mm. A carriage can move along the Rowland circle carrying the exit slit, and behind it a layer of sodium salicilate for he conversion of VUV radiation to the visible, together with a glass-enclosed photomultiplier (PM) tube, EMI type 9514 B. The anode current of the PM was amplified by a Keithly electrometer and displayed on an x-y recorder. A

---

[11]Blackwell, H. E., Bajwa, G. S., Shipp, G. S., and Weissler, G. L.,
J. Wuant. Spectry. Radiative Transfer 4, 249 (1964).

5 kOhm potentiometer was mounted on the gear, which is driving the PM carriage, thus providing a voltage proportional to the wavelength position of the carriage, which was fed into the x-input of the x-y recorder. The linearity of the Potentiometer was better than 0.1%. By this means, any backlash, caused by additional gears could be eliminated, a precaution which is of significance for line profile measurements.

Since the arc is rather long (13 cm) and because of the gradient of both the temperature and the electron density from the center of the arc column to the wall, therefore it was necessary to limit the aperture, allowing only light from the very center of the arc to enter the spectrograph. This was accomplished by limiting the height of the entrance slit and by using a rather small bore of 0.6 mm diameter between the arc and the differential pumping system.

Radiation leaving the arc end-on on the cathode side was focussed by means of an achromatic lens on the entrance slit of a Seya-Namioka monochromator which was used for diagnostic purposes of the arc plasma in the visible region. This monochromator was equipped with a grating blazed for 4000 Å in the first order of the spectrum and with an EMI Photomultiplier type 9-01 b with an S 11 cathode. The current of the PM is amplified by a Keithly electrometer madel 610 C, and the signal is recorded with a Leeds and Northrup recorder.

As previously mentioned, the arc was operated in a mixture of Argon and Hydrogen, and Fig.32 shows the gas inlets and outlets. Under normal conditions of temperature and pressure the following flow rates were used: 70 cm^3/sec of Argon through the cathode, 60 cm^3/sec through the anode, and about 15 cm^3/sec of Helium through the anode plate most of which was pumped away in the first stage of the differential pumping system. The gas outlet

was at Plate #2 measured from the anode, open to the room, thus equalizing the pressure in the arc to 1 atm. Hydrogen was fed in small amounts of 0.14 to 4.0 cm^3/sec into the arc at plate #15. From the position of the different gas inlets and outlets it follows that there was an overall Argon flow in the main part of the arc from the cathode to plate #2 of 70 cm^3/sec. The Argon flow from the anode to this outlet was too strong to allow any back-diffusion of Hydrogen into the anode region. Furthermore, the cold gas layers between the anode and the VUV spectrograph were kept clear by a flow of Helium in the end part. Helium and Hydrogen gases were purified by cooling them to liquid Nitrogen temperatures, thus freezing out N_2 and water. Argon was flowed through a bath of dry ice and Alcohol to freeze out water contaminations. In all cases, ultra pure gases from Airco were used. However their quality was not guaranteed and could not be checked.

Spectroscopic and Plasma Parameters

The intensity I_λ of a spectral line, emitted from a homogeneous plasma in LTE is given by:

$$I_\lambda = B_\lambda(T) \; [1-\exp(-\kappa \cdot \ell)] \tag{1}$$

and

$$\kappa_\lambda = (\pi e^2/mc^2) \; N_g \; f_{gk} \; \lambda o^2 \; P \; (\Delta\lambda) \; , \tag{2}$$

where $B_\lambda(T)$ is the Planck function of the source at a temperature T, κ_λ the absorption coefficient of the plasma at a wavelength λ, N_g the number density of atoms in the state g, ℓ the length of the emitting plasma layer, f_{gk} the absorption oscillator strength for the transition from the level g to the level k, $P(\Delta\lambda)$ the normalized line shape and $\Delta\lambda=(\lambda_o-\lambda)$, where λ_o is the central

wavelength of the line. If $\kappa \cdot \ell >> 1$, then $I_\lambda \cong B_\lambda$ and the radiation is said to be emitted from an optically thick layer. In this experiment, the peak intensities of the Ly-α and Ly-β lines correspond to this condition.

According to the old Holtsmark theory, which, as more recent theoretical and experimental investigations show, holds quite well for the line wing, the profile of the lines can be described by a rather simple relation:

$$P_H(\alpha) = \frac{C_H}{\alpha^{5/2}} , \quad \text{where } \alpha = \Delta\lambda/F_0 \quad \text{and } F_0 = 1.248 \quad 10^{-9} \, n_e^{2/3} .$$

C_H is the so-called Holtsmark constant, F_0 the local electric field, and n_e the electron density. Furthermore, we have, because of the normalization,

$$P(\Delta\lambda) = P(\alpha)/F_0.$$

It is often more convenient to express theoretical results in form of a correction factor to the old Holtsmark expression, i.e.

$$P(\alpha) = \frac{C_H}{\alpha^{5/2}} \cdot R(\alpha)$$

for $R(\alpha)$ is without dimension, of the order of unity, and shows with considerable sensitivity the deviations between the different theories and experimantal results. We then get

$$R(\Delta\lambda) = P(\Delta\lambda) \frac{\Delta\lambda^{5/2}}{C_H \, F_0^{3/2}} .$$

Substitution of eq. (2) yields

$$R(\Delta\lambda) = \frac{1}{C_H \, F_0^{3/2}} \frac{mc^1}{\pi e^2} \frac{1}{N_g \, f_{gk}} \frac{1}{\lambda_0^2} \Delta\lambda^{5/2} \cdot \kappa \cdot \ell$$

and eq. (1) in the form

$$\kappa = - 1/\ell \cdot \ln[1 - I_\lambda/B_\lambda]$$

gives

$$R(\Delta\lambda) = \frac{-1}{C_H F_o^{3/2}} \cdot \frac{mc^2}{\pi e^2} \cdot \frac{1}{N_g f_{gk}e} \cdot \frac{1}{\lambda_o^2} \cdot \Delta\lambda^{5/2} \ln[1-I_\lambda/B_\lambda] \ .$$

If particle densities and temperature are kept constant, we finally obtain

$$R(\Delta\lambda) = \text{Const.} \ \Delta\lambda^{5/2} \cdot \ln[1-I_\lambda/B_\lambda] \ .$$

If one assumes that wavelengths can be measured without appreciable errors, there only remain the errors in B and I, at least as far as relative measurements are concerned. Assuming rather small errors of $\Delta B = 2\%$ and $\Delta I=0.01 \ I_{max}$, the errors in R exceeds 10% if I_λ is either below 15% or above 85% of the peak intensity. Thus, the wavelengths range over which measurements could be carried out with fairly good accuracy was rather small. We therefore decided to follow a method formerly used by Boldt et al.: the profiles of Ly-α and Ly-β are recorded for a number of different Hydrogen concentrations (in steps of a factor of about 2), while temperature and electron density are kept constant. To check this condition we used the visible region spectrograph to measure, in conjunction with the profile of H-β, the Argon continuum at $\lambda = 46900 \ \overset{\circ}{A}$. This continuum, under the experimental conditions of T=12 5000 K and $n_e= 10^{17} \ cm^{-3}$ is emitted from an optically thin layer and

$$I_c \ \alpha \ n_e \ e^2/\sqrt{T} \ .$$

(The remaining weak dependance on T is negligible.) Assuming LTE we can apply the Saha equation for the first Argon ionization step and get:

$$\frac{n_i^A}{n_o^A} \ n_e = 2 \ \frac{u_i}{u_o} \ (\frac{2\pi m \ kt}{h^2})^{3/2} \ \ell^{-x/kT}$$

Because the Hydrogen admixtures were rather small ($\leq 4\%$) in all experiments we have $n_i^A \simeq n_e$ and obtain

$$n_e^2 = n_o^A \quad 2 \frac{u_i}{u_o}(\frac{2\pi m\, kt}{h^2})^{3/2} \, \ell^{-\chi i} kt \, ,$$

where χi is the ionization energy of Argon. It follows that

$$I_c \propto T \cdot \ell^{-\chi i/kt} \rightarrow \frac{dI_c}{I_c} = [1 + \frac{\chi}{kT}] \frac{dT}{T} \, ,$$

and with T=12 500 K,

$$\frac{dI_c}{I_c} = 15.6 \frac{dT}{T} \, .$$

One sees easily that the continuous intensity is very sensitive to temperature variations.

In addition to this check, the profile of H-β was measured several times for the different Hydrogen admixtures and used to determine the electron density by the following method: A straight line was drawn, which connected the two peaks of H-β, and the value at 4861 $\overset{\circ}{A}$ is taken as the peak intensity of the line. Taking into account the underlying continuum, the full, half, quarter, and eighth widths are read from the recorded profile. We then use the experimentally found relations between $\Delta\lambda_{1/2}$, $\Delta\lambda_{1/4}$ and $\Delta\lambda_{1/8}$ and the electron density, as determined by Wiese et al.[12] In our work these values of the electron density deviate by less than 5%. In experiments with higher Hydrogen concentrations (but less than 3%) the electron density is obtained with an accuracy[12] of about 6%. The different Ly-α and Ly-β recordings for the different Hydrogen concentrations were at first treated separately.

---

[12] Wiese, W. L., Kelleher, D. E., and Paguette, D. R.,
    Phys. Rev. A6, 1132 (1972).

The amplitudes A of the profiles (an example is shown in Fig. 37) were evaluated point-by-point according to

$$A_c - \Delta\lambda^{5/2} \; \ell n[1-I_\lambda/B_\lambda] = \text{const. } R(\Delta\lambda).$$ Because T and n_e were kept constant, the constant C should only contain the different Hydrogen densities as a variable. We therefore fitted profiles, i.e. A_c values in the range between 20 and 60% of I_{max} of the line wing, and finally normalized these values in the far wing (between 4.5 10^{-2} and 7.5 10^{-2} in the case of Ly-α to the calculated value of Vidal, Cooper and Smith.[3] The different Ly-α and Ly-β recordings (for the different Hydrogen concentrations) were first treated separately. A typical plot is shown in Fig. 36. Inspite of the rinsing the end part of the arc with purified Helium, there still remained a remarkable amount of self-absorption in the center of Ly-α, caused by cold boundary layers that could not be avoided. The NI impurity lines at 1199.6, 1200.7, and 1243.3Å, respectivey, were used, in conjunction with the self-absorption dip of Ly-α, to calibrate the wavelength scale, Fig. 37. The peak intensity of Ly-α was taken to be the relative Black Body Value B_λ and the profiles were evaluated according to:

$$R(\Delta\lambda) = C_1 \; \Delta\lambda^{5/2} \; \ell n[1-I_\lambda/B_\lambda].$$

Because T and n_e were kept constant, which was checked by measuring the Argon continuum in the visible part of the spectrum, the constant C should depend on the different Hydrogen concentrations only. We therefore fitted the different profile amplitudes in the wing in the range between 20 and 60% of the peak intensity I_{max} and finally constructed an average profile from several overlapping profiles, in the far blue wing of the line (in the case of Ly-α between 4.5 10^{-2} <α< 7.5 10^{-2}) to the calculated value of Vidal et al./3/. These results are shown in Fig. 38 and Fig. 39 for the blue and
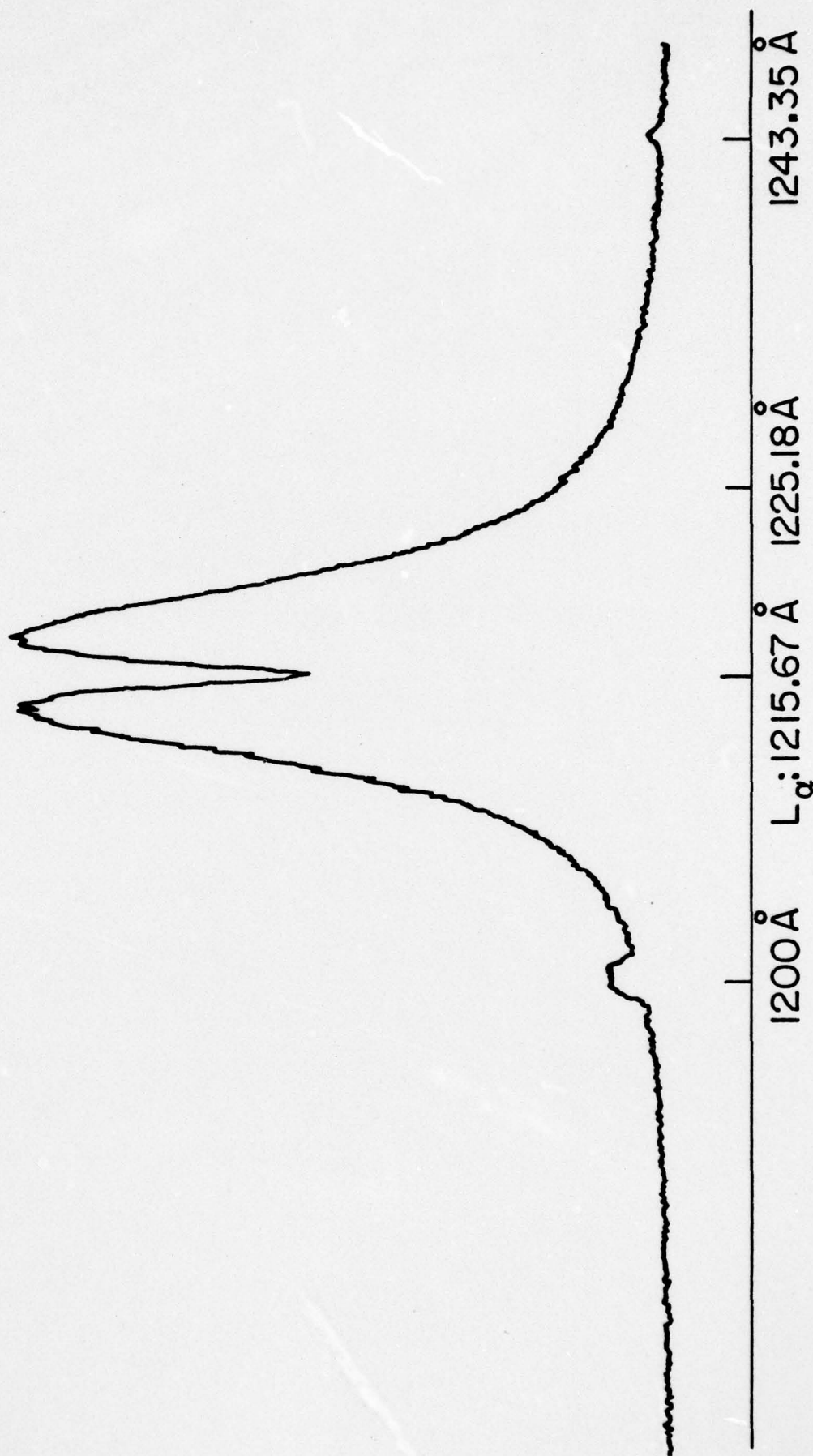
Fig. 36. Typical Recording Trace of Ly-α Used to Measure its Profile.

1243.18 } NI
1243.31 }

NI { 1225.03
     1225.37

NI { 1228.41
     1228.79

1199.55 } NI
1200.23 }
1200.71 }

NI: 1176.51

NI: 1177.69

(HI: 1215.67) L$_\alpha$

pen recorder paper motion
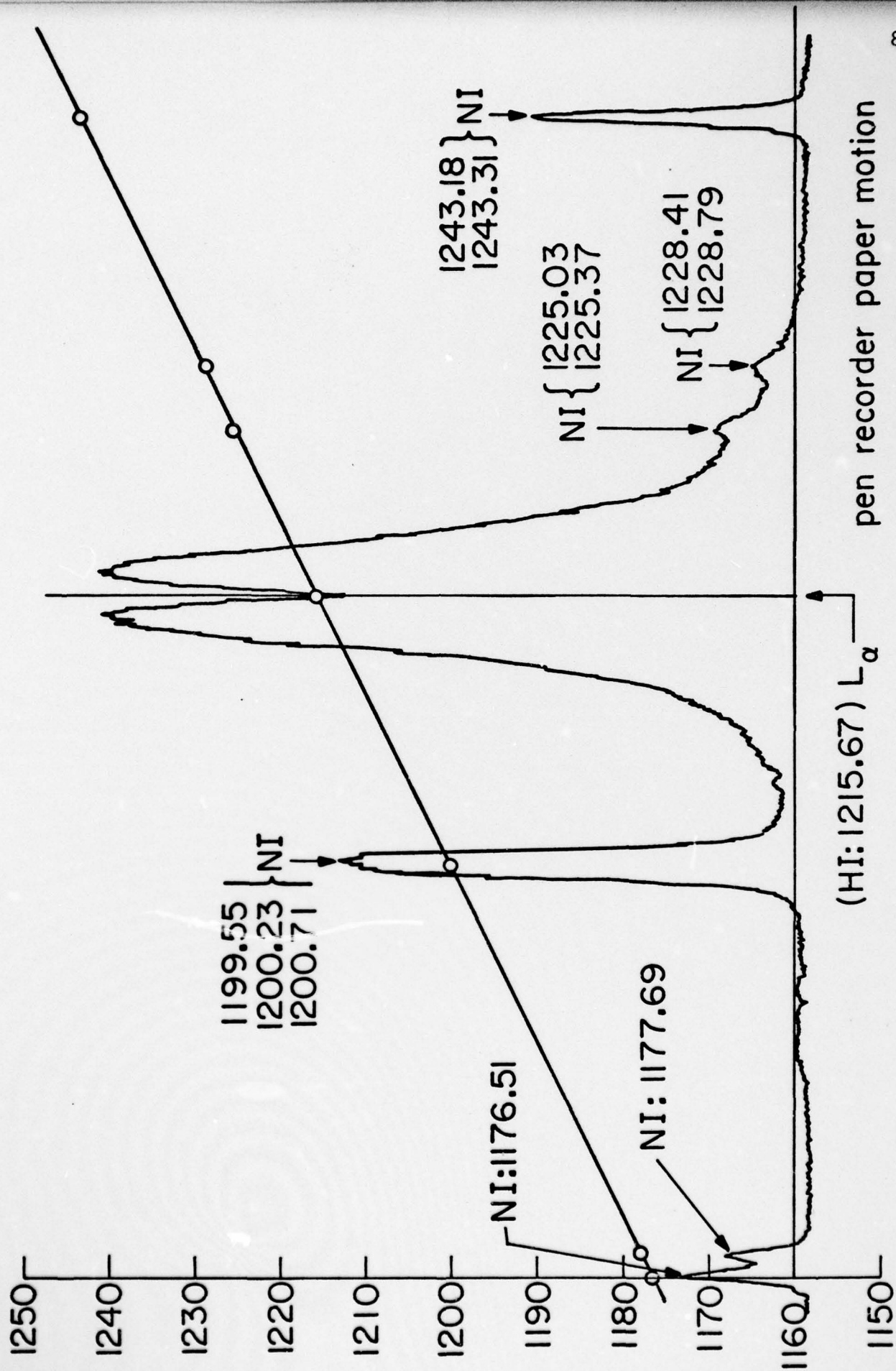
Fig. 37. Recording Trace of Ly-α with N$_2$ Added for Calibration of λ-Scale.

1250
1240
1230
1220
1210
1200
1190
1180
1170
1160
1150

END
DATE
FILMED
8-78
DDC

Fig. 38. The Blue Wing of Ly-α in Asymptotic Holtsmark Units versus $\alpha = \Delta\lambda/F_0$.

Fig. 39. The Red Wing of Ly-α in Asymptotic Holtsmark Units versus α = Δλ/F₀.

red wing of Ly-α, respectively. The profile is plotted in asymptotic Holtsmark units versus $\alpha = \Delta\lambda/F_o$. The solid curve represents the calculations of Vidal for the same electron density. Besides the fitting and normalization of the measured values, no other smoothing procedures have been applied. Therefore our measurements are rough data. We also did not account for the finite resolution of the spectrograph (no deconvolution). As Figs. 38 and 39 show, there is quite good agreement between theory and experiment as far as the blue wing of Ly-α is concerned, while in the red wing (for $\alpha > 2 \cdot 10^{-2}$) the measured values are higher than predicted by theory, a result which is in accordance with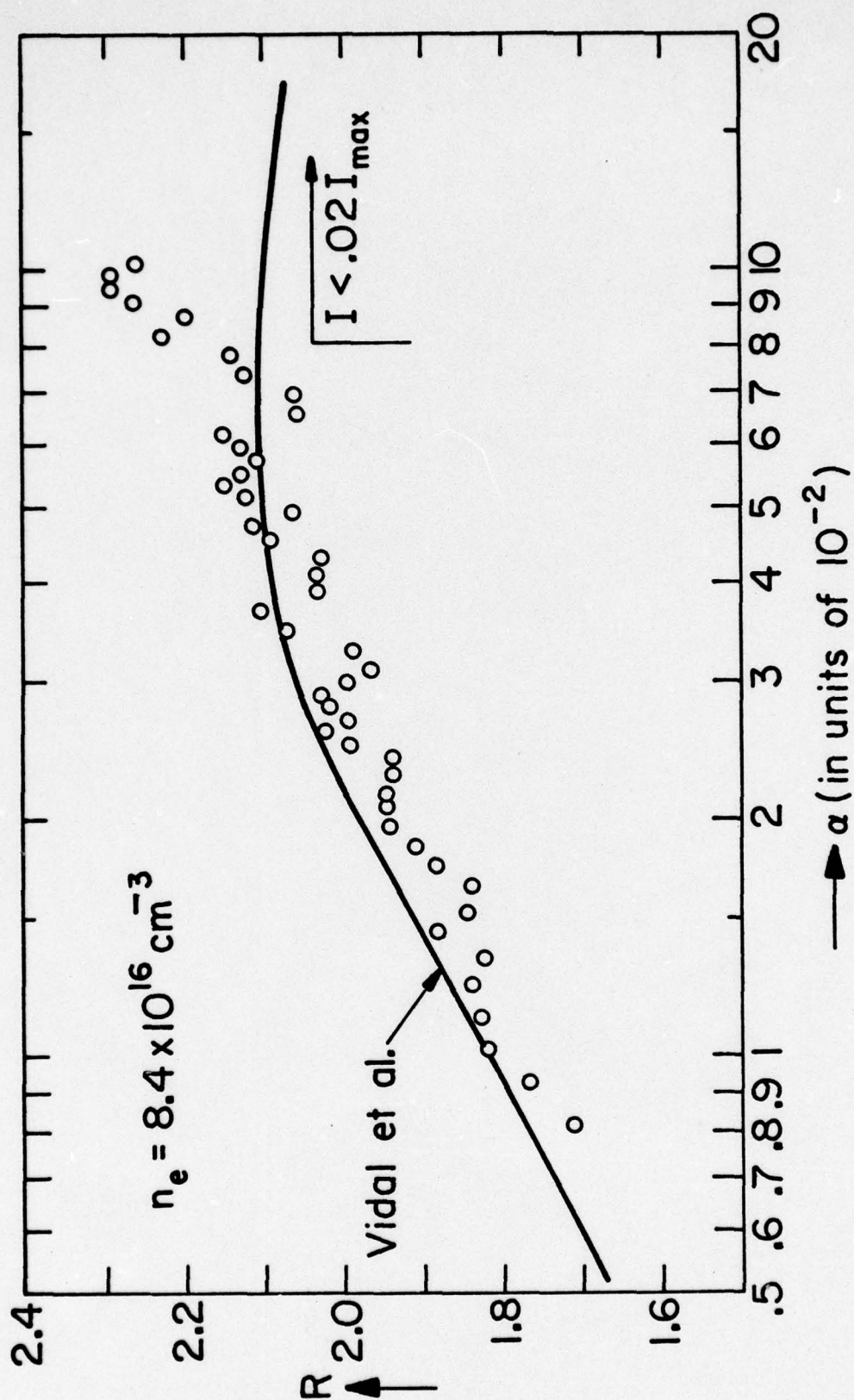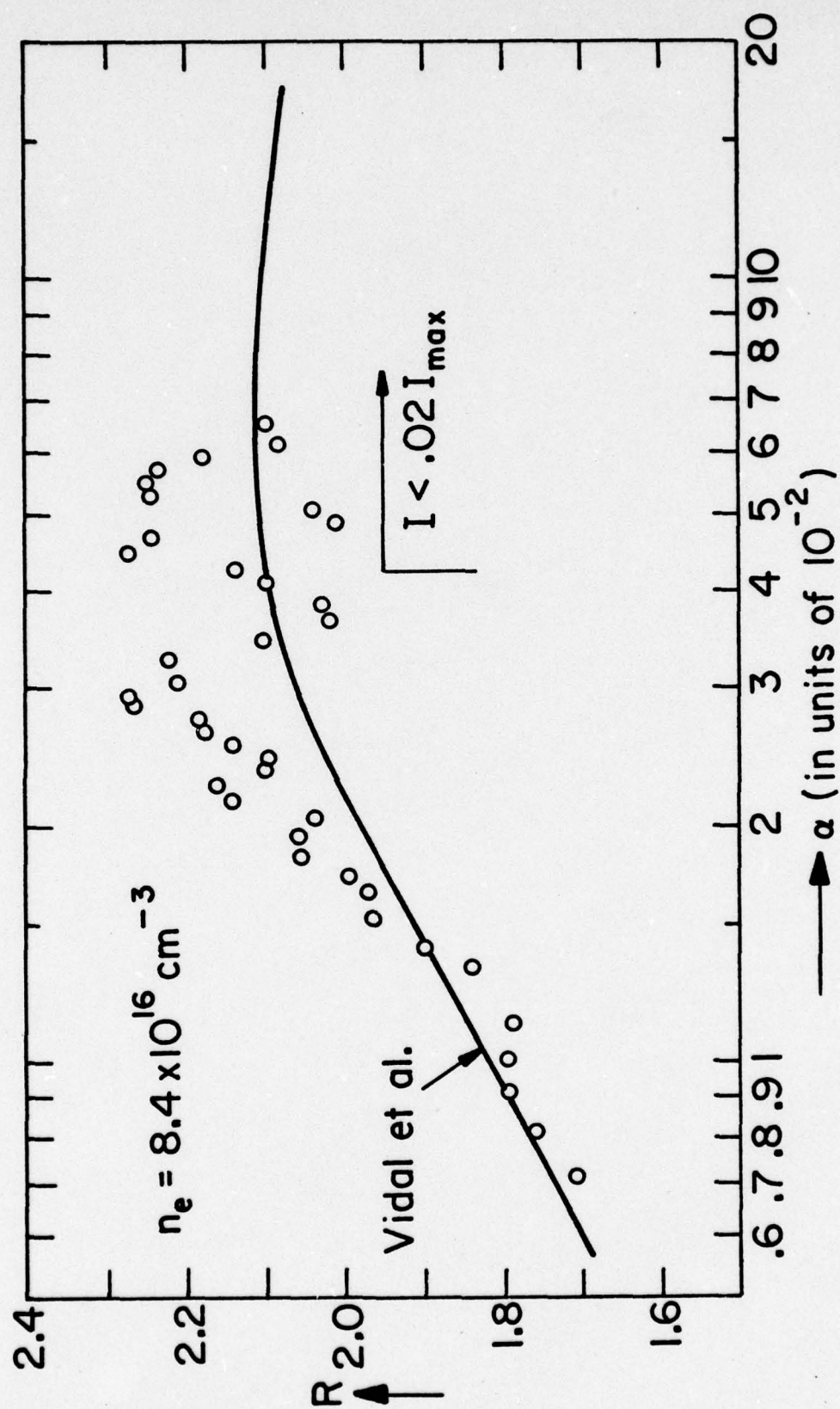 Boldt's experiments. (The red wing could not be evaluated for the highest Hydrogen concentrations because of a disturbance during the experiment, thus the limit $I \leq 0.02 \, I_{max}$ is already reached at $\alpha = 4 \times 10^{-2}$.) Unfortunately, it can not be decided whether the asymmetry is a true effect or caused by some other disturbance. This is because of two reasons: When large amount of Nitrogen were added to (Fig.37) the Argon-Hydrogen mixture, rather strong NI lines at 1225 and 1228 Å could be observed. These lines, although about a factor of ten weaker than the impurity line at 1243 Å, may have some effect, even if the arc is operated with a pure Argon-Hydrogen mixture.

The apparatus function of the spectrograph has not been measured; though unlikely, it could by asymmetric because of the rather astigmatic mounting.

The sattelite or asymmetry, due to proton interaction predicted by Voslamber should lie about 18 Å to the red from the line center of Ly-α. Assuming an electron density of $8.4 \cdot 10^{16} \, cm^{-3}$, this sould correspond to a value of $\alpha = 7.5 \cdot 10^{-2}$ which is outside the range of accuracy of this experiment. It was not possible to increase the intensity of Ly-α by adding more

Hydrogen to the Argon because the arc could not be stabilized for concentrations above 5%.

The blue wing of Ly-β is shown in Fig. 40, where the same kind of evaluation procedure has been applied as for Ly-α. Its red wing could not be measured at all because of very strong Nitrogen lines. The agreement with theory is rather poor, but the appartus profile has not been taken into account. The overall signal was small, so that wide slits had to be used at the entrance and exit of the spectrograph.

It should be pointed out here that after this report was finished, some new information has been published by Hans R. Griem[13] on the broadening of Ly-α in dense plasmas. Here he compares the various theoretical treatments with the most recently published data[14] of Ly-α line broadening at electron densities of $n_e=2$ to 4×10^{17} cm^{-3}. Our data presented here in Fig.s 38 and 39 at $n_e=8.4 \times 10^{16}$ cm^{-3} can be fitted easily to the lower theoretical curve (see Fig. 41) of reference 13, for which no experimental points were then available.

At least some of the difficulties just mentioned could be overcome by using a photon counting system instead of taking DC measurements. The overall sensitivity of the system could be increased and smaller slits could be used which would enhance the spectral resolution. A photon counting system would also eliminate any shift of the zero line due to changes in the amplification system. Thus it should be possible to measure the line profiles in the far wing with higher accuracy.

In addition, the apparatus profile of the spectrograph could be measured using a special light source, e.g. a spark, to produce narrow lines. In the evaluation procedure one could then apply a deconvolution procedure and take account of the inherent apparatus profile. Furthermore, if the resolution of the spectrograph could be increased, it would be possible to use optically thick lines (saturated centers) of KrI 1165Å and 1236Å and several NI lines in the neighborhood of Ly-α and Ly-β for an absolute calibration, thus determining the line profiles absolutely.

[13]H. R. Griem, Phys. Rev. A17, 214 (Jan. 1978).
[14]K. Grützmacher and B. Wende, Phys. Rev. A16, 243 (1977).
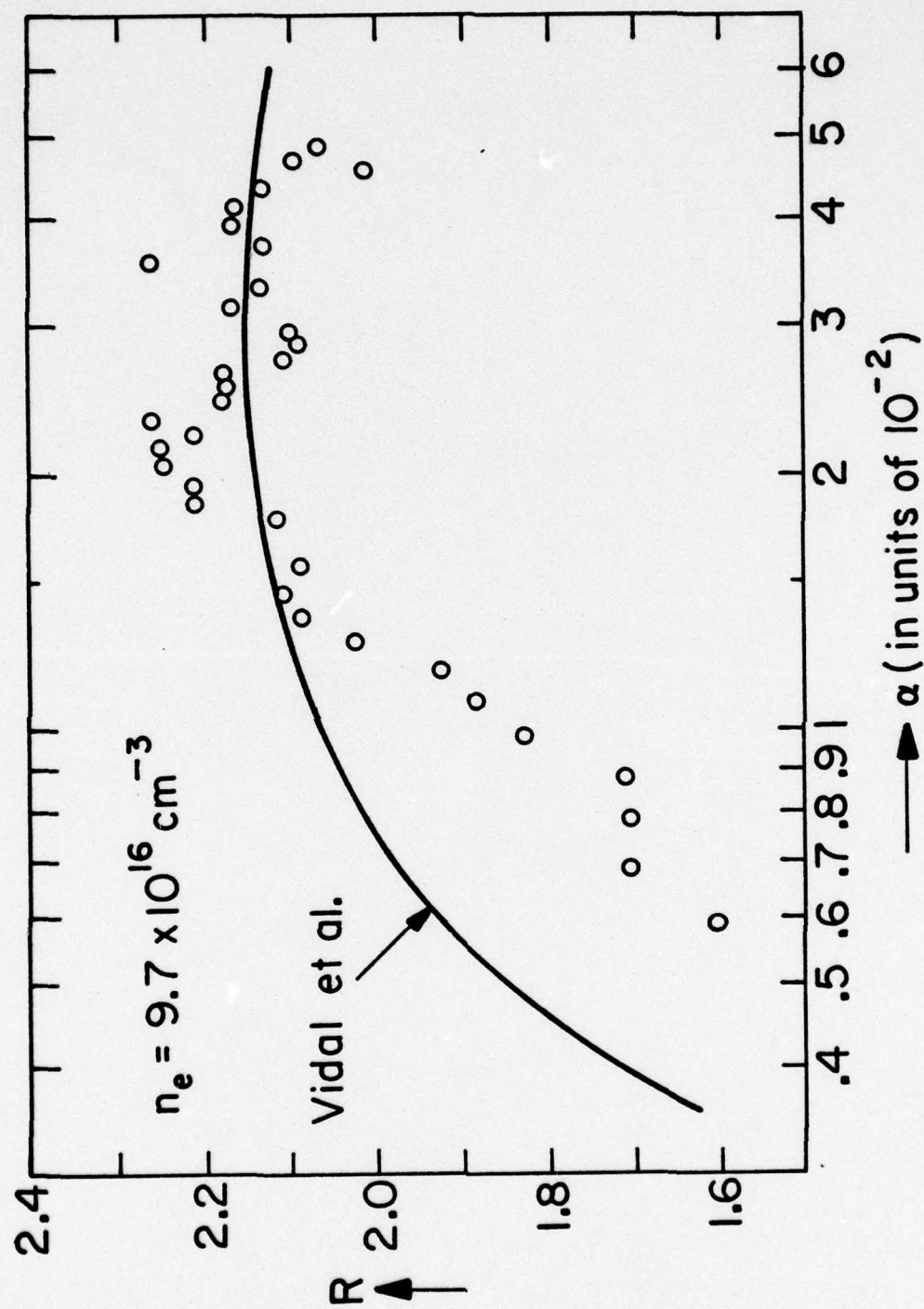
Fig. 40. The Blue Wing of Ly-β in Asymptotic Holtsmark Units versus α = Δλ/F₀.
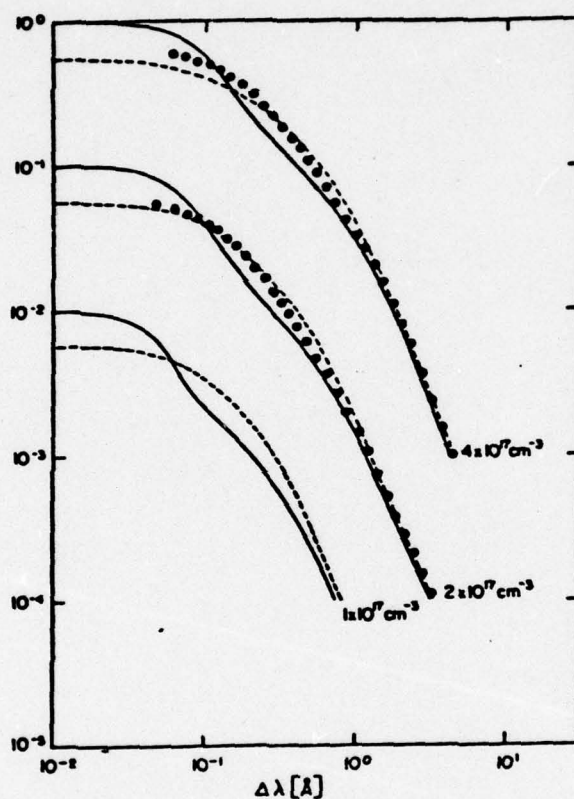
Fig. 41. Comparison of measured Lyman-α profiles
(solid dots, from Ref. 4) with calculated profiles not
accounting for electron-produced low-frequency fluctua-
tions (solid lines, from Ref. 8) and with profiles calcu-
lated as described in the present paper (dashed lines).
The profiles are normalized as in Ref. 4, except that the
areas are normalized to 0.1 and 0.01 for the lower-den-
sity cases.

III. OPTICAL AND PHOTOELECTRIC EFFECTS IN SOLIDS [33,63]
[18,19,26,31,33-35,41,43,45,47,56,57,62,63,67,70,76,77]
[79,82,83,92,95,97-100,103,104]

a) Photoelectric Yields of Surfaces. [18,19,26,31,33-35,41,43,45]

Interest in the interaction of vacuum u.v. photons with solids at U.S.C. arose out of the problem of understanding fundamental cathode phenomena in gas discharges. For this reason, the first study undertaken was the measurement of absolute photoelectric yields from a variety of polycrystalline materials subject to various surface treatments. Measurements were made on Ni, Cu, Pt, Au, W, Mo, Ag and Pd over the spectral range 473-1400 Å corresponding to photon energies from 25-8 eV. The samples used were normally commercial foils with thicknesses ranging from 0.5-5 mils and were measured in a vacuum of approximately 10^{-5} mm Hg.

Photoyields were measured first on foils cleaned with organic solvents; these were followed by measurements on surfaces heat treated in vacuum (5×10^{-5} mm Hg) for varying intervals of time. A few metals were tested after exposure to O_2, H_2, and air at various pressures, both at room temperature and above. Yields were also obtained for several metals while they were maintained at temperatures between 500°C and 1000°C. Later as more interest developed in the basic mechanism of the vacuum u.v. photoeffect, photoyield measurements were made on a variety of evaporated films prepared in situ at 3×10^{-5} mm Hg. Films of Al, In, Sn, Bi, Au, Ag, and Cd were studied.

Typical photoyield data are shown in Figs. 42-44. Figs. 43 & 44 contain data on simultaneous reflection and transmission measurements on the same materials. These optical data will be discussed later. The photoyield curves illustrate the several novel features observed for the far ultra-violet photo-
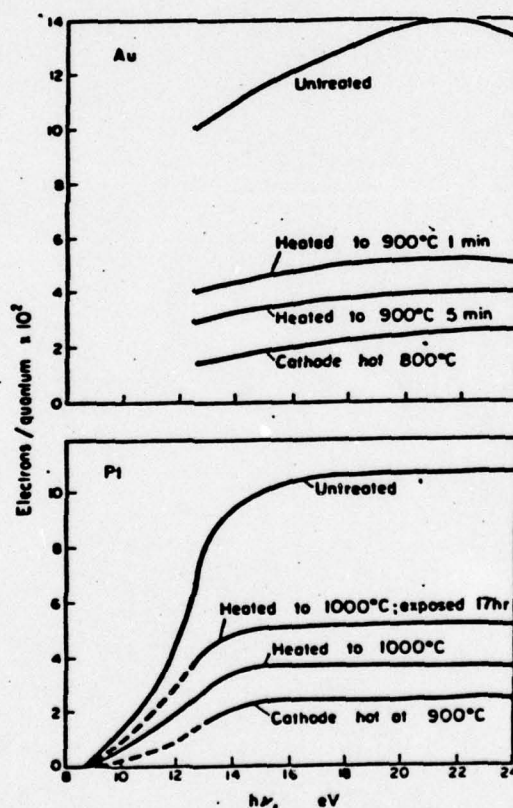
Fig. 42.. Photoelectric yield of Au and Pt. Measurements were made on polycrystalline foils in a vacuum of about 10⁻⁸ mm Hg.
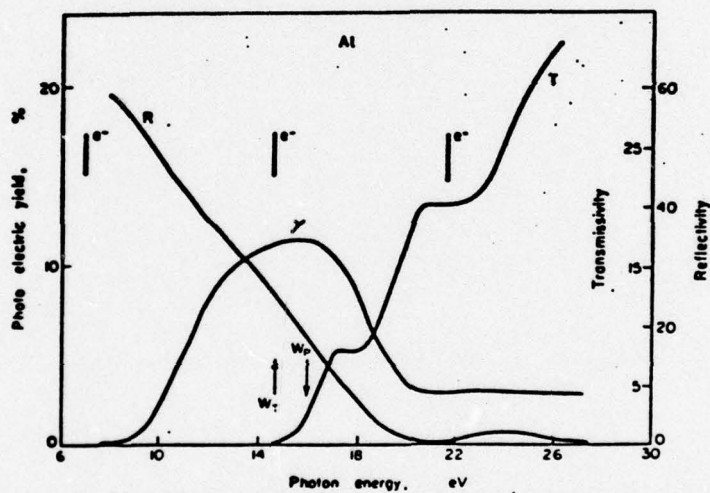
Fig. 43. Optical and photoelectric data for evaporated films of Al. Reflectivity (R) and Photoyield (γ) measured on a glass backed film 430 Å thick evaporated *in situ*. Transmissivity (T) from an unbacked film 1150 Å thick, evaporated outside the mono chromator. Arrow down denotes the free electron plasma frequency and arrow up the onset of optical transmission. Vertical lines labelled e⁻ denote measured electron energy losses.
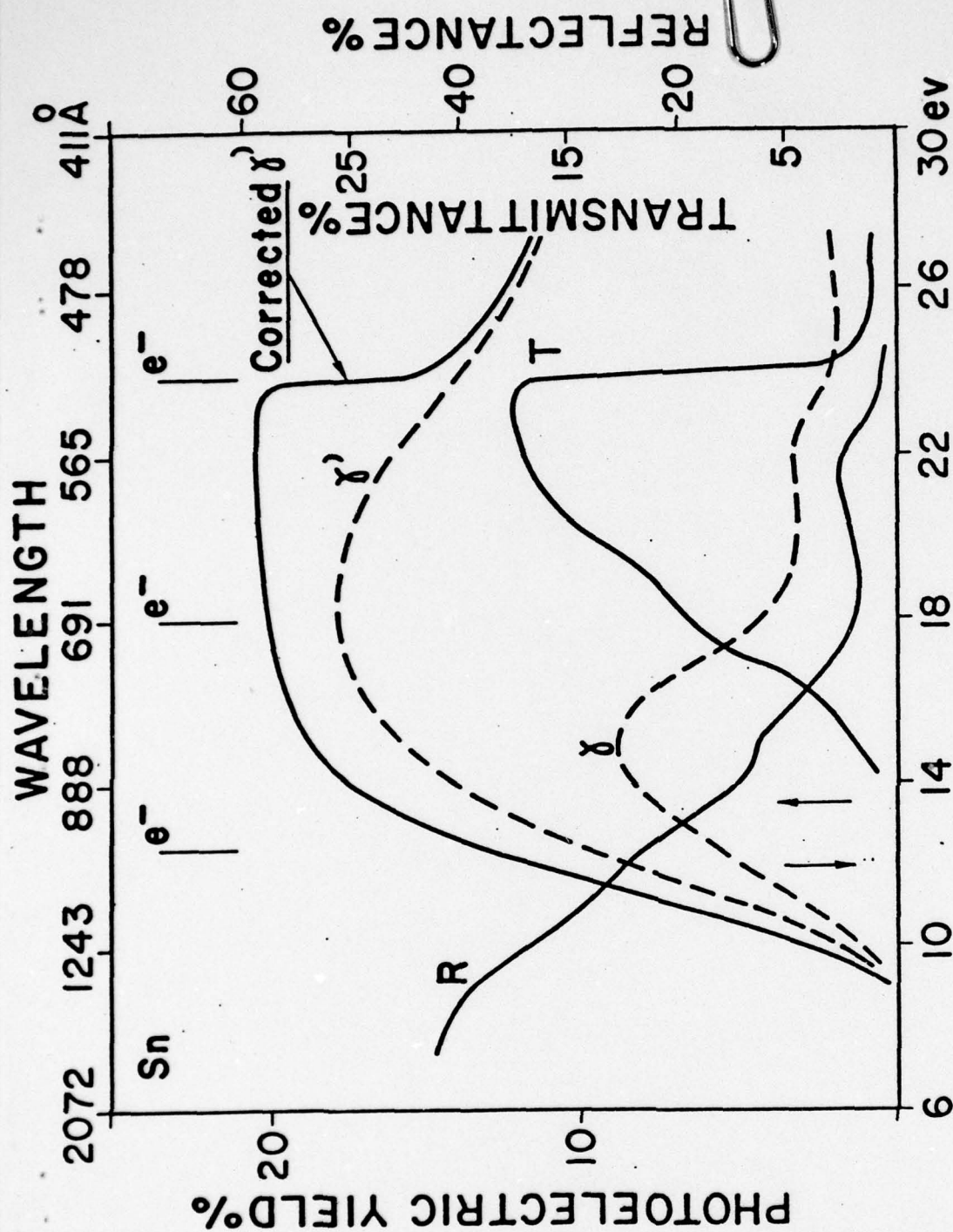
Fig. 44. Optical properties of Sn films. The reflectance R and the photoelectric yield γ based on the old definition of electrons emitted per photons incident, are presented for a glass-backed film of Sn, evaporated within the measuring chamber of a normal-incidence vacuum monochromator. The transmittance T and the total photoelectric emission γ' is shown for an unbacked film 1020 Å thick, evaporated outside the mono-chromator and floated off in water. The dashed curve labeled γ' takes into account only the incident photon flux, while the solid curve shows the corrected γ' values obtained by use of $\gamma = N_e / \{I_0 (1-R-T)\}$, where N_e is the total number of photoelectrons emitted, the reflectance $R = I_R / I_0$, and the transmittance $T = I_T / I_0$. All data were obtained with light normally incident on the sample. Arrow down denotes the theoretical plasma frequency and arrow up the onset of optical transmission. While the vertical lines labelled e^- show the positions of the known characteristic electron energy losses.

effect. First, the yields are 10-100 times larger (values of 1-10 per cent are typical) than those characteristic of the visible region. Second, the yields are less strongly influenced by surface treatment than are those at longer wavelengths. A decrease in yield of only a factor of ten is obtained in going from an untreated surface to as clean a surface as could be obtained under the existing vacuum conditions. Third, in all cases where the measurements extended far enough the yields show a sharp rise in the vicinity of 1400-1000 Å indicating a 'threshold' for the large yield effect between 9 and 12 eV. This threshold is particularly well defined in Ni, Pt, Al, Sn, and Bi. One final feature of the photoyield behavior in the vacuum u.v. which is of some practical importance is the relative constancy of the yields of several metals in the region 1000-500 Å. Gold for example when heat treated in vacuum gives reproducible yields which remain between 3-4 percent over the above region. Pt, Pd, and W show similar behavior to a lesser extent.

The above features of the photoyield behavior were interpreted on the basis of the onset of a 'volume' photoeffect near 10 eV. In order to investigate the influence of the 'volume effect' on the nature of the emission, electron energy distributions were measured on Au for several photon energies in the range 10-20 eV. These data are shown in Fig. 45. The ordinate is the number of electrons, in percent, emitted with energies between E and E+dE per incident photon divided by the photoelectric yield. A striking feature of these curves is the large proportion of low energy electrons emitted for photon energies several eV larger than the Fermi band width. The vertical arrows indicate the lowest electron energy expected from the 14·9 and 17·6 eV photons on the basis of the surface photoeffect model. A reasonable interpretation of this behavior is that the electrons are emitted from the volume of
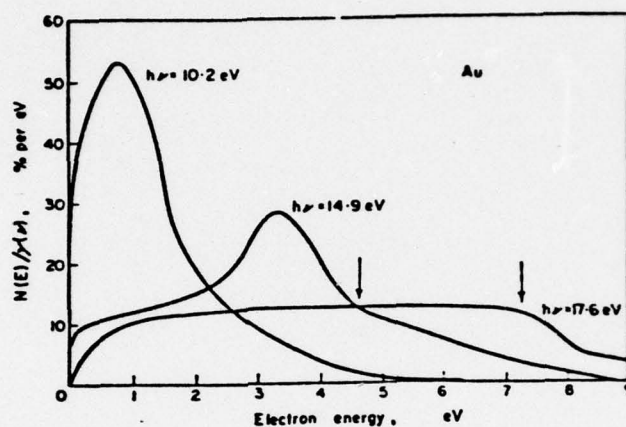
Fig. 45.   Photoelectron energy distributions from Au. Incident
photon energies were 10.2, 14.9, and 17.6 eV. The vertical
arrows indicate the lowest electron energy expected for the
surface effect. A work function of 4 eV was estimated from
the current saturation curve.

the metal and undergo multiple electron-electron scattering before emerging. In each case the mechanism of electron-electron scattering seems to offer a plausible explanation. It is possible to exploit this effect to study electron-electron collisions in metals and semiconductors by making careful electron distribution measurements at several photon energies in the region of the volume effect. The ratio of low to high energy electrons as a function of photon energy should peak near the energy corresponding to the maximum cross section.

b) <u>Optical Properties of Surfaces</u>. [43,45,47,56,57,62,63,67,70,76,77,79, 82,83,92,95,97-100,103,104]

In 1956 a new series of experiments was begun aimed at making simultaneous measurements of optical and photoelectric properties of single crystals and evaporated films of a wide range of materials in the spectral region from 1500-500 Å. Aside from the value of these measurements in elucidating the volume photoeffect they are significant from several other points of view. Thin film optical transmission data correlate optical behavior and electron energy loss information in a variety of materials. In this case the determination of the onset of plasma transmission predicted by both the Drude theory and the more modern Bohm-Pines theory is sought. Reflectivity data at normal incidence, analyzed by the Kramer's-Kronig dispersion relation, yield values for the optical constants n and k of the material. Since very little data on optical constants were available for the spectral region below 1500 Å, these experiments revealed a wealth of new and exciting results. Measurements were made of optical transmission of unbacked evaporated films of Al, In, Sn, Bi, and Ti and of Sb, Te, and Ge evaporated onto a fluorescent substrate. Simultaneous measurements of reflectivity and photoyields were made on films of Al, In, Sn, Bi, Au, Ag, and Cd. The reflectivity spectrum of a single crystal of Ge was measured at several angles of incidence and the optical constants calculated by applying the Kramer's-Kroniz relation. Examples of the results obtained are shown in Figs. 43, 44, 46 and 47.

Perhaps the most interesting result is the onset of transmission beginning in the region 12-18 eV and its sudden drop for some materials at energies of a few eV from the onset. In addition to the materials shown, this behavior was observed in In, Bi, Te, and Ti. The Drude free electron model predicts such an onset at the frequency $\omega_p = (4\pi n_0 e^2/m)^{\frac{1}{2}}$ where n_0 is the free
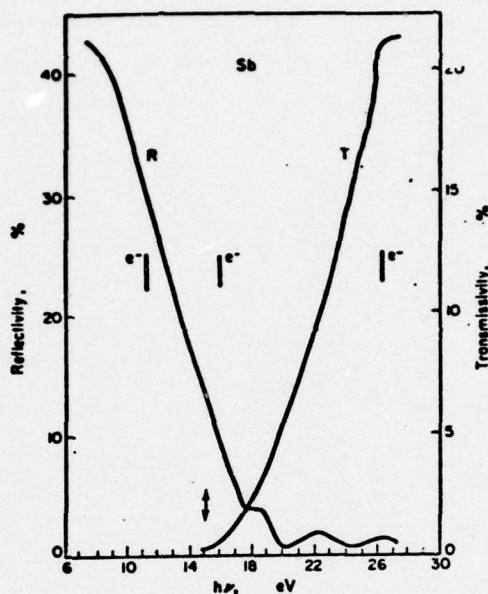
Fig. 46. Optical data for evaporated Sb films. Reflectivity (R) of a glass backed film, 860 Å thick, evaporated in situ. Transmissivity (T) of a stilbene-backed film 1330 Å thick, evaporated in an external chamber. Arrow down denotes the free electron plasma frequency and arrow up the onset of optical transmission. Vertical lines marked e⁻ denote electron eigenlosses.
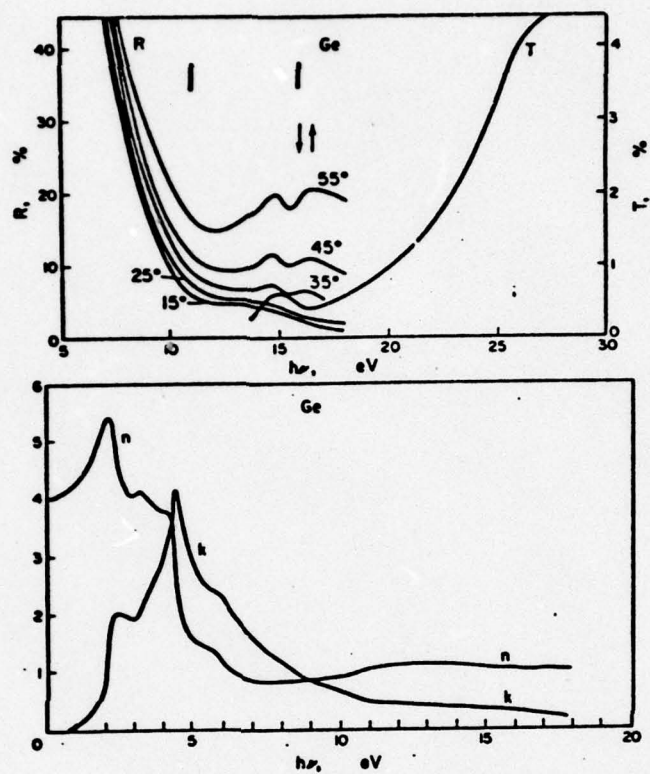
Fig. 47.   Optical data and the results of a dispersion relation
  calculation of n and k for Ge. Reflectivity (R) of a single
  crystal of Ge at various angles of incidence. Transmissivity
  (T) of an evaporated film 800 Å thick.

electron density, and e and m have the usual meaning for electrons. The position of the onset is considered carefully in the Bohm-Pines theory which modifies the simple picture by introducing plasma modes, the electron effective mass, and the possibility of interband transitions. In many materials values close to the free electron plasma frequency are predicted. Reference to Figs. 43,44,46 show that this is true to a good approximation in several materials. The general shift of the transmission onset to values a few tenths of an eV lower than the observed eigenlosses corresponding to plasma excitations has been explained by Mendlowitz as due to the different dependence of the two phenomena on the real and imaginary parts of the complex dielectric constant. The sharp drop in transmission at higher energies can be identified with $d \rightarrow s,p$ band transitions and gives for the position of this transition the following values: Sn(24.3eV), In(16.8 eV), and Bi(24 eV). Correlations of the reflectivity, transmissivity, and photoyields from these data show definitely that an absorption mechanism (volume photoeffect) sets in at about 8-10 eV for most of these materials. Additional structure in the transmission curves of Al, Sn, and Sb seems to coincide with prominent electron eigenloss values but as yet no definite conclusions can be drawn from the optical data regarding the mechanism involved.

Figure 47 shows reflectivity data and the results of the dispersion analysis for a single crystal of Ge. This analysis was carried out by combining the reflectivity measurements of Rustgi at U.S.C. between 7.6-18 eV with those of Phillip and Taft of G.E. between 0-10 eV. A comparison of n and k with the transmission curve is interesting for Ge since the difference between the free electron plasma frequency ω_p, which for 4 electrons per atom corresponds to 16 eV, and the transmission onset given by n=k is significant. The condition n=k yields a value near 9 eV for the plasma frequency compared to 16 eV for ω_p.

Prominent energy losses are found near each of these values. The transmission curve for a Ge film evaporated onto a fluorescing substrate indicates a weak transmission onset at an energy lower than 16 eV together with an apparent stronger transmission beginning at 16 eV.

An investigation of the absorption band of X-irradiated LiF in the long wavelength tail of the exciton absorption edge is also underway. Figures 48 and 49 show some of the early results of this work. The reflection spectrum of a cleaved Harshaw crystal was obtained at room temperature at an angle of incidence of 20°. The structure observed agrees substantially with that obtained in absorption by Milgram and Givens and clearly shows the large exciton peak near 970 Å. Peaks seen at shorter wavelengths can be associated with electronic transitions on the F^- ion. Transmission data on a thin cleaved LiF crystal which was irradiated for 2 hr at room temperature with 35 keV X-rays from a Cu target are shown in Fig. 49. The measurements were made by comparing the transmission of the X-irradiated sample to that of a control sample. Transmission through both samples was measured before irradiation. X-irradiation increased the absorption over the entire region measured, however, there is clear evidence of a new absorption band centered near 1130 Å. This band can be bleached slightly by LiF F-light (2536 Å) and thus behaves similarly to the β band observed in other alkali halides.
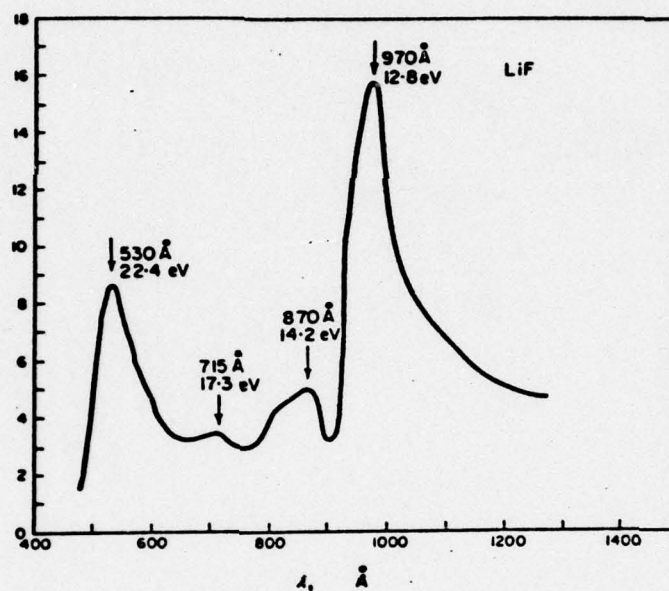
Fig. 48. Extreme u.v. reflection spectrum
of LiF. Measurements made at room tem-
perature at an angle of incidence of 20°.
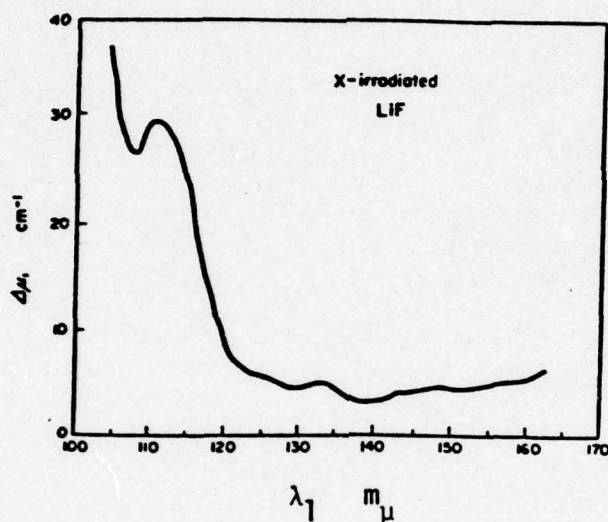
Fig. 49.   Incremental absorption of X-irradiated LiF.   Data
from a cleaved Harshaw crystal, irradiated for 2 hr at
35 kV and 20 mA with X-rays from a Cu target tube.   Samples
placed 8 cm from the beryllium exit window of the X-ray
tube were uniformly colored by this treatment.   The ordin-
ate represents the difference between the absorption
coefficients of the irradiated sample and an unirradiated
control sample.

c) Optical Constants under Ultrahigh Vacuum Conditions. [82,97-100]

The optical properties of evaporated barium films have been investigated in the wavelength range from 1500 to 3000 Å. The complex index of refraction is n' = n-ik, where n is the real part and k is the extinction coefficient. If we define here the complex dielectric constant

$$\varepsilon = (n^2 - k^2) - 2ink,$$

then

$$Im(1/\varepsilon) = 2nk/(n^2 - k^2)^2$$

and

$$Im\{1/(\varepsilon+1)\} = 2nk/\{(n^2 - k^2 + 1)^2 + 4n^2k^2\}.$$

Reflectance measurements were made at angles of incidence of 17.5° and 72.5° (Figure 50) and the complex index of refraction obtained from graphical solutions of the Fresnel reflection equations (Fig's. 51-53). The films were prepared in an ultrahigh-vacuum reflectometer (Fig. 54) having a base pressure of about 5 x 10^{-10} torr. Radiation from a hydrogen glow-discharge source was dispersed by a normal-incidence vacuum monochromator which was optically connected to the ultrahigh-vacuum system by means of a sapphire window (Fig. 55). The energy-loss function Im(1/ε), as computed from the optical constants, is compared with published characteristic electron-loss (CEL) data. The complex index of refraction was fitted to a Drude model for which the plasma energy was fixed at 7.4 eV and the damping at 1.6 x 10^{-16}sec. (Fig. 56).

Using the same apparatus as for the barium work described above, zirconium films were investigated. The reflectance for both parallel and perpendicularly polarized light was measured near the plasma frequency of Zr, and the ratio of R_p/R_S exhibited a peak at 790 Å (15.7 eV), while a character- istic energy loss of 15.6 eV was experimentally determined by Lynch and Swan, Austral. J. Phys. 21, 811 (1968), compared to a theoretical prediction of 15.4eV (Fig. 57).
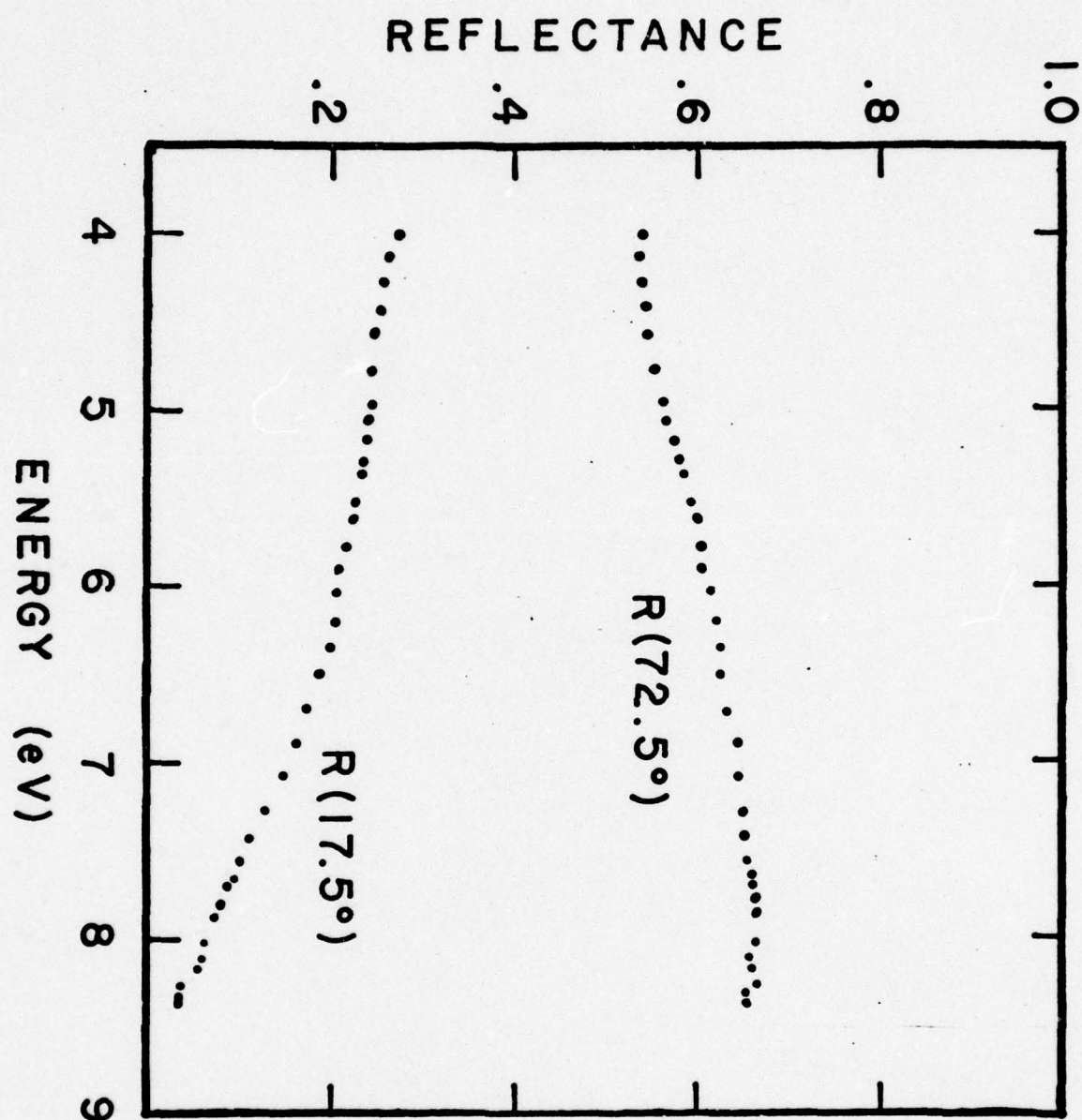
Fig. 50. Reflectance data for Barium.
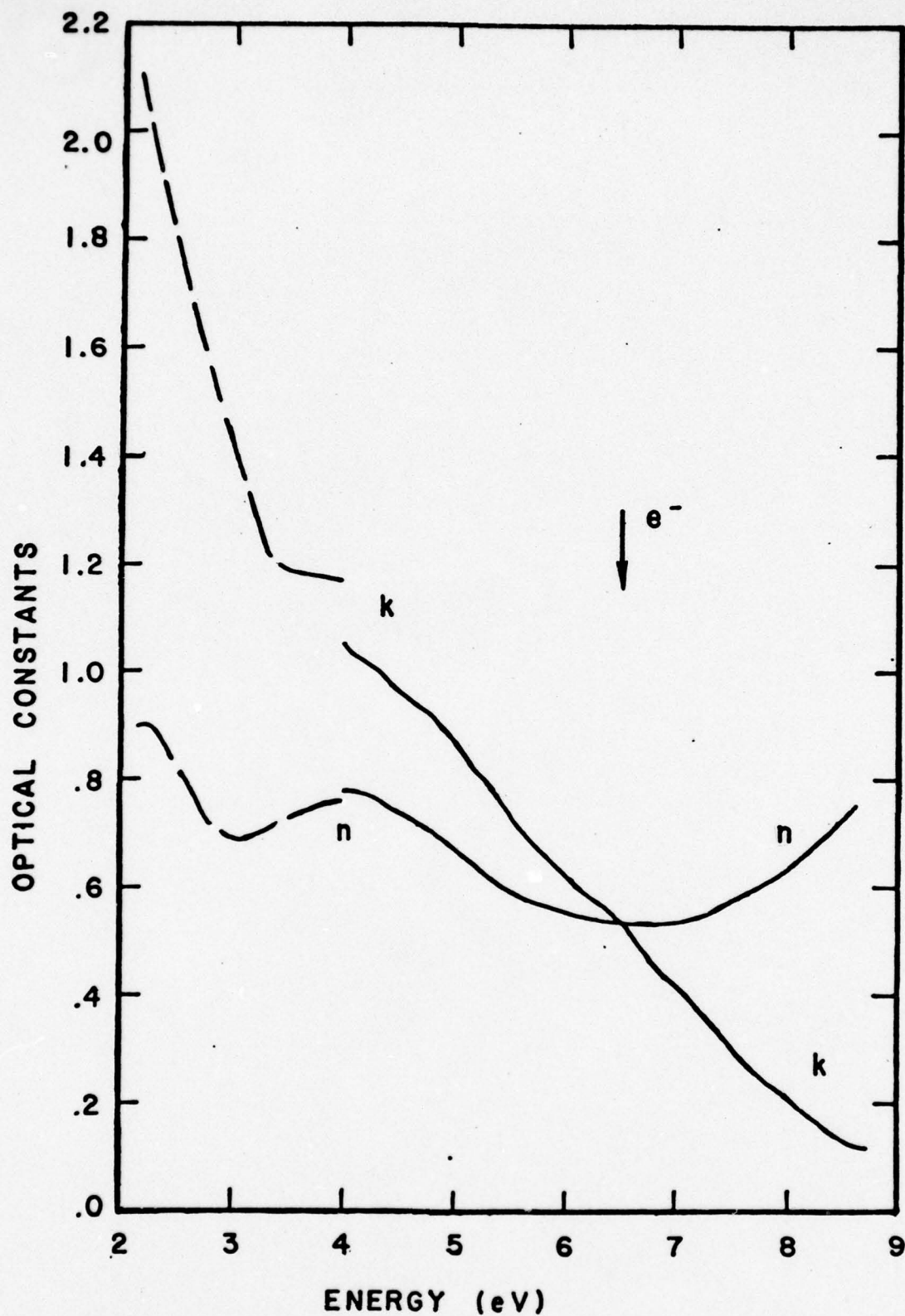
Fig. 51. Optical constants of Barium. The solid curves represent the present data. The dashed curves were obtained from Maurer. The flags indicate the effects of an assumed ± 10% polarization of the incident radiation.
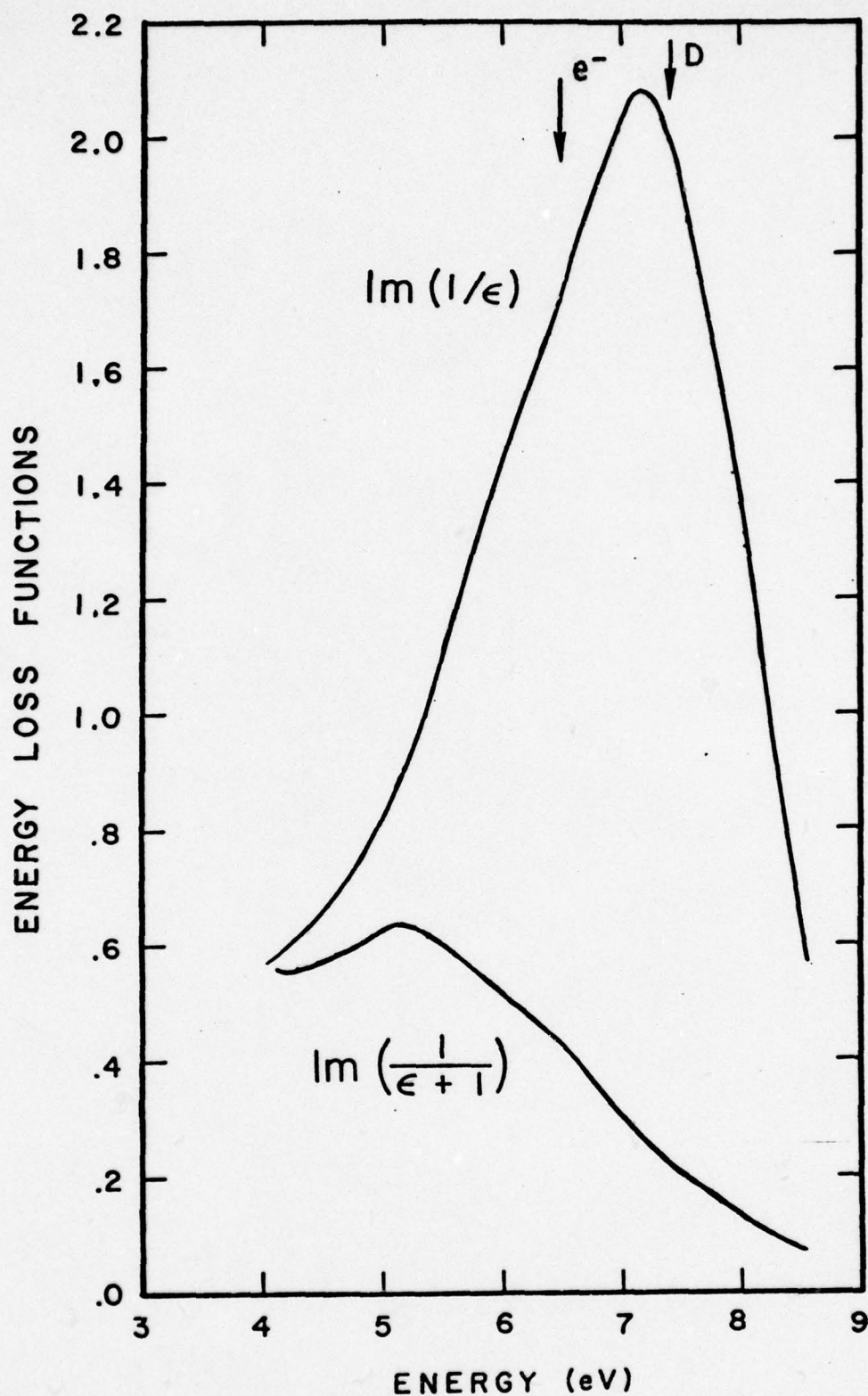
Fig. 52. Energy-loss functions for Barium. The upper curve is the bulk loss and the lower curve the surface loss. The arrow labeled e- is at 6.5 eV, the energy loss reported by Robins and Best, and the one labeled D at 7.4 eV corresponds to the plasma energy obtained for the curve fitting shown in Fig. 6
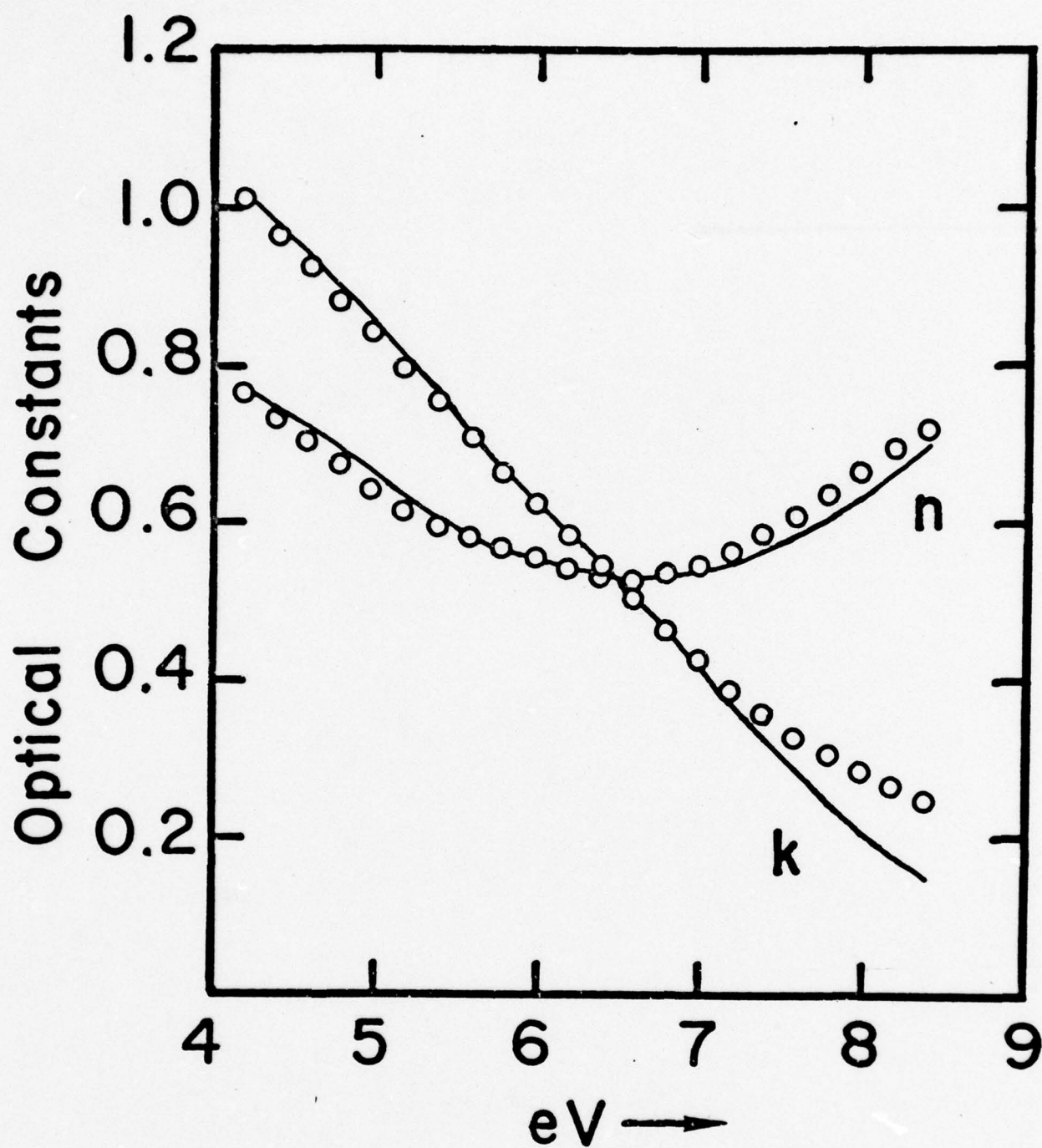
Fig. 53. The experimental data fitted to a Drude model having a plasma energy of 7.4 eV and a relaxation time of 1.6×10^{-16} sec. The solid curves are the experimental data, and the circles and dots represent points on the Drude curves.
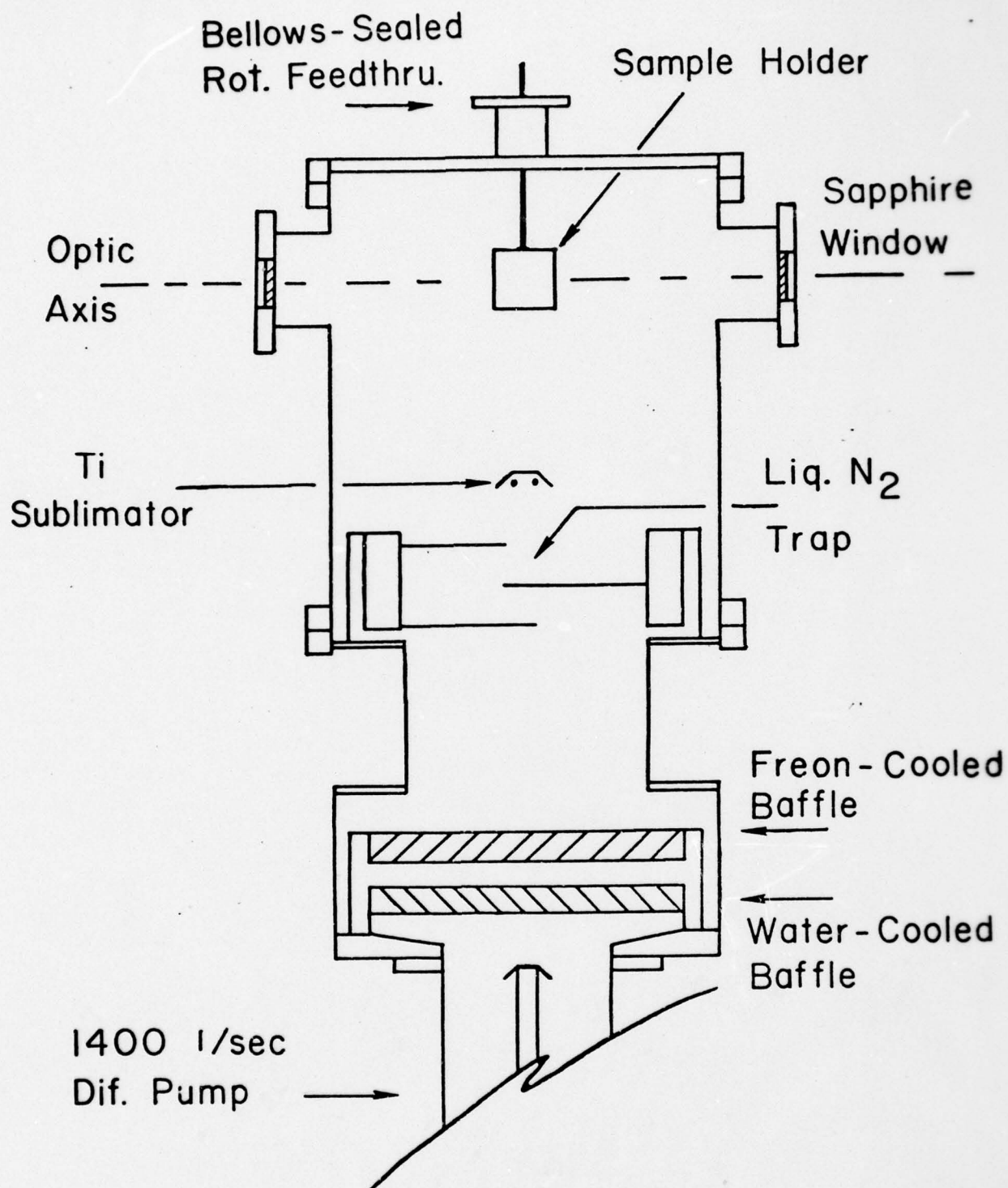
Fig. 54. Cross section of the reflectometer. The optic axis is indicated by the line of dashes through the sapphire windows and the experimental sample.
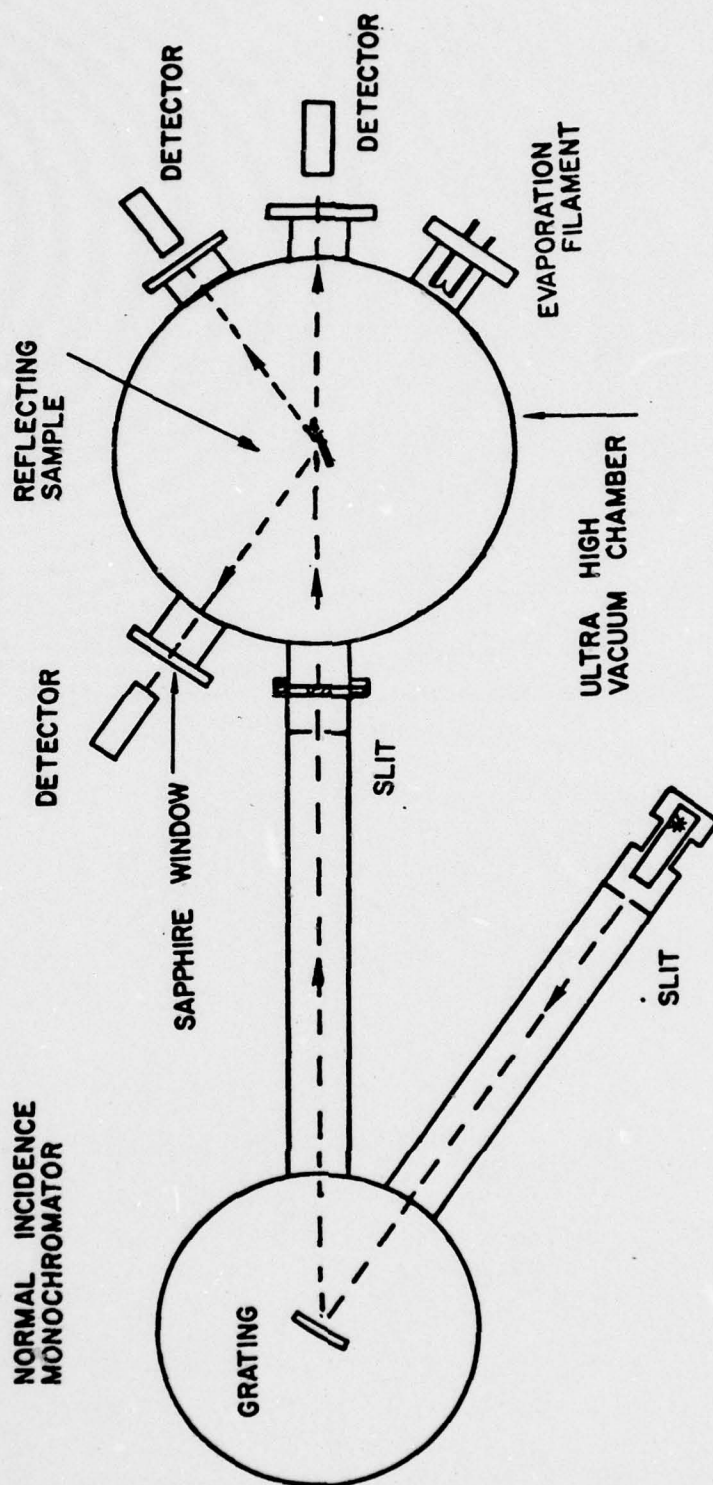
Fig. 55. Experimental arrangement. The right-hand circle represents the ultrahigh-vacuum reflectometer and the left-hand circle the normal-incidence monochromator. The exit arm of the monochromator is sealed to the reflectometer by means of an elastomer gasket. A sapphire window at this point isolates the relatively poor vacuum of the monochromator from the ultrahigh vacuum of the reflectometer. The movable detector is indicated outside the three exit ports of the reflectometer. The evaporator is shown on the remaining flange.
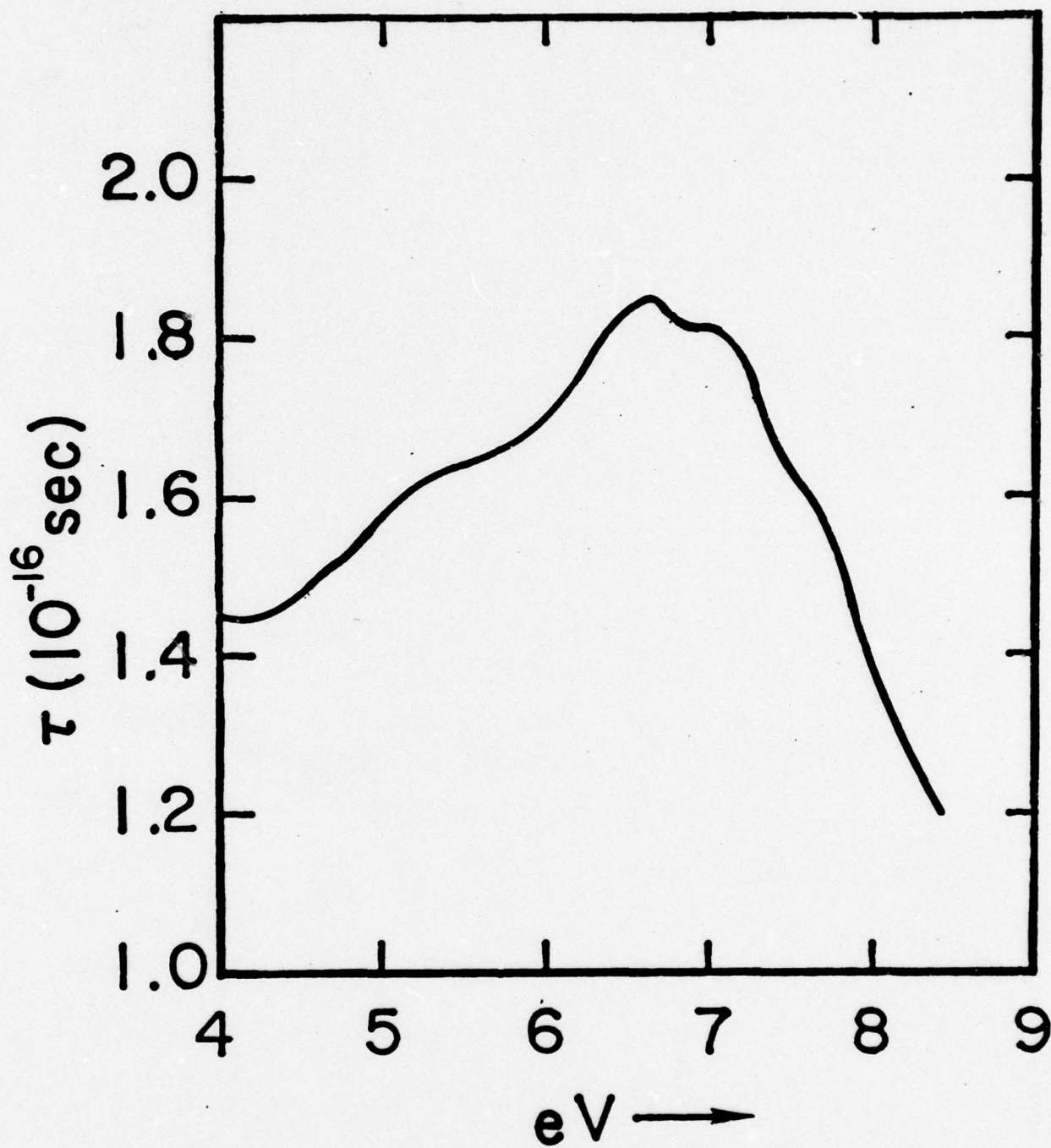
Fig. 56. The energy dependent relaxation time corresponding to curve fitting shown in the previous figure.
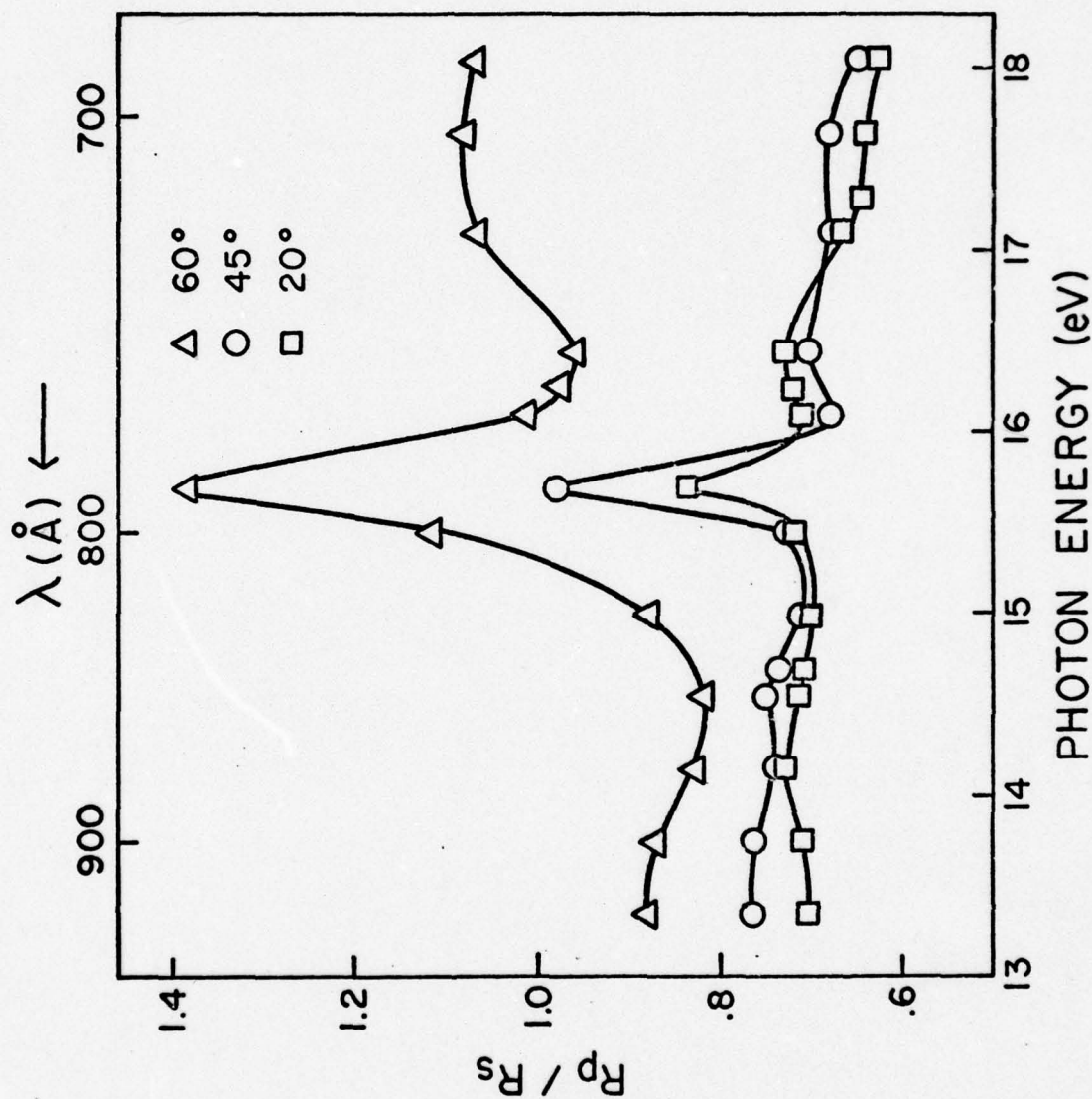
Fig. 57. Photon energy versus ratio of the reflectance for p-polarized (R_s) light of a Zr thin film of about 200 Å thickness for three angles of incidence.

d) Optical and Photoelectric Properties of Gold and Aluminum in the Extreme Ultraviolet Wavelength Region, to 173 Å. [92,95]

Continuing the type of research described on the previous pages, the optical and photoelectric properties of thin films of gold and aluminum have been investigated in the spectral region of 100 to 1000 Å. (See Fig. 58) Particular attention has been paid to the effects of polarization (Fig. 59) and angle of incidence on the total yield and energy distribution of the photoelectrons, Fig. 60. The reflectance, Fig.'s 61-64, which was measured as an essentially continuous function of the angle of incidence in order to obtain yields per absorbed photon, was also used in conjunction with the Fresnel relations to calculate the optical constants and polarization of the incident beam. To check these results, the polarization was measured directly, and in addition, the reflectance was measured at several angles of incidence with the plane of incidence rotated 90°. The calculated optical constants and the complementary polarization data were then used to predict the original reflectance curves. A spherical retarding potential system was employed to obtain data providing total yields, while an electron multiplier with a retarding grid system measured the photoelectron energy distribution, Fig. 60. It was found that the variation of photoelectric yield, Fig.'s 65-68, with angle of incidence depends promarily on the absorption depth of the photons, Fig.'s 69 & 70. The effect of the direction of polarization relative to the plane of incidence was small and could only be seen in terms of the yield of low energy photoelectrons, Fig.'s 71 & 72.
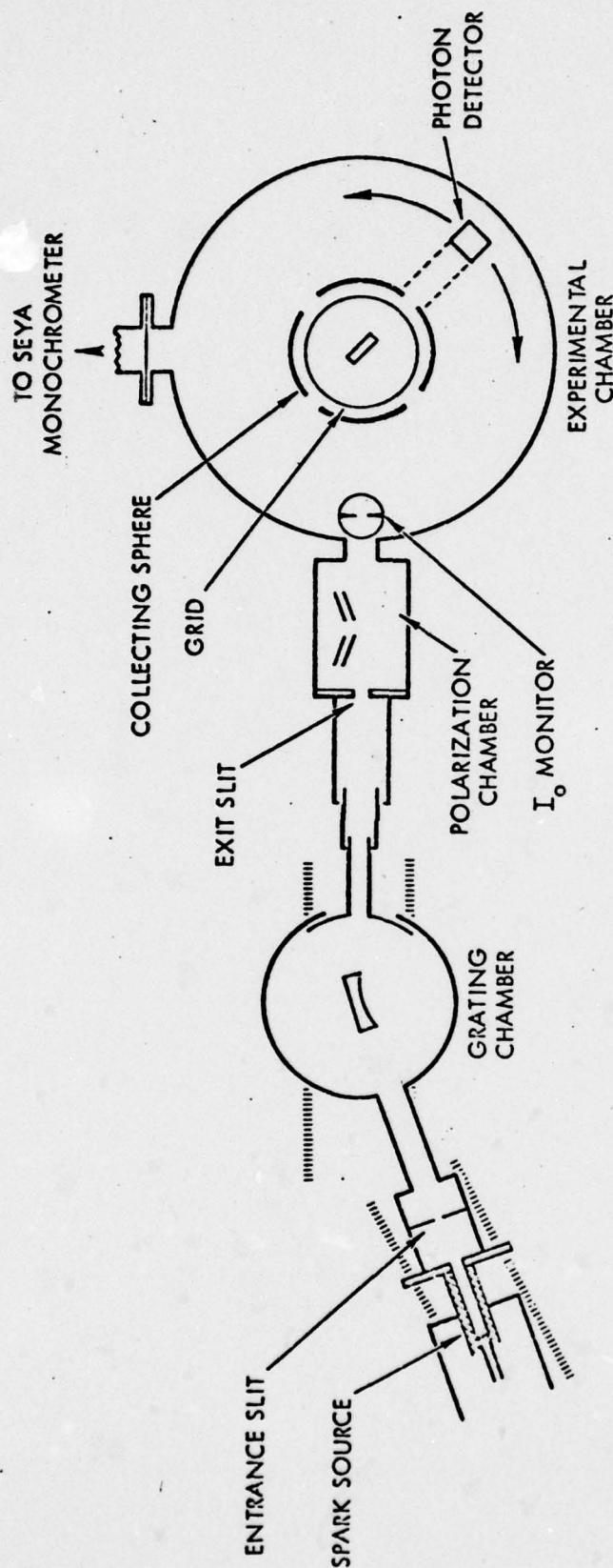
Fig. 58. The Vodar Grazing Incidence Monochromator and the Experimental Chamber. The desired monochromatic radiation is selected by moving the grating chamber to along the horizontal rails, the source and entrance slit assembly following along the diagonal rails. Both the length of the entrance arm and the angle of incidence remain constant. This radiation, whose polarization can be determined in the preliminary polarization chamber, is monitored for intensity fluctuation at the entrance of the experimental chamber. It then strikes the sample, and the reflectance and photoelectric properties of the sample are measured.
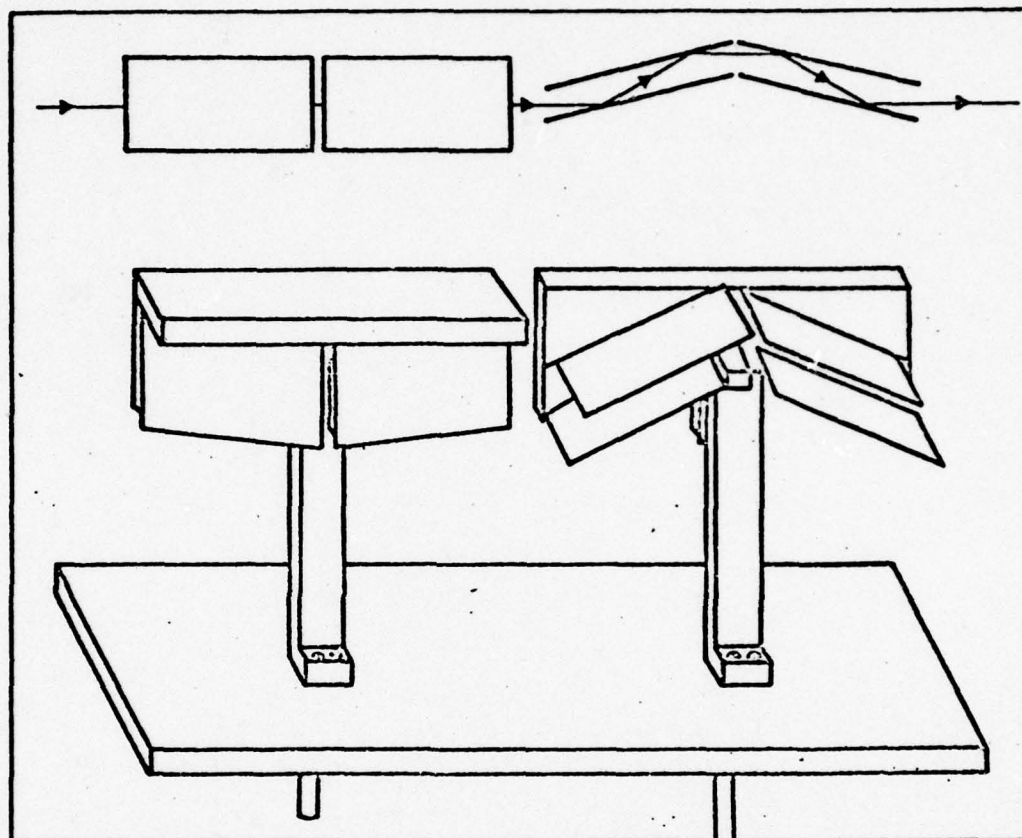
Fig. 59. The Polarizer-Analyzer System. The
polarizer and analyzer are shown in one of the two
crossed positions. By measuring the transmitted intensity
in the four possible orientations, the polarization of
the impinging beam can be determined assuming the
polarizer and analyzer are identical. The two different
crossed positions should have the same transmittance and
hence serve as a check on the required equality of the
polarizing efficiency of the two sections.
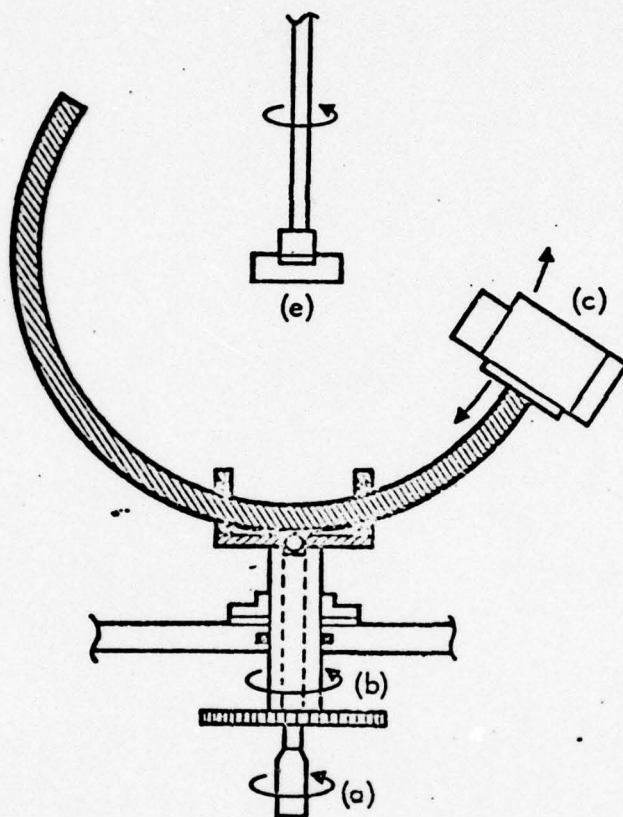
Fig. 60. The Scanning Electron Multiplier-
Retarding Potential System. The electron multiplier and
retarding system can be positioned so as to observe either
ultraviolet photons, or photoelectrons coming from the
sample in a continuous range of solid angles. The altitude
and azimuth of the electron multiplier (c), relative to
the sample (e) are varied by the rotations indicated
at (a) and (b), respectively.
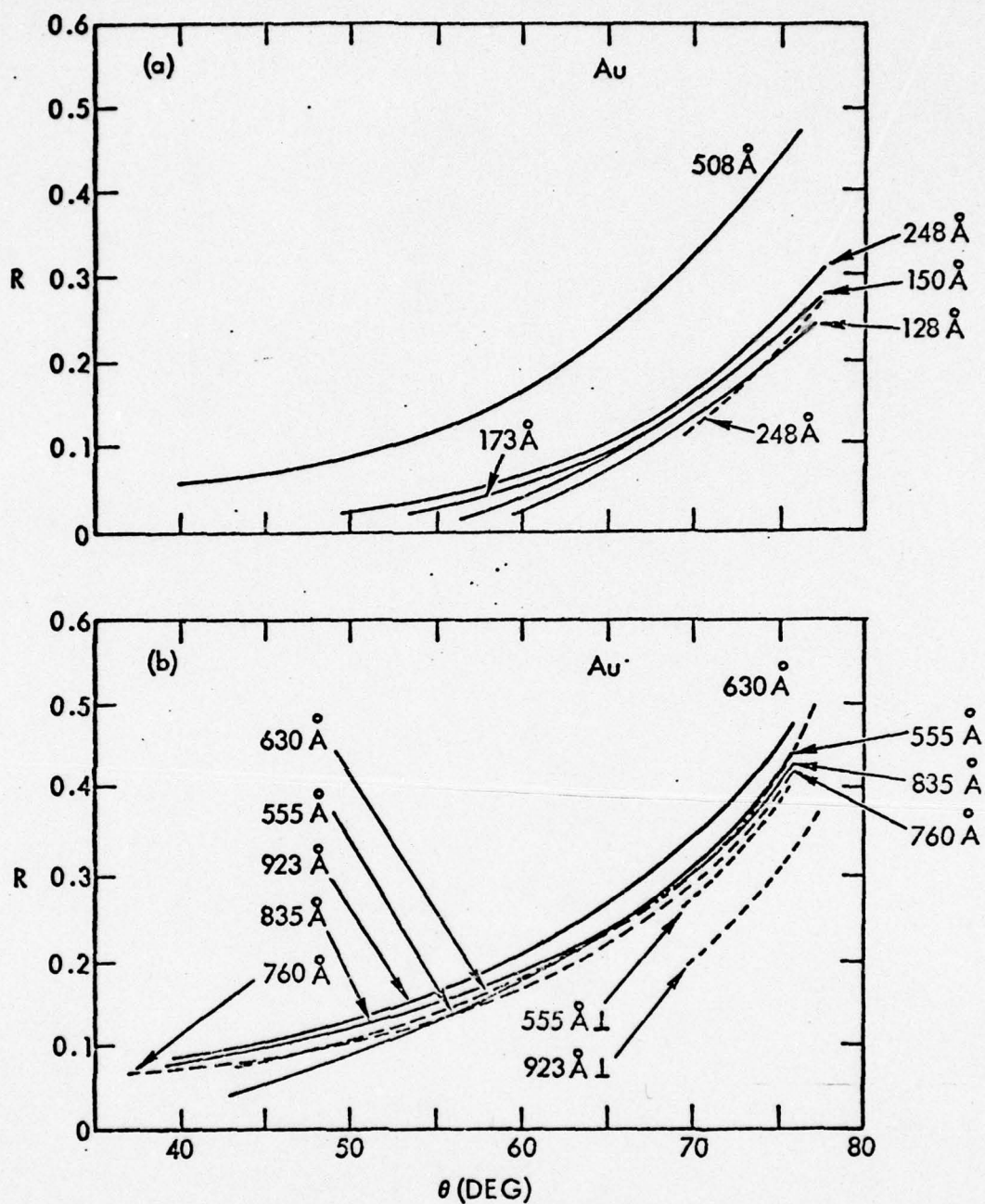
Fig. 61. Measured Reflectance of an Evaporated
Gold Film. The curves are labeled by the wavelength of
the incident photons, measured in angstroms. The dotted
curves are for the plane of incidence perpendicular to
the plane of incidence of the monochromator and are
correspondingly labeled by the ⊥ symbol after the
wavelength. For all other curves, the two planes of
incidence are identical.
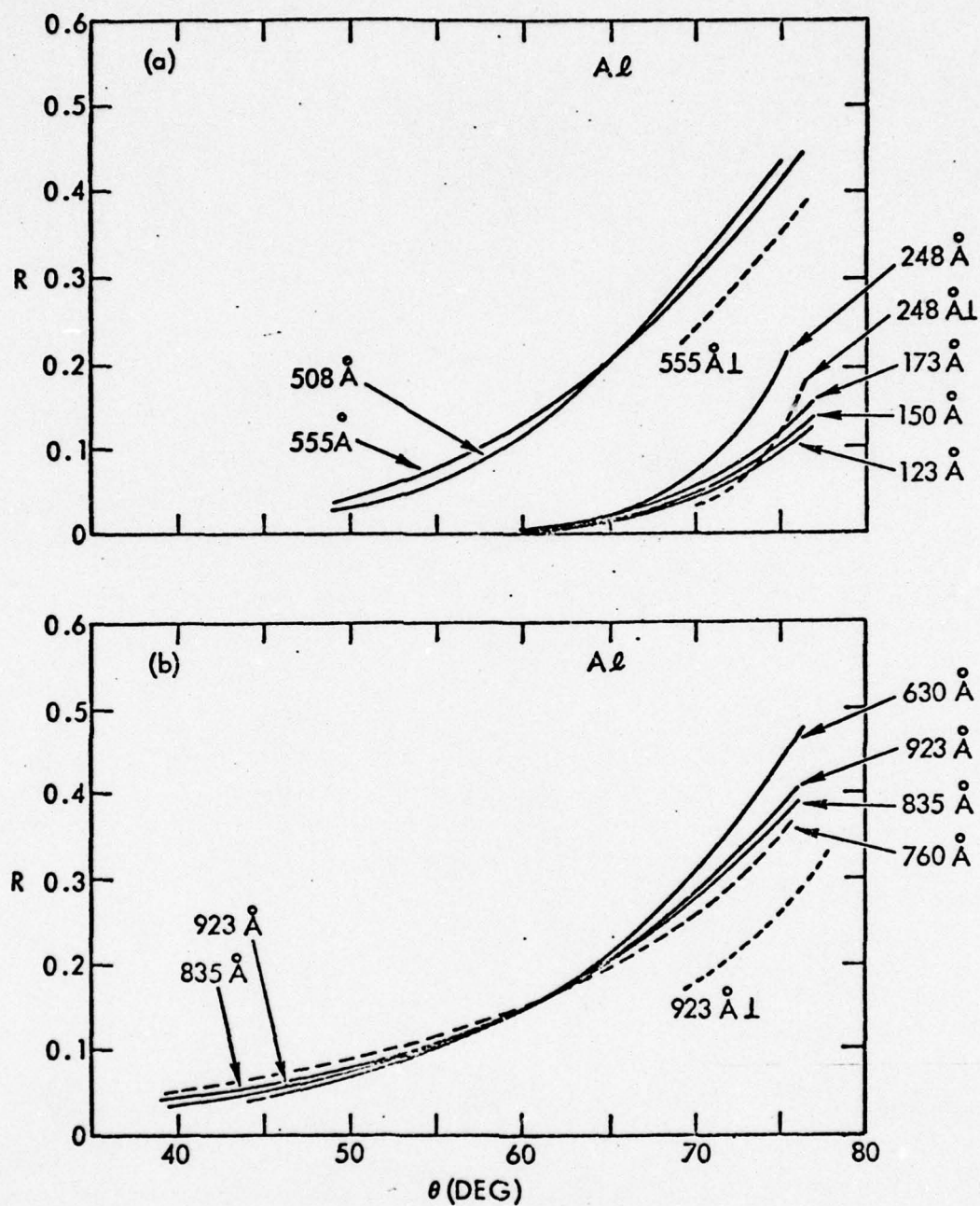
Fig. 62. Measured Reflectance of an Evaporated and Oxidized Aluminum Film. The curves are labeled as in the previous figure. The film had been oxidized by several days' exposure to the atmosphere.
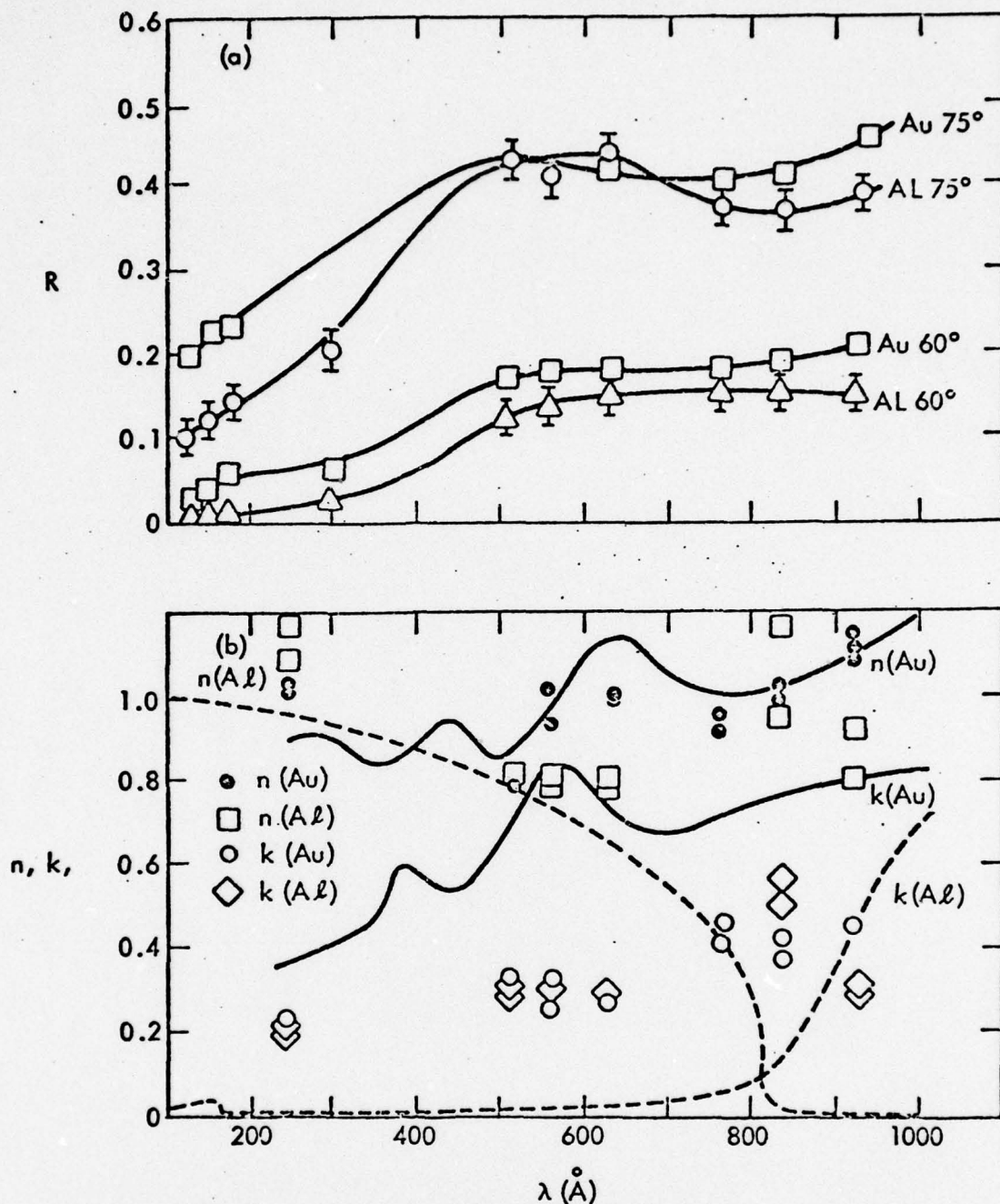
Fig. 63. Reflectance and Computed Optical
Constants of Gold and Aluminum. The curves in (a) give
the reflectances of the two films at 60° and 75°. The
points plotted in (b) show the values of n and k necessary
to produce the reflectance curves shown in Figs. 14 and
15. The solid and dashed curves show respectively the
variation of n and k for gold and aluminum as reported
by Hunter[19] and by Canfield, Hass and Hunter.[20]
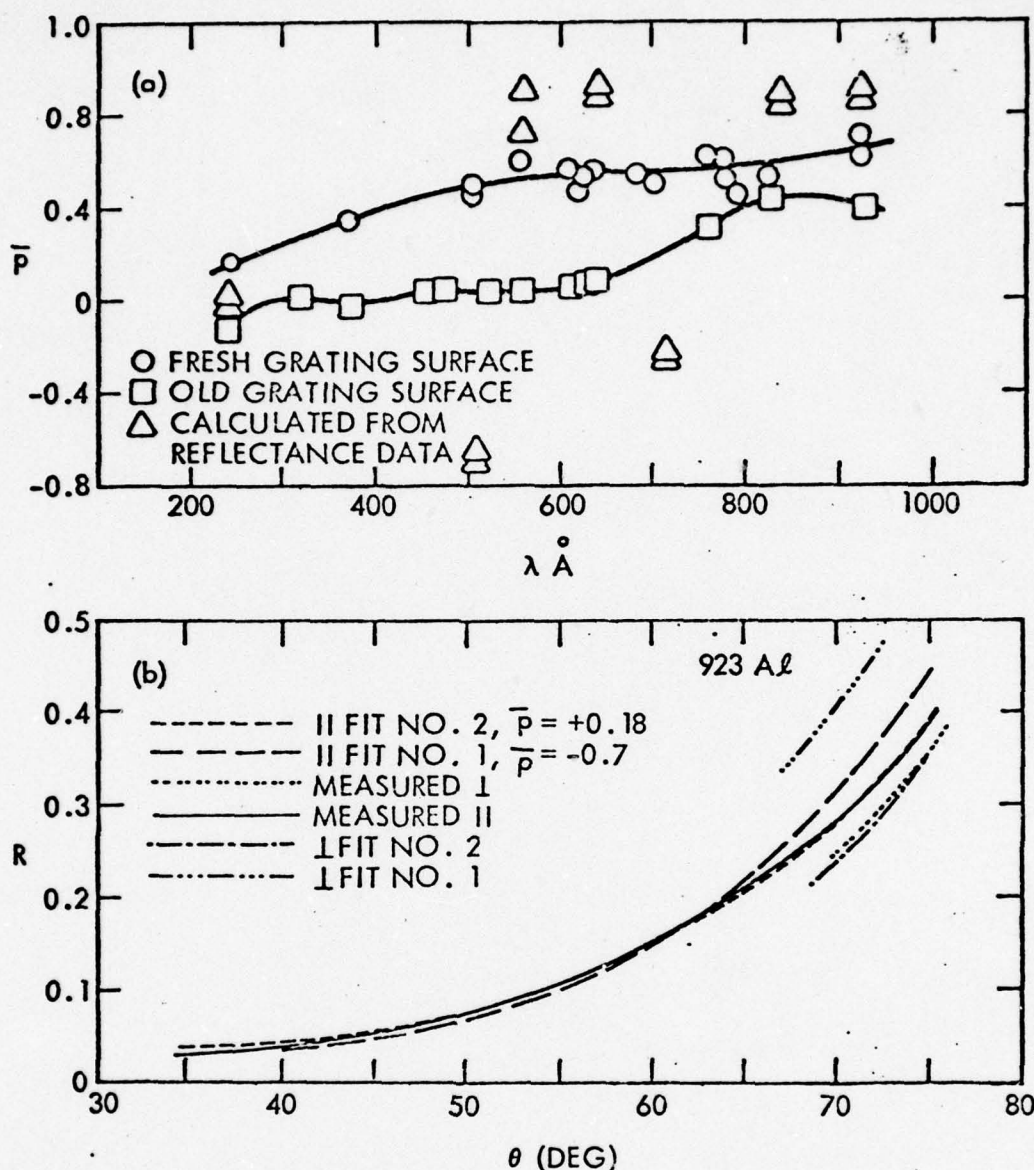
Fig. 64. Polarization Measurements and
Calculations. In (a) are shown the results of the
polarizer-analyzer measurements of the polarization of
the incident beam. The top curve is for freshly-cleaned
glass Siegbahn grating, while the lower one is for the
same surface about six months after cleaning. The effect
of grating contamination is then only moderately
noticeable in terms of scattered light background below
about 250Å. In (b) is shown several of the reflectance
curves seen previously in conjunction with computed
reflectance curves based on the calculated values of
n and k in Fig. 16. It was found that these curves are
very insensitive to polarization when both n and k can
be adjusted to optimize the fit.
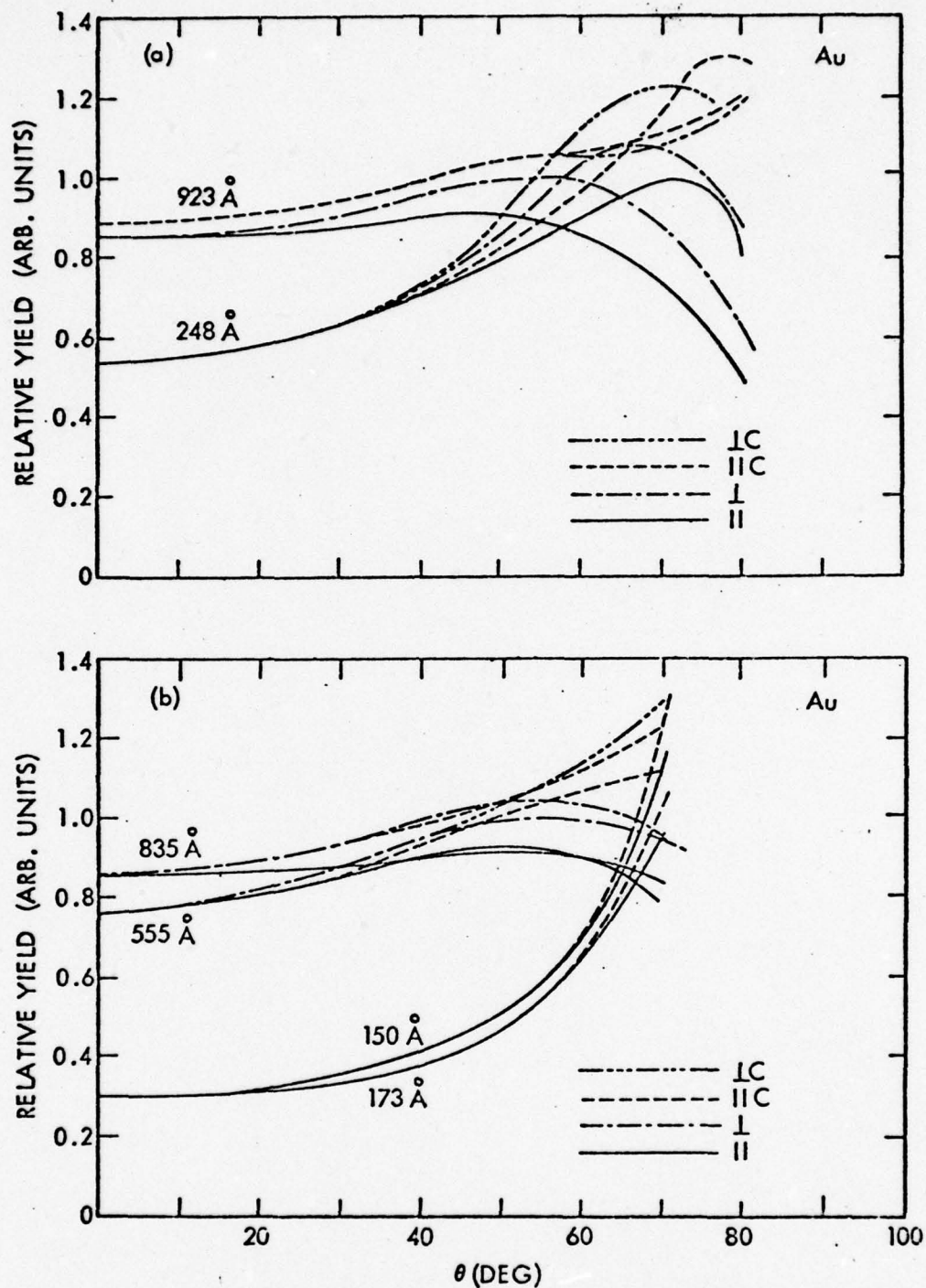
Fig. 65. Photoelectric Yield of Gold as a Function of the Angle of Incidence. The solid curves show the yield per incident photon as directly measured, while the dashed sections give the yield per absorbed photon.
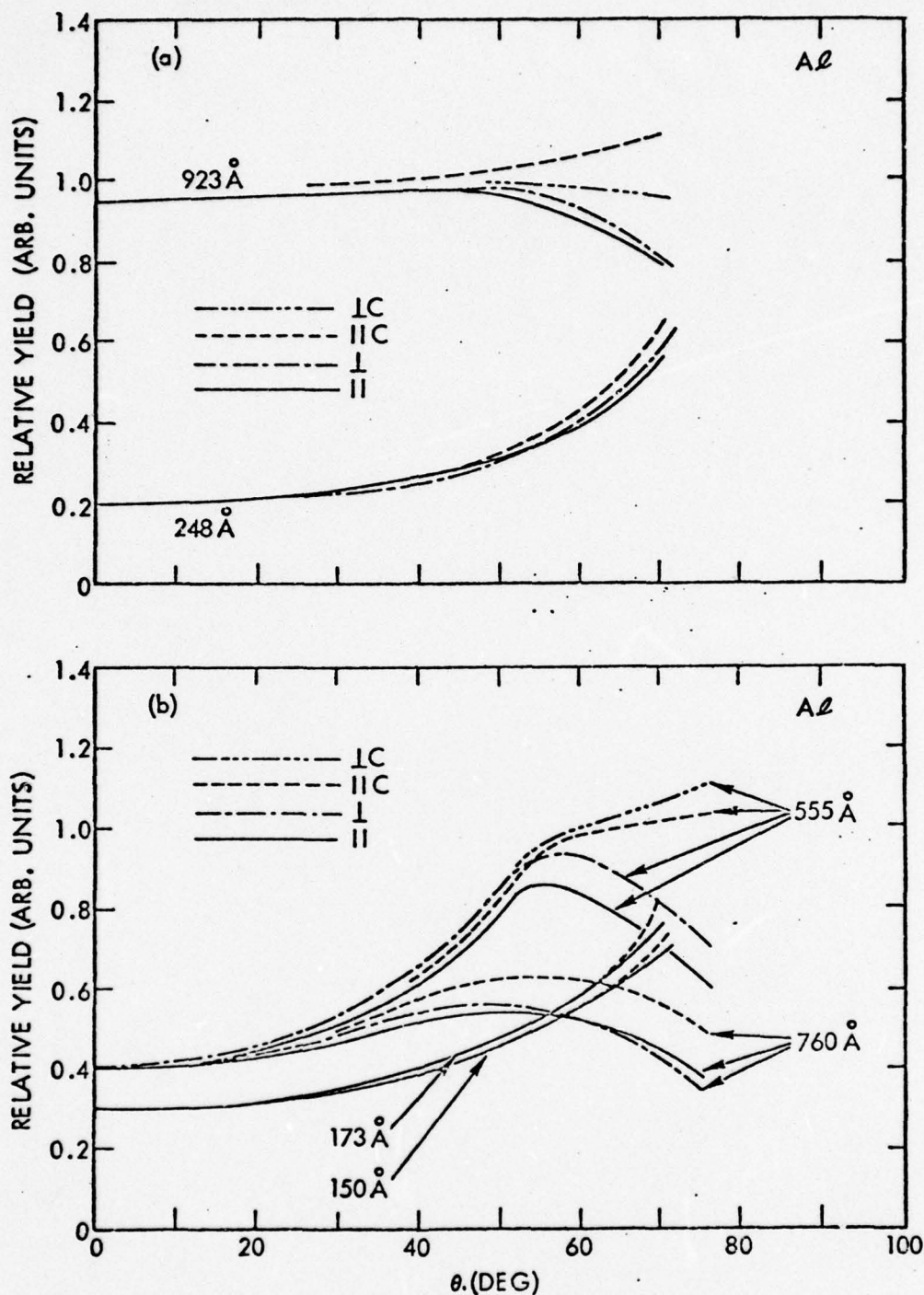
Fig. 66. Photoelectric Yield of Aluminum as a Function of The Angle of Incidence. The solid curves show the yield per incident photon while the dashed sections give the yield per absorbed photon. The effect of polarization in the yield per absorbed photon is small, but seems significant.
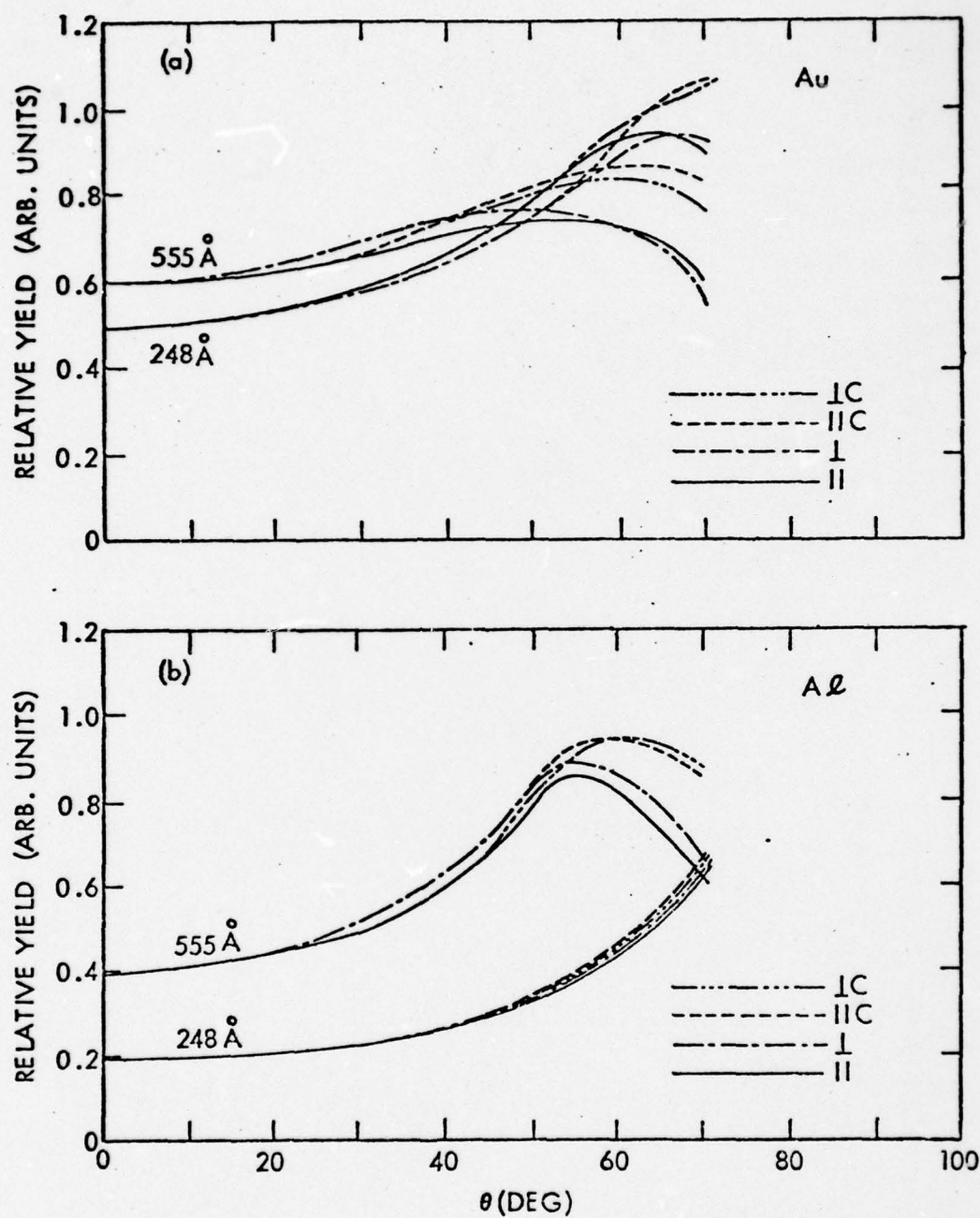
Fig. 67. The Yield of Photoelectrons with Energies Greater than a Few eV. The effects of polarization seem to have nearly vanished.
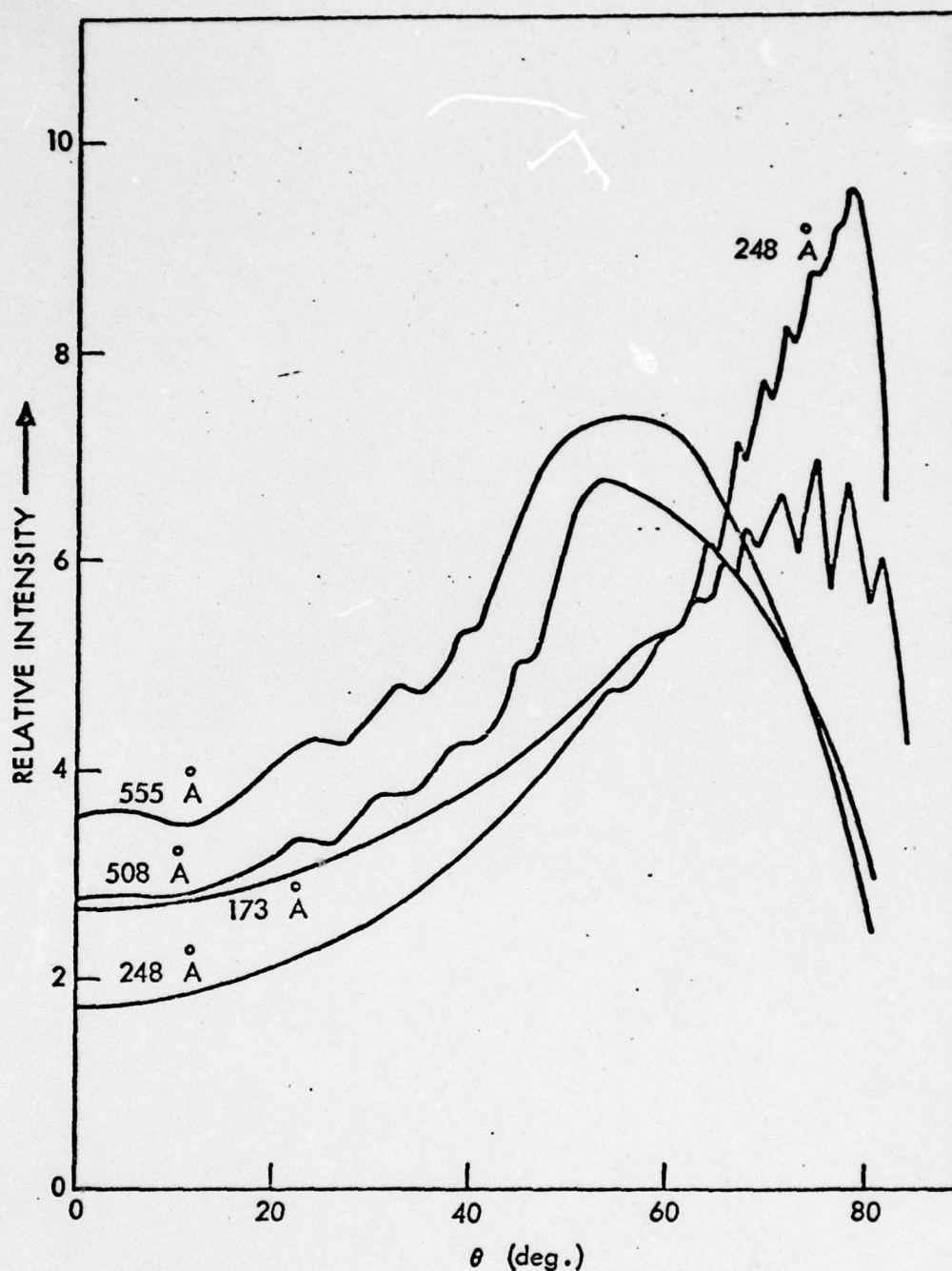
Fig. 68 . The Photoelectric Yield per Incident Photon of a Thin Aluminum Film. The structure is due to interference of the light reflected from the front and back surfaces. The spacing of the interference maxima and minima can be used to calculate both the index of refraction and the film thickness.
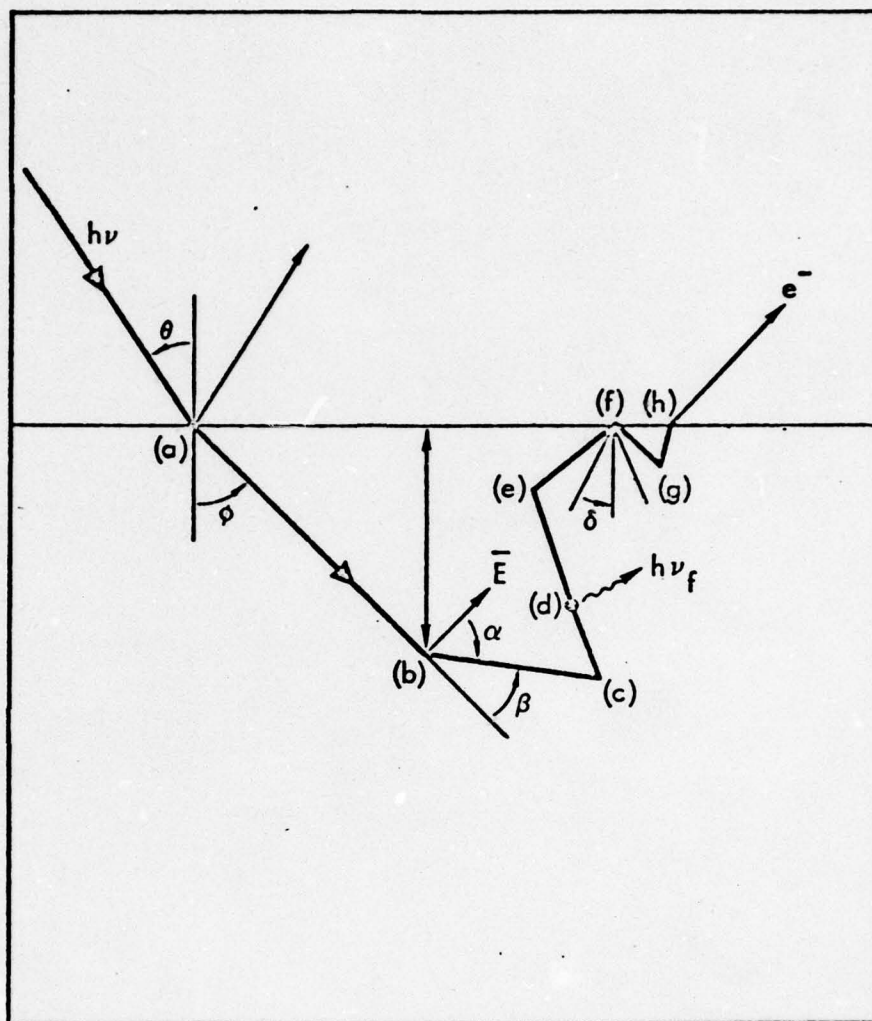
Fig. 69. Typical Processes in Photon Absorption and Photoemission. The incident photon is reflected or refracted at (a). At (b), the photon is absorbed producing an internal photoelectron whose initial direction may depend on both the local lattice orientation, and the polarization of the photon. The electron is scattered elastically at (c) and at (d) makes a direct transition to a lower energy band. At (e) the electron is inelastically scattered toward the surface with an angle of incidence greater than the maximum escape angle δ, and at (f) is totally reflected. At (g) it is scattered to within the escape cone, and at (h) escapes from the solid, after being refracted away from the normal.
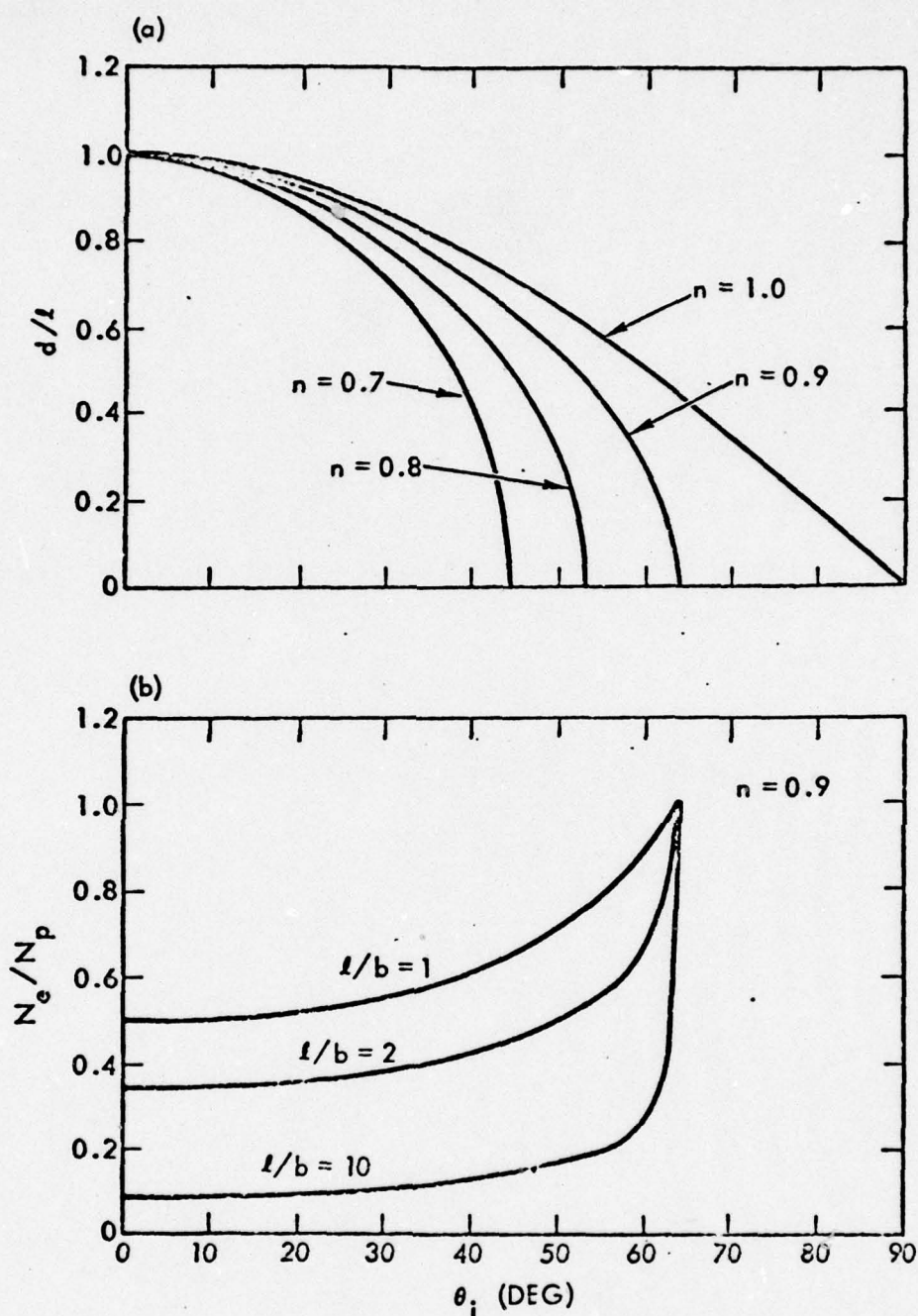
Fig. 70. The Effect of Absorption Depth on
Photoelectric Yield. The curves in (a) give the mean
absorption depth d, relative to the photon mean free
path ℓ, as a function of the angle of incidence for
various refractive indices. In (b) the calculated yield
per absorbed photon of photoelectrons of mean free path
b is shown for various ratios of mean free paths ℓ/b.
These curves are for a medium of refractive index
n = 0.9.
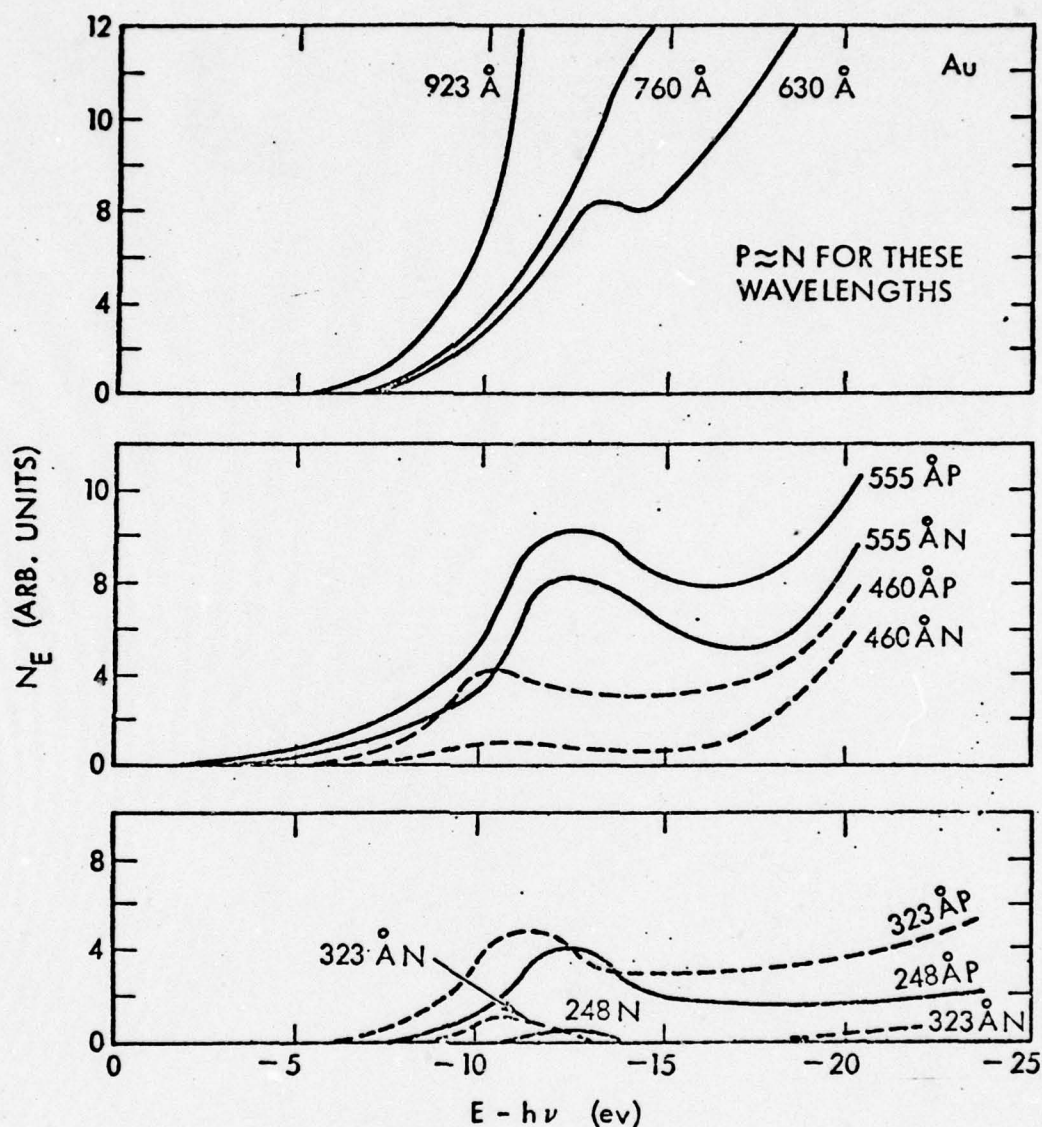
Fig. 71 . Energy Distribution of Photoelectric
from Gold. In most cases curves are given for both normal
incidence and the angle of incidence giving the peak
yield per incident photon, identified by N and P,
respectively. In order to compare the shape and energy
loss of the higher energy electrons, the abscissa shows
the energy difference between the photoelectron and the
incident photon.
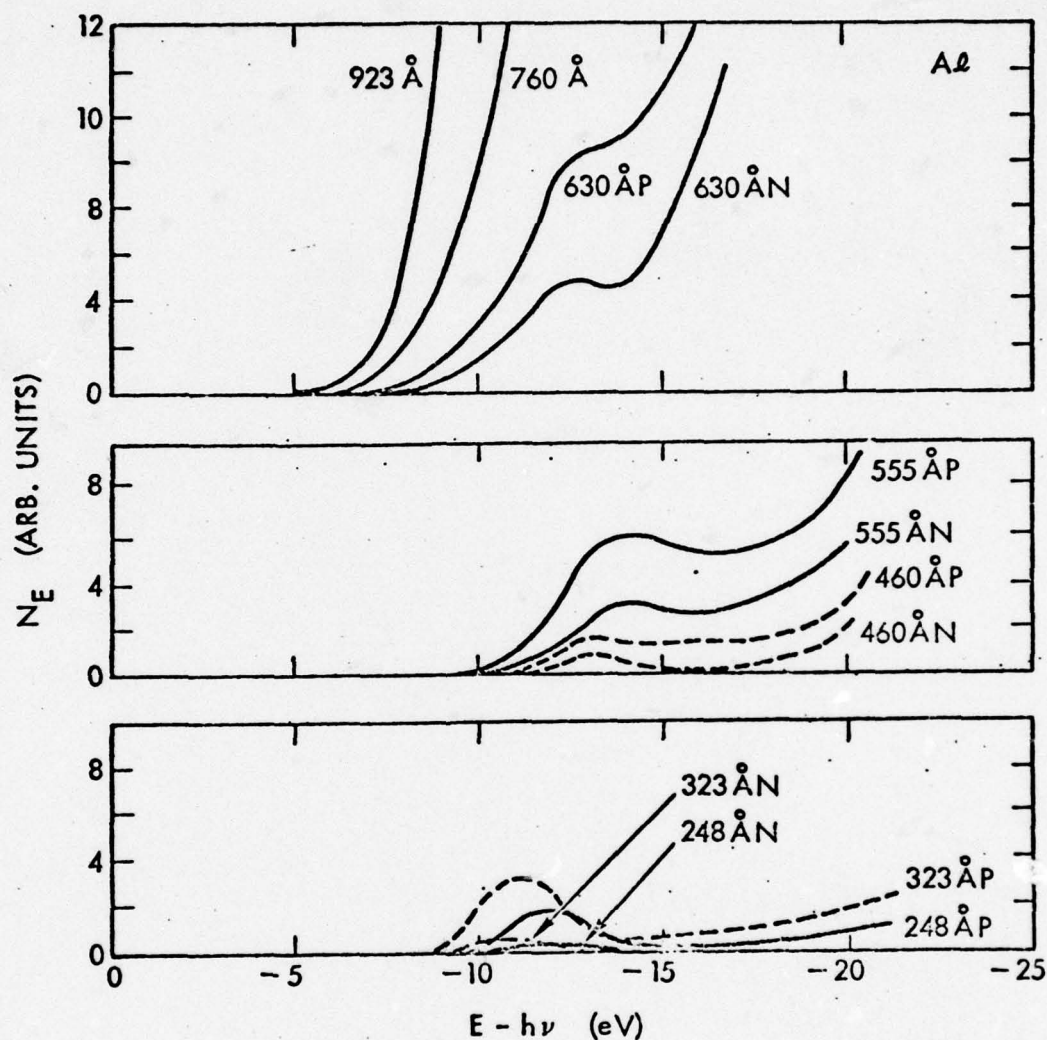
Fig. 72. Energy Distribution of Photoelectrons from Aluminum. In most cases, curves are given both for normal incidence and for the angle of incidence giving the peak yield per incident photon, as indicated by N and P, respectively. In order to compare the shape and energy loss of the higher energy electrons, the abscissa shows the energy difference between the photoelectron and the incident photon.

e) <u>The Efficiency of Concave Gratings in the Extreme Ultraviolet Region, to 150Å.</u> [90]

Using the same instrumentation as in d) above, Fig.'s 46-48, the efficiency of five blazed and two Siegbahn type gratings has been measured in the wavelength range of 150 Å to 1000 Å. In particular, data are presented for angles of incidence varying in 5° increments from normal to 80° for the four wavelengths, 150, 248, 555 and 923 angstrom units. Three of these gratings were replicas of the same master, having different surface coatings, Pt, Au, and Al, in order to allow particular attention to be paid to the effect of material on grating efficiency. The results are shown to be consistent with a simple model giving the overall efficiency as the product of the reflectance and a geometrical efficiency depending only on the structure of the grating surface. It is also concluded that light reflected from the grooves of the Siegbahn type gratings contributes substantially to the performance of these gratings.

*[90]

IV. <u>CONCLUDING REMARKS</u>

For those readers of this report, which in a general way characterizes the types of thinking of this era, it should be pointed out in all fairness that a new wave of research, a rejuvenation if you please, was started in the mid-sixties, couriously enough with the advent of a new light source for vacuum uv, soft and hard X-rays, namely synchrotron radiation, first proposed by the late Professor D. H. Tomboulian of Cornell University and first translated into an effective research group at the

Deutsche Elektronen-Synchrotron (DESY)

in Hamburg under the leadership of Prof. R. Haensel.

This was followed rapidly by other such user groups being established at NBS, the University of Wisconsin, and Stanford in the late sixties and early seventies in the USA, at Daresbury in England, in Tokyo, at Orsay in France, in Bonn and most recently in West-Berlin, and in other places. (Unfortunately, this writer is not sufficiently well informed about similar efforts in the Soviet Union.)

Such local users groups, each made up of investigators from many different institutions and universities, have developed because of close contact and cross-fertilization of ideas into effective nuclei of expanding research horizons. It must be sufficient to mention at this point only two new and exciting directions, namely aspects of surface physics and macromolecular investigations in biological systems.

The reader who is interested in more detailed surveys of these synchrotron radiation research activities should try to obtain the readily available programs of the various user group meetings and/or the published proceedings of the IVth (in Hamburg in 1974) and Vth (in Montpellier in 1977) International Conference on Vacuum UV Radiation Physics.

PUBLICATIONS OF G. L. WEISSLER AND ASSOCIATES

Department of Physics
University of Southern California
Los Angeles, California   90007

(Phys. Soc. Meeting Abstracts (A), Letters-to-the-Editor (L), and Technical Reports
are included only if no full-length paper has been published.)

1. "Positive and Negative Corona in Pure and Impure Hydrogen, Nitrogen, and
    Argon," G. L. Weissler, Phys. Rev. 63, 96 (1943).

2. "Apparent Breakdown of Meek's Criterion due to Failure of Townsend's Func-
    tion," L. Fisher and G. L. Weissler, Phys. Rev. 66, 95 (1944).

3. "Electrodeless Discharges at High Frequencies and Low Pressures," Nisewanger,
    Holmes, and Weissler, J. Opt. Soc. Am. 36, 581 (1946).

4. "Positive Corona in Freon-Air Mixtures," E. I. Mohr and G. L. Weissler, Phys.
    Rev. 72, 289 (1947).

5. "Negative Corona in Freon-Air Mixtures," G. L. Weissler and E. I. Mohr, Phys.
    Rev. 72, 294 (1947).

6. "Sensitivity of a Positive Ion Space-Charge Detector," R. R. Eggleston and
    G. L. Weissler, Phys. Rev. 78, 91 (1950).   (A)

7. "Ion Pulses in the Positive Ion Space-Charge Detector," N. Wainfan and
    G. L. Weissler, Phys. Rev. 82, 569 (1951).   (A)

8. "Absolute Absorption Coefficients of Nitrogen in the Vacuum Ultraviolet,"
    G. L. Weissler, Po Lee and E. I. Mohr, J. Opt. Soc. Am. 42, 84 (1952).

9. "Absorption Coefficients of Oxygen in the Vacuum Ultraviolet," G. L. Weissler
    and Po Lee, J. Opt. Soc. Am. 42, 200 (1952).

10. "A Semi-Automatic Graphical Computer with Use in Spectroscopy," G. L. Weissler,
    A. E. Einarsson, and J. McClelland, Rev. Scien. Instr. 23, 209 (1952).

11. "A Constant Intensity Vacuum Spectroscopic Light Source, G. L. Weissler,
    J. Opt. Soc. Am. 42, 80 (1952).

12. "On the Absolute.Absorption of Radiation by Molecular Nitrogen and Oxygen
    Between 300 A and 1300 A," G. L. Weissler, Mem. Soc. Roy. Sci. Liege 12,
    281 (1952).

13. "Absolute Absorption of the H_2 Continuum," Po Lee and G. L. Weissler, Astro-phys. J. <u>115</u>, 570 (1952). (L)

14. "An Estimate of the Energies of the Positive Ions in a Negative Point-to-Plane Corona," G. L. Weissler and Mark Schindler, J. Appl. Phys. <u>23</u>, 844 (1952).

15. "Work Functions of Gas-Coated Tungsten and Silver Surfaces," G. L. Weissler, and T. N. Wilson, J. Appl. Phys. <u>24</u>, 472 (1953).

16. "The Characteristics of Ultraviolet-Sensitized Photographic Plates in the Vacuum Ultraviolet," Po Lee and G. L. Weissler, J. Opt. Soc. Am. <u>43</u>, 512 (1953).

17. "The Photoionization Cross Section of Neon," Po Lee and G. L. Weissler, Proc. Roy. Soc. Lond., Ser. <u>A219</u>, 71 (1953); also J. Opt. Soc. Am. <u>42</u>, 214 (1952). (L)

18. "Preliminary Results on Photoelectric Yields of Pt and Ta and on Photoioniza-tion in O_2 and N_2 in the Vacuum Ultraviolet," N. Wainfan, W. C. Walker, and G. L. Weissler, J. Appl. Phys. <u>24</u>, 1318 (1953).

19. "Energy Distributions of Photoelectrons from Au and Ge in the Far Ultraviolet, W. C. Walker and G. L. Weissler, Phys. Rev. <u>97</u>, 1178 (1955). (L)

20. "Absorption Cross Sections of Methane and Ammonia in the Vacuum Ultraviolet," H. Sun and G. L. Weissler, J. Chem. Phys. <u>23</u>, 1160 (1955).

21. "Absorption Cross Sections of CO_2 and CO in the Vacuum Ultraviolet," H. Sun and G. L. Weissler, J. Chem. Phys. <u>23</u>, 1625 (1955).

22. "Absorption Cross Sections of Argon and Helium in the Region of Their Respective Ionization Continua," Po Lee and G. L. Weissler, Phys. Rev. <u>99</u>, 540 (1955).

23. "Photoionization Efficiencies and Cross Sections in O_2, N_2, CO_2, A, H_2O, H_2, and CH_4," N. Wainfan, W. C. Walker, and G. L. Weissler, Phys. Rev. <u>99</u>, 542 (1955).

24. "Photodissociation and Photionization of O_2 as Inferred from Measured Absorp-tion Coefficients," Po Lee, J. Opt. Soc. Am. <u>45</u>, 703 (1955).

25. "Absorption Coefficients of Nitric Oxide in the Vacuum Ultraviolet," H. Sun and G. L. Weissler, J. Chem. Phys. <u>23</u>, 1372 (1955). (L)

26. "Photoelectric Yields in the Vacuum Ultraviolet," W. C. Walker, N. Wainfan, and G. L. Weissler, J. Appl. Phys. $\underline{26}$, 1366 (1955).

27. "Photoionization Cross Sections in NO and N_2O," W. C. Walker and G. L. Weissler, J. Chem. Phys. $\underline{23}$, 1962 (1955). (L)

28. "Preliminary Data on Photoionization Efficiencies and Cross Sections in C_2H_2, and C_2H_4," W. C. Walker, and G. L. Weissler, J. Chem. Phys. $\underline{23}$, 1547 (1955). (L)

29. "Photoionization Efficiencies and Cross Sections in NH_3," W. C. Walker and G. L. Weissler, J. Chem. Phys. $\underline{23}$, 1540 (1955). (L)

30. "The Ultraviolet Absorption of Atomic Nitrogen in its Ionization Continuum," A. W. Ehler and G. L. Weissler, J. Opt. Soc. Am. $\underline{45}$, 1035 (1955).

31. "The Absorption of Thin Films in the Vacuum Ultraviolet," G. L. Weissler and L. Maudlin, paper presented at the Amer. Phys. Soc. Meeting, Dec. 28 to 30, 1955, at U.S.C., Los Angeles, California.

32. "Photoionization in Gases," G. L. Weissler, invited paper presented at the annual Amer. Phys. Soc. Meeting, Jan. 30 to Feb. $\underline{3}$, 1956, New York, New York.

33. "Photionization in Gases and the Photoelectric Effect from Solids," G. L. Weissler, Chapter 24, Vol. $\underline{21}$, p. 304, Handbuch der Physik, Springer Verlag, Berlin: 1956.

34. "Photoionization in Gases and Photoemission from Surfaces, G. L. Weissler, invited paper presented at the "Third International Conference of Ionization Phenomena," June 11-17, 1957, in Venice, Italy, held under the auspices of the Italian Physical Society. Paper was published in a special volume of the Conference Proceedings in Milan, October, 1957.

35. "Optical Properties of Al for hv between 10 and 26 eV, W. C. Walker, J. A. R. Samson, O. P. Rustgi, and G. L. Weissler, J. Opt. Soc. Am. $\underline{48}$, 71 (1958).

36. "Absorption Coefficients of O_3 in the Vacuum Ultraviolet Region," M. Ogawa, G. R. Cook, and G. L. Weissler, J. Chem. Phys. $\underline{28}$, 173 (1958).

37. "Absorption Coefficients of Methyl, Ethyl, n-Propyl, and n-Butyl Alcohols," M. Ogawa, G. R. Cook, and G. L. Weissler, J. Chem. Phys. $\underline{28}$, 747 (1958).

38. "Absorption Coefficients of C_6H_6 and H_2 in the Vacuum Ultraviolet," S. M. Bunch, G. R. Cook, M. Ogawa, A. W. Ehler, and G. L. Weissler, J. Chem. Phys. $\underline{28}$, 740 (1958).

39. "Photoionization Analysis by Mass Spectroscopy," G. L. Weissler, G. R. Cook, M. Ogawa, and J. A. R. Samson, Bull. Am. Phys. Soc. 3, 259 (1958). (A)

40. "Mass Analysis of Photionization Products in N_2 and N_2O," G. L. Weissler, J. A. R. Samson, and G. R. Cook, Bull. Am. Phys. Soc. 3, 413 (1958). (A)

41. "Vacuum U.V. Optical and Photoelectric Properties of Evaporated Metal Films," G. L. Weissler, W. C. Walker, and O. P. Rustgi, Bull. Am. Phys. Soc. 3, 414 (1958).(A)

42. "Photon Absorption Mechanisms and Electrical Discharges Through Gases," G. L. Weissler, Invited paper, Bull. Am. Phys. Soc. 3, 420 (1958).

43. "Optical Transmissions of Evaporated In, Sn, and Bi Films in the Vacuum U.V." G. L. Weissler, W. C. Walker, and O. P. Rustgi, J. Opt. Soc. Am. 48, 1017 (1958). (L)

44. "Photoionization Analysis of 10 Gases by Mass Spectroscopy," G. L. Weissler, J. A. R. Samson, M. Ogawa, and G. R. Cook, J. Opt. Soc. Am. 49, 338 (1959).

45. "Optical and Photoelectric Properties of Thin Metallic Films (8 Metals) in the Vacuum U.V.," G. L. Weissler, W. C. Walker, and O. P. Rustgi, J. Opt. Soc. Am. 49, 471 (1959).

46. "Photoionization Induced Ion-Molecule Reactions in H_2, CH_4, and an N_2-H_2 Mixture," G. L. Weissler, G. Cook, and J. A. R. Samson, U.S.C. Technical Report, 1959 (see also ref. 50, p. 5).
    Gilbert R. Cook, Ph.D. Dissertation, Univ. of So.Calif.,Los Angeles, June 1959.

47. "Optical Transmission of Sb, Te, and Other Films in the Vacuum U.V.," G. L. Weissler, W. C. Walker, and O. P. Rustgi, Bull. Am. Phys. Soc. 4, 226 (1959). (A)

48. "Methods of Experimental Physics," J. R. Holmes and G. L. Weissler, Vol. I, Part 7: OPTICS, Academic Press, Inc., New York, 1959.

49. POOK REVIEW of "The Photoelectric Effect and its Applications," by R. Suhrmann and H. Simon, Springer-Verlag, Berlin: 1958: J. Am. Chem. Soc. (September 1959).

50. "Radiation Processes in Gases," G. L. Weissler, invited paper, Proceedings of the "Fourth International Conference on Ionization Phenomena," Uppsala, August 1959, Vol. I, p. 195 (North-Holland Publishing Co., Amsterdam: 1960).

51. "Intensity Distribution of Vacuum Ultraviolet Radiation Emitted from Magnetically Driven Shock Plasmas," G. L. Weissler, J. A. R. Samson, and D. Robinson, Bull. Am. Phys. Soc. 4, 450 (1959) G7.

52. "Monochromatic Photoionization of Ammonia with Mass Analysis of Ions," G. L. Weissler, G. R. Cook, and J. A. R. Samson, Bull. Am. Phys. Soc. 4, 454 (1959) J6.

53. "Photionization of Water Vapor with Mass Analysis of Ions," G. L. Weissler, J. A. R. Samson, and G. R. Cook, Bull. Am. Phys. Soc. 4, 454 (1959) J5.

54. "Photoionization Studies with a Vacuum U.V. Monochromator Crossed with a Mass Spectrometer," G. L. Weissler, invited paper, Opt. Soc. Meeting, Ottawa, Canada, October, 1959.

55. "The Absorption Cross Section of Sodium Vapor Between 1800 Å and 1100 Å," R. D. Hudson, Bull. Am. Phys. Soc. 5, 496 (1960) (F-8).

56. "Optical Constants of Ge in the Region of 0 to 27 eV," O. P. Rustgi, J. S. Nodvik, and G. L. Weissler, Phys. Rev. 122, 1131 (1961).

57. "Optical Properties of Sb, Te, and Ti Films in the Vacuum Ultraviolet," O. P. Rustgi, W. C. Walker, and G. L. Weissler, J. Opt. Soc. Am. 51, 1357 (1961).

58. "Fluorescence Induced by Vacuum Ultraviolet Radiation," R. I. Schoen, D. L. Judge, and G. L. Weissler, Proc. V. Int'l. Conf. on "Ionization Phenomena," Munich, August 28 to September 1, 1961, Vol. 1, page 25; North-Holland Publishing Co., Amsterdam: 1962; H. Maecker, ed.

59. "Efficiency of Aluminized Gratings in the Spectral Range 555 to 1600 Å," J. A. R. Samson, J. Opt. Soc. Am. 52, 525 (1962).

60. "A Theoretical and Experimental Analysis of an Eighteen Stage Radio-Frequency Mass Spectrometer," G. S. Bajwa, Tech. Rep., July 31, 1962.

61. "Cross Section Measurements for Some Photon-Gas Interaction Processes," G. L. Weissler, J. Quant. Spectr. Radiative Transfer 2, 383 (1962).

62. "Vacuum Ultraviolet Optical and Photoelectric Effects in Solids," W. C. Walker and G. L. Weissler, J. Quant. Spectr. Radiative Transfer 2, 613 (1962).

63. Proceedings of the "International Conference on Vacuum Ultraviolet Radiation Physics," J. Quant. Spectr. Radiative Transfer 2, pp. 315 to 725, Pergamon Press, Oxford: 1962; G. L. Weissler, Editor.

64. "Absorption, Ionization and Ion-Fragmentation Cross Sections in Hydrocarbon Vapors under Vacuum Ultraviolet Radiation," R. I. Schoen, J. Chem. Phys. 37, 2032 (1962).

65. "Wavelength Analysis of Fluorescence from Gases Excited by Vacuum Ultraviolet Radiation," D. L. Judge, A. L. Morse, and G. L. Weissler; "Proc. VI Int'l. Conf. on Ionization Phenomena in Gases," Paris, July 8-13, 1963; edited by P. Hubert and E. Cremieu-Alcan; Vol. III, p. 373, S.E.R.M.A., Paris, 1963.

66. "Molecular Fragmentation and Excitation by Vacuum Ultraviolet Radiation," R. I. Schoen and G. L. Weissler, invited paper, Symposium on Unimolecular Reactions in the Mass Spectrometer and Related Topics in Chemical Kinetics sponsored by the Division of Physical Chemistry of the Am. Chem. Soc., July 7-10, 1963, University of Utah, Salt Lake City.

67. "Optical Constants of Metals in the Vacuum UV Region," W. Steinmann, E. I. Fisher, and G. L. Weissler, USC-Tech. Report, dated January 15, 1964.

68. "Vacuum Ultraviolet Radiation as a Probe of Rare Gas Plasmas," H. E. Blackwell G. S. Bajwa, G. S. Shipp, and G. L. Weissler, J. Quant. Spectr. Radiative Transfer 4, 249 (1964); see also contributed paper to the Int'l. Symposium on Plasma Phenomena and Measurement, Oct. 29-31, 1963, San Diego: I.E.E.E. Transactions on Nuclear Sciences, NS-11, 199 (1964).

69. "Time-Delayed Fluorescence from Excited Ionic States of CO, CO_2, O_2, and N_2O," D. L. Judge, A. L. Morse, S. Furmanski, and G. L. Weissler, Bull. Am. Phys. Soc. 9, 183 (1964) (B3).

70. "An Apparatus for Measuring the Reflection, Transmission, and Photoelectron Yields of Thin Metallic Films in the Extreme UV," Boyd MacNaughton, M.S. Thesis, USC 1964; also Tech. Report dated February 15, 1964.

71. "Far Ultraviolet Response of Silicon P-N Junction Photo-diodes," D. B. Medved, Electro-Optical Systems, Inc., W. F. Crevier, A. L. Morse, USC, Bull. Am. Phys. Soc. 9, 644 (1964) (01); see also USC Tech. Report No. USC-Vac UV-101, June 15, 1965.

72. "Some Instrumentation Problems Below 1000 Å," G. L. Weissler, ICO Conf., Tokyo, Sept. 2-8, 1964; Japan J. Appl. Phys. 4 (Supplement I), 486 (1965).

73. "A Rapidly Operating Vacuum Spark Source forthe Vacuum Ultraviolet Region," (in French), G. Balloffet, J. Physique 25, 73A (1964).

74. "Absorption Cross Sections of Argon and Methane Between 600 and 170 Å," O. P. Rustgi, J. Opt. Soc. Am. 54, 464 (1964).

75. "Absorption Cross Sections and f-Values of Krypton and Xenon in their Ionization Continuum," O. P. Rustgi, E. I. Fisher, and G. H. Fuller, J. Opt. Soc. Am. <u>54</u>, 745 (1964).

76. "Transmittance of Thin Metallic Films (Ti, Te, Sb, Be, Al, Au, and Ag) in the Vacuum Ultraviolet Region Below 1000 Å," O. P. Rustgi, J. Opt. Soc. Am. <u>55</u>, 630 (1965).

77. "Optical and Photoelectric Properties of Thin Metallic Films in the Vacuum Ultraviolet," O. P. Rustgi and G. L. Weissler, J. Opt. Soc. Am. <u>55</u>, 456 (1965).

78. "Mobilities of Oxygen and Nitrogen Ions," James A. R. Samson and G. L. Weissler, Phys. Rev. <u>137A</u>, 381 (1965).

79. "Optical Constants and Photoelectric Yields in the Soft X-Ray Region," G. L. Weissler, invited pape æ to the "Int'l. Conf. on the Physics of X-Rays," Cornell Univ., June 22-24, 1965; Bull. Am. Phys. Soc. <u>10</u>, 1224 (1965).

80. "Fluorescence from N_2^{+*} Excited by Vacuum Ultraviolet Radiation, D. L. Judge and G. L. Weissler, Bull. Am. Phys. Soc. <u>10</u>, 739 (1965).

81. "Photo-Excitation, -Ionization, and Dissociative Photoionization of Some Simple Molecules," G. L. Weissler, invited paper to the 10th Annual Meeting of the Health Physics Society, Los Angeles, June 14-16, 1965.

82. "Optical Constants of Barium and Silver in the Vacuum Ultraviolet," E. I. Fisher, I. Fujita, and G. L. Weissler, J. Opt. Soc. Am. <u>56</u>, 1560 (1966); see also Tech. Report No. USC-Vac UV-108, dated 1 May 1966, by the same title. See also Edward I. Fisher, Ph.D. Dissertation, USC, Jan. 1964.

83. "Photoemission from Al Films in the Extreme Ultraviolet," A. L. Morse and J. E. Rudisill, Bull. Am. Phys. Soc. <u>10</u>, 1186 (1965) (A).

84. "Properties of a Plane Grating Predisperser Used with a Grazing Incidence Vacuum Spectrograph," H. E. Blackwell, G. S. Shipp, M. Ogawa, and G. L. Weissler, J. Opt. Soc. Am. <u>56</u>, 665 (1966).

85. "Vacuum Ultraviolet Radiation from Plasmas Produced by a Laser on Metal Surfaces," A. W. Ehler and G. L. Weissler, Appl. Physics Letters <u>8</u>, 89 (1966).

86. "Fluorescence Spectra of Molecular Ions Excited by Vacuum Ultraviolet Radiation," G. L. Weissler and D. L. Judge, Int'l. Conf. on "Ultraviolet and X-Ray Spectroscopy of Laboratory and Astrophysical Plasmas," Culham Lab., England, March 29 to April 1, 1966.

87. "Absorption, Photionization, and Scattering Cross Sections," J. A. R. Samson and G. L. Weissler, pages 142-178, in "Methods of Experimental Physics," Vol. 7, Part A: "Atomic and Electron Physics--Atomic Interactions," edited by B. Bederson and W. L. Fite, Academic Press, Inc., New York, 1968.

88. "Light Sources and Detectors for Work in the Vacuum Ultraviolet Region of the Spectrum," G. L. Weissler in "Aerospace Measurement Techniques," ed. G. G. Manella, pages 229-261, NASA SP-132, U. S. Government Printing Office, Washington: 1967.

89. "Thermopiles, Thermistor Bolometers, and Silicon p-n Junction Photodiodes as Vacuum UV Detectors," G. L. Weissler and W. F. Crevier, Tech. Report No. USC-Vac UV-102, dated July 1, 1965 (Contract DA-ARO (D)-31-124-G509).

90. "The Efficiency of Concave Gratings inthe Extreme Ultraviolet," A. L. Morse and G. L. Weissler, Sci. Light (Tokyo) 15, 22 (1966).

91. "Fluorescence Spectra (and Cross Sections) of the Excited Ion N_2^+ Resulting from Vacuum Ultraviolet Photon Impact on N_2," D. L. Judge and G. L. Weissler, J. Chem. Phys. 48, 4590 (1968).

92. "Photoemission Processes in Au and Al in the Extreme UV," A. L. Morse, Bull. Am. Phys. Soc. 13, 196 (1968); see also Arthur Morse, Ph.D. Dissertation, Univ. of Southern California, Los Angeles, Jan. 1968.

93. "Remeasurement of the Conversion Constant, Λ," H. A. Kirkpatrick, J. W. M. DuMond, and E. R. Cohen in the Proceedings of the Third International Conference on Atomic Masses, ed. R. C. Barber, Univ. of Manitoba Press, page 347; Winnipeg, 1967.

94. "A Vacuum Spark Light Source for the Extreme Ultraviolet Region," N. Wainfan and J. E. Rudisill, J. Appl. Opt. 8, 345 (1969).

95. "Optical and Photoelectric Properties, Including Polarization Effects of Gold and Aluminum in the Extreme Ultraviolet," A. L. Morse, Tech. Report No. USC-VacUV-109, dated January 5, 1968.

96. "Vacuum UV Emission and Absorption by Moderate Temperature Arc Plasmas, and Temperature Measurements in a High Pressure Arc Plasma," H. E. Blackwell, M. Whitson, and G. L. Weissler, Tech. Report No. USC-VacUV-110, dated August 1, 1968.

97. "The Combination of an Ultrahigh Vacuum Seya Monochromator with an Ultrahigh Vacuum Reflectometer for Measurement of the Optical Constants of Solids in the Extreme UV," Hayden H. Bower, M.S. Thesis, University of Southern California, January, 1969.

98. "On the Polarization Produced by a Normal Incidence Vacuum Monochromator,' Lawrence R. Whalley, M.S. Thesis, January 1970, U.S.C.

99. "Observations of Plasma Resonance at 790 Å in Reflection from Thin Zr Films,' J. E. Rudisill, A. Matsui, and G. L. Weissler, Optics Communications 2, 39 (1970).

100. "On the Polarization Produced by the Same Grating in the Seya and in the Normal Incidence Mounting," T. Knowles, L. R. Whalley, and G. L. Weissler (in preparation, April 1970).

101. 'Measurement of the Photoionization Cross Section in the Resonance Continuum of Carbon-I Using a Wall-Stabilized Arc," W. Hofmann and G. L. Weissler, USC Tech. Report No. USC-Vac UV-121, issued April 1, 1970. J. Opt. Soc. Am. 61, 223 (1971).

102. 'Temperature Measurements of Argon Plasma Arcs Operated Between 100 and 760 Torr, and Preliminary f-value Measurements of Ly-β, -γ, -S,' S. Ogawa and G. L. Weissler, Tech. Report No. USC-Vac UV-122, April 15, 1970.

103. "The Combination of an Ultrahigh Vacuum Seya Monochromator with an Ultrahigh Vacuum Reflectometer for Measurement of the Optical Constants of Solids in the Extreme Ultraviolet," Hayden H. Bower, M.S. Thesis at USC, January 1969.

104. 'Observation of Plasma Resonance at 790 Å in Reflectance from Thin Zirconium Films," J. E. Rudisill and G. L. Weissler, to be submitted for publication in the J. Am. Opt. Soc.; see also Tech. Report No. USC-Vac-UV-123 by the same title, dated September 1, 1970 and USC Ph.D. Dissertation J. E. Rudisill, August, 1970.

105. "Absorption of O_2, CO_2, and CS_2; Fluorescence of CS_2; and Photoionization of Atomic Carbon," G. L. Weissler, M. Ogawa, and D. L. Judge, contributed paper to the "International Colloquium on Simple and Multiple Electron Transitions in the X-Ray and Far-Ultraviolet Regions;' Paris, Sept. 21 to 25, 1970. *Journal de Physique, Supplément, Vol. 20 (Oct. 1971)*

page 154

106. "Vacuum UV Spectroscopy with Wall-Stabilized Arcs; Absorption Series of CO and its Photoionization Fluorescence,' G. L. Weissler, M. Ogawa, and D. L. Judge, contributed paper to the '3rd Int'l Conf. on Vacuum UV Radiation Physics," Aug. 30 to Sept. 2, 1971, Tokyo, Japan, to be published.

107. "Conference Summary Talk, given at the conclusion of the 3rd Int'l. Conf. on Vacuum UV Radiation Physics," by G. L. Weissler, Science of Light, Tokyo (Japan), Vol. 20, p. 95 (Dec. 1971).

108. "Methods of Measurement of Photoionization Processes Including Arc Plasma Spectroscopy," G. L. Weissler, paper presented at U.S.-Japan Seminar, Aug. 24, 1971, in Tokyo (Japan); Science of Light, Tokyo 21, 89 (June 1972); also in Japanese in the J. Spectroscop. Soc. Japan 21, 150 (1972).

109. "A Wall-Stabilized Arc as a Standard Light Source Below 1100Å, G.L. Weissler and Santosh K. Srivastava; contributed paper to the Twenty-Fourth Annual Gaseous Electronics Conference and Third Arc Symposium, Oct. 5-8, 1971; Univ. of Florida, Gainesville, abstract published in Bull. Am. Phys. Soc. 17, 383 (1972) (B-1).

110. "The Question of Local Thermodynamic Equilibrium of Argon in a Helium Plasma and the Measurement of the Photoionization Cross Section of Argon, M.S. Thesis by Scott C. Daubin, Jr., Univ. of Southern Calif., January 1972.

111. "U.S.-Japan Seminar on Current Problems in Spectroscopy," Tokyo, 24-27 Aug. 1971; reviewed by G. L. Weissler, Appl. Opt. 11, 962 (1972).

112. "Third International Conference on Vacuum UV Radiation Physics," Tokyo, Aug. 30-Sept. 2, 1971; reviewed by G. L. Weissler, Appl. Opt. 11, 2395 (1972).

113. "A Wall-Stabilized Double Arc as a Standard Intensity Source in the Vac. UV," G. L. Weissler and Santosh K. Srivastava; IX Int'l. Commission on Optics (ICO), Santa Monica, Calif., Oct. 9-13, 1972; page 196. See also "Space Optics," Proceed. IX. Int'l. Congress of the Int'l. Comm. for Optics, B. J. Thompson and R. R. Shannon, Ed's.; Nat'l. Acad. Sci., Washington, 1974, page 772.

114. "f-Values of Nine ArII Lines in the Vac. UV," Santosh K. Srivastava and G. L. Weissler, paper presented at the "25th Annual Gaseous Electronics Conference" at the Univ. of Western Ontario, London, Ontario, Oct. 17-20, 1972; paper JA 5. Bull. Am. Phys. Soc. 18, 794 (JA5) (May 1973).

115. "Lowering of the Ionization Potential of an Atom in a High-Temperature and High-Density Plasma," S. K. Srivastava and G. L. Weissler, internal Tech. Report No.: USC-Vac UV-131, dated Dec. 1, 1972; and USC-Vac. UV-132, dated Sept. 1, 1973.

116. "Vacuum UV Plasma Spectroscopy on a Double Arc, with Measurements on Line Strengths and Shapes, and on the Lowering of Ionization Potentials," Santosh K. Srivastava, Dissertation: August 1973; Univ. of Southern California, Los Angeles, CA 90007.

117. "The Lowering of the Hydrogen Ionization Potential in an Argon Arc Plasma," S. K. Srivastava and G. L. Weissler, Bull. Am. Phys. Soc. 19, 166 (PB-1) (Feb. 1974).

118. "The Lowering of the Spectral Series Limit of Hydrogen and Carbon," Santosh Srivastava and G. L. Weissler, IEEE Transactions on Plasma Science, vol. PS-1, 17 (Dec. 1973).

119. "The Lowering of the Hydrogen Ionization Potential in an Argon Arc Plasma", S. K. Srivastava and G. L. Weissler, Bull. Am. Phys. Soc. 19, 166 (PB-1)(Feb. 1974).

120. "Vacuum UV Spectroscopy with Plasma Arcs", G. L. Weissler, p. 160, in "Procceedings of the Fourth International Conference on Vacuum UV Radiation Physics"; Hamburg, July 22-26, 1974; to be published by the North-Holland Publishing Co.

121. "Absorption Spectroscopy of Metal Atoms in the Vacuum UV via Electron Impact and Spectroscopy", P. I. at USC: G. L. Weissler; P. I. at J.P.L.: S. K. Srivastava - Proposal to the President's Fund, Caltech, Jan. 14, '75.

122. "Measurements of Ly-α and -β Line Profiles in an Argon Arc", G. L. Weissler and H.-H. Carls, 28th Annual Gaseous Electronics Conference, Oct. 21-24, 1975 in Rolla, Missouri, contributed paper DA-5; Bull. Am. Phys. Soc. 21, 159 (DA-5)(Feb. 1976).

123. "Some High-Resolution Work with Various Gratings at both Normal and Grazing Incidence", G. L. Weissler, invited paper given at U.S.-Japan Seminar on the subject of "Diffraction Gratings", Oct. 14-17, 1975, Washington, D.C.

124. "f-Values of Nine Argon-II Lines Measured in a High Current Arc," S. K. Srivastava and G. L. Weissler, internal Tech. Report No. USC-Vac UV-160, dated Feb. 1, 1978.

125. "Measurements of the Hydrogen Lyman-Alpha and Lyman-Beta Line Profiles in an Argon Arc," H. H. Carls and G. L. Weissler, internal Tech. Report No. USC-Vac UV-161, dated Feb. 15, 1978.

MASARU OGAWA

PUBLICATION LIST

1. "On the New Emission Spectrum of Nitric Oxide in the Visible Region," M. Ogawa and Y. Tanaka, J. Sci. Res. Inst. 44, 1 (1949).

2. "On the Emission Band of the γ and ε Systems of Nitric Oxide," M. Ogawa, Sci. of Light 1, 19 (1951).

3. "On the Origin of Sodium D-lines in the Night Sky Emission and Twilight Flash," Y. Tanaka and M. Ogawa, Sci. of Light 1, 61 (1951).

4. "Band Spectra of Nitric Oxide in the Visible and Near Infrared Regions," M. Ogawa, Sci. of Light 2, 87 (1953).

5. "The Band Spectrum of Nitric Oxide in the Near Infrared Region," M. Ogawa, Sci. of Light 3, 39 (1954).

6. "On the Origin of Sodium D-lines in the Nightglow and Twilight Flash," M. Ogawa, Sci. of Light 3, 47 (1954).

7. "Spectroscopy and Dissociation Energy of Diatomic Molecules," M. Ogawa, J. Spectrosc. Soc. Japan 10, 17 (1954).

8. "On the Emission Spectrum of the β-, γ-, and ε-systems of Nitric Oxide," M. Ogawa, Sci. of Light 3, 90 (1955).

9. "Photoelectric Studies of Near Infrared OH Emissions of the Night Sky (1)," M. Ogawa, N. Nakamura, and A. Hashizume, Sci. of Light 5, 139 (1956).

10. "Rotational Constants of B'State of Nitric Oxide," M. Ogawa and M. Shimauchi, Sci. of Light 5, 146 (1956).

11. "Absorption Coefficients of O_3 in the Vacuum Ultraviolet Region," (L), M. Ogawa and G. R. Cook, J. Chem. Phys. 28, 173 (1958).

12. "Absorption Coefficients of C_6H_6 and H_2 in the Vacuum Ultraviolet," (L), S. H. Bunch, G. R. Cook, M. Ogawa, and A. W. Ehler, J. Chem. Phys. 28, 740 (1958).

13. "Absorption Coefficients of Methyl, Ethyl, n-Propyl, and n-Butyl Alcohols," (L), M. Ogawa and G. R. Cook, J. Chem. Phys. 28, 747 (1958).

14. "Photoionization Analysis by Mass Spectroscopy, G. L. Weissler, J.A.R. Samson, M. Ogawa, and G. R. Cook, J. Opt. Soc. Am. 49, 338 (1959).

15. "New Emission Bands of N_2 in the Vacuum Ultraviolet Region", (L), M. Ogawa and Y. Tanaka, J. Chem. Phys. 30, 1354 (1959).

16. "New Emission Bands of Forbidden Systems of Nitrogen in the Vacuum Ultraviolet Region", M. Ogawa and Y. Tanaka, J. Chem. Phys. 32, 754 (1960).

17. "Emission Spectrum of S_2 in the Vacuum Ultraviolet Region", Y. Tanaka and M. Ogawa, J. Chem. Phys. 36, 726 (1962).

18. "Rydberg Absorption Series of CO_2 Converging to the $^2\Pi_u$ State of CO_2^+", Y. Tanaka and M. Ogawa, Can. J. Phys. 40, 879 (1962).

19. "Rydberg Absorption Series of N_2", M. Ogawa and Y. Tanaka, Can. J. Phys. 40 1593 (1962).

20. "The b $^4\Sigma_g^- \leftarrow X\ ^3\Sigma_g^-$ Rydberg Series of the Oxygen Molecule", T. Namioka, M. Ogawa, and Y. Tanaka, International Symposium on Molecular Structure and Spectroscopy, Tokyo, September 10 to 15, 1962.

21. "Forbidden Absorption Bands of N_2 in the Vacuum Ultraviolet Region", Y. Tanaka, M. Ogawa, and A. S. Jursa, J. Chem. Phys. 40, 3690 (1964).

22. "Vacuum Ultraviolet Light Sources", M. Ogawa, J. Spectrosc. Soc. Japan 11, 199 (1963).

23. "Isotope Shift of the Absorption Bands of N_2 in the Vacuum Ultraviolet Region", M. Ogawa, Y. Tanaka, and A. S. Jursa, Can. J. Phys. 42, 1716 (1964).

24. "Absorption Spectrum of Electrically Excited Nitrogen Molecules in the Vacuum UV Region", M. Ogawa, Y. Tanaka, and A. S. Jursa, J. Chem. Phys. 41, 3351 (1964).

25. "Vibrational Isotope Shifts of Absorption Bands of N_2 in the Spectral Region 720Å to 830Å", M. Ogawa, Can. J. Phys. 42, 1087 (1964).

26. "The Absorption of Hydrogen Lyman Gamma Radiation by Molecular Nitrogen", M. Ogawa and R. B. Cairns, Planet. Space Sci. 12, 656 (1964).

27. "Photoionization of N_2 in the 734-805Å Region", G. R. Cook and M. Ogawa, Can. J. Phys. 43, 256 (1965).

28. "Rydberg Series Converging to the $B^2\Sigma^+$ State of CO^+", (L), M. Ogawa, J. Chem. Phys. 43, 2142 (1965).

29. "Absorption, Photoionization, and Fluorescence of CO", G. R. Cook P. H. Metzger, and M. Ogawa, Can. J. Phys. 43, 1706 (1965).

30. Absorption Photoionization, and Fluorescence of CO_2", G. R. Cook, P. H. Metzger, and M. Ogawa, J. Chem. Phys. 44, 2935 (1966).

31. "Properties of a Plane Grating Predisperser Used with a Grazing Incidence Vacuum Spectrograph", H. E. Blackwell, G. S. Shipp, M. Ogawa, and G. L. Weissler, J. Opt. Soc. Am. 56, 665 (1966).

32. "Absorption Spectrum of Electrically Excited Oxygen Molecules in the Ultraviolet Region", M. Ogawa, Science of Light (Tokyo), 15, 97 (1966).

33. "Absorption, Photoionization, and Fluorescence of NO", G. R. Cook, P. H. Metzger, and M. Ogawa, Can. J. Phys. 45, 203 (1967).

34. "Photoionization and Absorption Coefficients of N_2O", G. R. Cook, P. H. Metzger, and M. Ogawa, J. Opt. Soc. Am. 58, 129 (1968).

35. "Tanaka-Takamine Rydberg Series of O_2", M. Ogawa, Can. J. Phys. 46, 312 (1968).

36. "Absorption Coefficient of O_2 at the L_α and its Vicinity", M. Ogawa, J. Geophys. Res. 73, 6759 (1968).

37. "Absorption Spectrum of Electrically Excited Oxygen Molecules, Part II", M. Ogawa and Han-chuan Chang, Science of Light (Tokyo), 17, 45 (1968).

38. "Forbidden Absorption Bands of O_2 in the Argon Continuum Region", M. Ogawa and K. R. Yamawaki, Can. J. Phys. 47, 1805 (1969).

39. "Photoionization and Absorption Coefficients of OCS", G. R. Cook and M. Ogawa, J. Chem. Phys. 51, 647 (1969).

40. "Photoionization, Absorption, and Fluorescence of CS_2", G. R. Cook and M. Ogawa, J. Chem. Phys. 51, 2419 (1969).

41. "Fluorescence Spectra Resulting from VUV Photon Impact on COS" D. L. Judge and M. Ogawa, J. Chem. Phys. 51, 2305 (1969).

42. "Oscillator Strengths of The Hopfield Absorption Series of N_2," G. R. Cook and M. Ogawa, J. Chem. Phys. 53, 1292 (1970).

43. "Absorption Coefficients of O_2 at the Lyman-α Line and Other O_2 Transmission Window," (L), M. Ogawa and K. R. Yamawaki, Applied Optics, $\underline{9}$, 1709 (1970).

44. "Absorption Spectrum of CS_2 in the Region from 600 to 1015Å," M. Ogawa and H. C. Chang, Can. J. Phys. $\underline{48}$, 2455 (1970).

45. "Absorption Coefficients of O_2 in the Metastable State, $a^1\Delta_g$", (L), M. Ogawa, J. Chem. Phys. 53, pg. 3754 (1970).

46. "Absorption Cross Sections of O_2 and CO_2 Continua in the Schumann and Far UV Regions," M. Ogawa, J. Chem. Phys. $\underline{54}$, 2550 (1971).

47. "Absorption Spectrum of CO in the Helium Continuum Region, 500-1020Å," M. Ogawa and S. Ogawa, J. Molec. Spec. $\underline{41}$, 393 (1972).

48. "Rotational Analysis of a High-Resolution Absorption Band of O_2 at 1161Å," (L) H. C. Chang and M. Ogawa, J. Molec. Spec. $\underline{44}$, 405 (1972).

49. "Photoabsorption Cross Section of Argon in the 180-700Å Wavelength Region," (L) R. W. Carlson, D. L. Judge, M. Ogawa and L. C. Lee, Applied Optics 12, 409 (1973).

50. "Photodissociation Continua of N_2 and O_2," G. R. Cook, M. Ogawa and R. W. Carlson, J. Geophys. Res. $\underline{78}$, 1663 (1973).

51. "Fluorescence of Atomic Nitrogen Produced in the Photoabsorption of Extreme Ultraviolet Radiation by N ," L. C. Lee, R. W. Carlson, D. L. Judge and M. Ogawa. Chem. Phys. Letter, $\underline{19}$, 183 (1973).

52. "The Absorption Cross Sections of N_2, O_2, CO, NO, CO_2, N_2O, CH_4, C_2H_4, C_2H_6 and C_4H_{10} from 180-700Å," L. C. Lee, R. W. Carlson, D. L. Judge and M. Ogawa, J. Quant. Spect. Rad. Trans. $\underline{13}$, 1023 (1973).

53. "Photoionization Excitation of the CO_2^+ ($B^2\Sigma_u^+ - x^2\pi_g$) 2290Å Band," R.W. Carlson, D.L. Judge, and M. Ogawa, J. Geophys. Res. $\underline{78}$, 3194 (1973).

54. "Observation of Autoionization Process in the Production of Excited CO_2^+ Ions,"(L) R.W. Carlson, D.L. Judge, and M. Ogawa, J. Phys. B. $\underline{6}$, 343 (1973).

55. "Absorption Spectrum of CO_2 in the Hopfield Helium Continuum Region. Rydberg Bands Converging to the $X^2\Sigma^+$ State of CO^+ in the Region, 960-1080Å." S. Ogawa and M. Ogawa, J. Molec. Spec. $\underline{49}$, 454 (1974).

56. "Absorption Cross Sections of $O_2(a^1\Delta_g)$ and $O_2(X^3\Sigma_g^-)$ in the Region from 1087 to 1700 A", S. Ogawa and M. Ogawa, Can. J. Phys. $\underline{24}$, 1845-52 (1975).

57. "Rotational Analysis of the Absorption Spectrum of Heavy Oxygen ($^{18}O_2$) in the Region 1200-1285 A", Masaru Ogawa, Can. J. Phys. $\underline{24}$, 2703-11 (1975).